Mechanisms of Microvascular Dysfunction Following Subarachnoid Hemorrhage

By

Dominic A. Siler

A DISSERTATION

Presented to the Neuroscience Graduate Program

and the Oregon Health & Science University

School of Medicine

in partial fulfillment of

the requirements for the degree of

Doctor of Philosophy

June, 2014

School of Medicine

Oregon Health & Science University

CERTIFICATE OF APPROVAL

This is to certify that the PhD dissertation of

Dominic A. Siler

has been approved

_____

Mentor: Nabil J. Alkayed, MD, PhD

_____

Committee Chair: Mary M. Heinricher, PhD

_____

Member: Justin S. Cetas, MD, PhD

_____

Member: Edward A. Neuwelt, MD

_____

Member: Steven L. Jacques, PhD

_____

Member: David B. Jacoby, MD

TABLE OF CONTENTS

LIST OF FIGURES

LIST OF TABLES

LIST OF ABBREVIATIONS

AA	Arachidonic Acid
ABP	Arterial Blood Pressure
aCSF	Artificial cerebrospinal fluid
ADP	Adenosine diphosphate
AMP	Adenosine monophosphate
ANOVA	Analysis of variance
ATP	Adenosine triphosphate
AUC	Area under the curve
BBB	Blood-brain Barrier
BHT	Butylated hydroxytoluene
CBF	Cerebral blood flow
CBV	Cerebral blood volume
CSF	Cerebrospinal fluid
CT	Computed tomography
CYP	Cytochrome P450
DCI	Delayed cerebral ischemia
DHET	dihydroxyeicosatrienoic acid
EBI	Early brain injury
EDH	Endothelial derived hyperpolarizations
EDHF	Endothelial derived hyperpolarizing factor

EET	Epoxyeicosatrienoic acid
JNK	c-Jun N-terminal kinase
KOH	Potassium hydroxide
LC-MS/MS	Liquid chromatography tandem mass spectrometry
LDF	Laser Doppler flowmetry
LR	Lindegaard ratio
MAP	Mean arterial pressure
MCA	Middle cerebral artery
MPIO	Micron-sized iron oxide
MR	Magnetic resonance
MRI	Magnetic resonance imager
NF-kB	Nuclear factor-kB
NO^-	Nitric oxide
OCT	Optical coherence tomography
HETE	Hydroxyeicosatetraenoic acid
Hb	Hemoglobin
ICP	Intracranial pressure
GMP	Guanosine monophosphate
OMAG	Optical microangiography
PBS	Phosphate-buffered saline

PCR	Polymerase chain reaction
PE	Polyethylene
RBC	Red blood cell
ROC	Receiver operator characteristics
TNF-a	Tumor necrosis factor-alpha
tPA	Tissue plasminogen activator
TPP	Triphenylphosphine
VCAM	Vascular cell adhesion factor
WT	Wild type
SAH	Subarachnoid hemorrhage
sEH	Soluble epoxide hydrolase
sEHKO	Soluble epoxide hydrolase knockout
TIA	Transient ischemic attack

ACKNOWLEDGEMENTS

Five years seems like a long time, but I cannot imagine how long it would take me to figure out on my own everything I have learned during my time here under my mentor Nabil Alkayed. His expertise in the profession of being a scientist and his willingness to share everything he himself has learned is a priceless gift that I will take with me for the rest of my life.

I'd like to also thank my co-mentors Mary Heinricher and Justin Cetas. Their unique perspectives and dedication to the core principle of being a scientist were and always will be welcome in shaping my view of the science.

Thanks to my committee members Steven Jacques and Edward Neuwelt whose top concern was always my success as a scientist and my well-being as a student. Thank you for the suggestions that have helped guide my work over the years.

My lab mates Kasia Davis, Jonathan Nelson, Kristen Zuloaga, Jeff Iliff, Nicole Libal, Jennifer Young, Amanda Casper, Doug Zeppenfeld and Wenri Zhang have all played critical roles in getting me to this point. Not only did they offer training and help with experiments, they were there for me when I was unsure about myself and needed a friend who understood.

I'd also like to thank my family for supporting me from near and far all these years as I worked toward my PhD. My brother Josh taught me to write a compelling grant application that was successfully funded. My talented sister Maria contributed artwork to manuscripts that really classed up my clumsy figures. Most especially, I'd like to thank my father, who took the time to become an expert on subarachnoid hemorrhage himself so that we could have in depth discussions on my work.

Finally, deep thanks to my wife Janelle, who never doubted me for a second, even when I was convinced I would fail. She is always there to place support in just the right way to keep me standing and moving forward. With her, I can do anything.

DEDICATION

To my wife Janelle, whose love is worth a hundred PhDs.

ABSTRACT

Subarachnoid Hemorrhage (SAH) is a devastating form of stroke caused by rupture of a large cerebral artery. This catastrophic event is associated with high mortality and long term neurological disability. SAH is also associated with other complications, which are severe and common. The complications are biphasic in nature, with some appearing very early after ictus such as acute hydrocephalus and cerebral edema, while others manifest days later; for example, delayed cerebral ischemia (DCI). The mechanisms underlying these complications are poorly understood but growing evidence suggests that dysfunction of the cerebral microvasculature plays a significant role in their development. The work in this thesis will first seek to characterize one of the earliest causes of impaired microvascular perfusion after SAH related to impaired CSF flow. Second, this work will study changes in the epoxyeicosanoid pathway in humans after SAH and then test its role as a protective mechanism in both early and delayed microvascular dysfunction.

Blood entering the cerebrospinal fluid (CSF) space is a primary pathology in SAH. The protein, cellular and ionic content of the blood are all capable of disrupting normal brain function. Fibrinogen is the third most abundant protein found in the blood and key component of the hemostatic system. In experimental SAH, I found that blood, containing fibrinogen, flows into CSF spaces within minutes following SAH induction in the mouse. This fibrinogen forms an insoluble barrier within the CSF flow spaces, blocking CSF flow and leading to elevated intracranial pressure (ICP), which compresses underlying cortical tissue and impairs cortical perfusion. Clearance of fibrin with tissue plasminogen activator (tPA) 1 hour after SAH restores CSF flow in the mouse, lowers ICP and improves cortical perfusion within 24 hours. Lowering ICP without clearing fibrin deposits does not have the same effect on cortical perfusion. Thus, blockade of CSF flow leads to impaired microvascular blood flow after SAH in an ICP dependent and ICP independent manner.

Delayed cerebral ischemia (DCI) is a common and life threatening complication of SAH that commonly occurs between 3-14 days after vessel rupture. It has been well documented that the eicosanoid 20-hydroxyeicosatetraenoic acid (20-HETE) plays a

detrimental role in DCI after SAH, but little is known about the role of epoxyeicosatrienoic acids (EETs), which are vasodilators in the microcirculation. In SAH patients, I found that CSF levels of both 20-HETE and 14,15-EET are elevated after SAH and those with the highest concentrations of both are more likely to experience DCI than those with lower concentrations. SAH in mice causes immediate vasoconstriction of pial arteries and delayed decreases in microvascular perfusion. Genetically modified mice with higher levels of 14,15-EET, due to deletion of its metabolizing enzyme soluble epoxide hydrolase (sEH), also exhibit pial artery constriction, but are nonetheless protected from microvascular perfusion deficits after SAH. Thus, both 20-HETE and 14,15-EET are increased after SAH. Although 20-HETE may contribute to DCI, 14,15-EET plays a protective role against delayed microvascular perfusion deficits and may represent a therapeutic target in SAH.

Early complications of SAH include acute hydrocephalus and global cerebral edema, both of which contribute to poor outcome after SAH. EETs have potent anti-inflammatory effects that may serve a protective role in these early complications. In mice with SAH, I found that acute communicating hydrocephalus develops within hours of hemorrhage induction. Cerebral edema and brain swelling also occur early after SAH and lead to disruption of the cortical white matter. Mice with genetically elevated levels of EETs are not protected from hydrocephalus but have reduced cerebral edema and less disruption of the white matter. Mice with higher levels of EETs also have better behavioral outcome than wild type mice.

Collectively, these results show that a component of the extravasated blood, fibrinogen, is capable of causing microvascular dysfunction within minutes of SAH by blocking CSF flow. The EETs pathway is activated after SAH and represents an important therapeutic target for treating both early and delayed complications of SAH.

Chapter 1

Introduction

1.1 Overview of Subarachnoid Hemorrhage

1.1.1 Definition

The subarachnoid space is a large causeway for cerebrospinal fluid that exists between the inner two layers of cells surrounding the brain, layers known as the *pia mater* and the *arachnoid mater* (figure 1). This space is shared by the large vessels of the cerebral arterial circulation, which bring oxygenated blood from the carotid and vertebral arteries to the brain. When the vessel wall of a large artery weakens, a defect known as cerebral aneurysm can form. Some of these aneurysms grow over time and rupture, causing blood to extravasate violently into the subarachnoid space. At the moment a subarachnoid hemorrhage (SAH) occurs, the arterial circulation, which operates at a pressure of 100 mmHg or more, becomes in direct communication with the subarachnoid space, whose pressure normally resides at a mere 10 mmHg. This pressure differential causes blood to pour into the subarachnoid space, leading to a rapid rise of intracranial pressure (ICP). In most cases, the actual hemorrhage itself lasts only a few minutes, but the damage done and the multitude of complications that follow this rapid and violent disease has earned it a characterization as a catastrophic cerebral event.

1.1.2 Epidemiology

Currently, 1-2% of the US population is living with a cerebral aneurysm [1]. A small percentage of those, an estimated 33,000 patients, will suffer from SAH in the US annually. The 30-day mortality rate is between 35-50% [2,3], with a high rate of disability among survivors [4,5]. Current monitoring and treatment strategies require prolonged stays in the intensive care unit, at high institutional and patient cost. The financial burden of SAH on the US healthcare system is nearly 3 billion dollars annually [6] and has an indirect societal cost greater than that of ischemic stroke [7], despite being less frequent.

1.1.3 Clinical Course of the Patient

Nearly 15% of SAH patients die before arriving at the hospital. Of those who survive to admission, 15% will have a second SAH, which confers an 80% risk of death or permanent disability [8]. Acute neurological complications include hydrocephalus, a build-up of fluid within the ventricular system of the brain which occurs in 20% of patients [9]. Additionally, cerebral edema, fluid accumulation within the brain parenchyma itself, befalls 20% of patients [10]. Delayed cerebral ischemia (DCI), new symptomatic cerebral infarcts that arise late in recovery, is seen in 30% of initial bleed survivors [11] and can manifest anywhere from 3-14 days [12] after the initial hemorrhage. Other complications include neurogenic fever, pulmonary edema, cerebral salt wasting and cardiac arrhythmias [13]. Overall, ~ 80% of SAH victims are either dead or left with a long term neurological deficit as the result of this disease [14].

1.1.4 Standard of Care

Aside from surgical clipping or endovascular coiling to prevent secondary bleeds, current standard of care for SAH is tailored to address prevailing symptoms while minimizing iatrogenic complications [15,16]. Management of DCI includes nimodipine and “triple-H” therapy (hemodilution, hypertension, hypervolemia) followed by endovascular intervention to reverse large vessel vasospasm. Exacerbation of cerebral edema and intracranial hypertension are possible complications of triple-H therapy and can be treated with osmotic diuresis. Symptomatic hydrocephalus is treated with CSF diversion and semi-permanent shunts are placed for those with unremitting disease. Overall, current SAH treatments are stop-gap techniques that reflect a lack of understanding of the underlying mechanisms behind these common complications.

1.2 A Shift in Focus: From Delayed to Early; from Large to Small

From its first characterization in 1951 [17], cerebral vasospasm of the large conduit arteries has been the presumed cause of DCI and the focus of intense research to improve the outcomes of SAH patients. Much of our current understanding of the pathology caused by SAH comes from work focused on treating this common

complication. Recently however, the field's focus has shifted away from large vessel disease and toward disease of the microvasculature [18]. This shift is entirely attributable to the preclinical success but ultimate failure of the endothelin receptor antagonist clasozentan in preventing DCI after SAH [19]. Endothelin-1 is a potent vasoconstrictor peptide found in the circulation and endothelial cells of the cerebral vasculature [20]. In preclinical studies, antagonism of the endothelin receptor with clazosentan was found to have a profound effect on vasospasm [21]. The treatment was quickly moved into clinical trials in SAH patients, where clasozentan was found to excel at preventing large vessel vasopasm. However, preventing vasospasm had no effect on neurological outcome [19]. Further work in animal models revealed that the effects of endothelin-1 antagonism were limited to the large vasculature, and did not affect many of the microvascular pathologies found in patients and in animal models of SAH [22].

At the same time that researchers were beginning to realize that preventing vasospasm directly would not improve the outcomes of their patients, clinical evidence was building that many of the early complications such as cerebral edema, global ischemia and acute hydrocephalus were themselves contributors to poor neurological outcome despite current treatment paradigms [10,23]. Hence the field has slowly begun to focus on understanding the mechanisms behind these complications with the hope of improving neurological outcome and preventing the development of DCI.

1.2. Primary Pathology in Subarachnoid Hemorrhage

Before describing the pathology found within the cerebral microvasculature, an understanding of the complicated situation that develops in SAH must be appreciated. As soon as SAH occurs, multiple pathological processes are activated, which feed into each other and create a vicious loop of pathological processes, making it difficult to determine which mechanisms are primary and which secondary or even tertiary.

1.2.1 Intracranial Hypertension and Transient Global Ischemia

In the late 18th century, Alexander Monro and George Kelli set the foundation of what would become the Monro-Kellie doctrine [24]. This states that the volume inside the cranium is fixed, and incompressible. This was further refined to describe the three compartments that make up the volume of the cranium; parenchyma, cerebrospinal fluid (CSF) and blood. An alteration in the volume one of these compartments requires compensation in another to maintain favorable pressure gradients to support maintenance of cerebral blood flow (CBF). Normally, any alterations in blood or brain volume within the cranium are compensated for by alterations in CSF volume to maintain favorable intracranial pressure (ICP). This favorable ICP allows the development of a pressure gradient that permits flow from the high pressure arterioles into the low pressure venous circulation and out of the cranium. During SAH, blood fills the CSF space. As extra volume is added within the cranium, pressure rises sharply. This leads to collapse of low-pressure vessels and a loss of the pressure gradient that drives CBF. The resulting cessation of CBF is called transient global ischemia and lasts several minutes following SAH. Global ischemia itself is known to cause cerebral inflammation, BBB disruption, and neuronal apoptosis [25]. While the initial extreme intracranial hypertension lasts only a few minutes, there often persists a sustained elevation in ICP which is not enough to arrest circulation but represents a poorly understood mechanism of damage in SAH [26].

1.2.2 Blood Products in the Subarachnoid Space

The CSF is a normally pristine fluid containing very little protein or cells. Its production is highly regulated by the brain and it is chemically distinct from blood. When SAH occurs, blood pours directly into the CSF space and brings with it a number of “contaminants” that are directly toxic to neurons and are capable of initiating an inflammatory response. The exact constituents of the blood that cause inflammation and neurotoxicity are unknown. Electron microscopy studies have documented leukocytes phagocytosing red blood cells in the subarachnoid space [27]. Constituents of the blood are also capable of causing vasoconstriction [28]. The best characterized of these is

hemoglobin which, when in its oxyhemoglobin form, is a strong scavenger of nitric oxide (NO^-) and is capable of inducing vasoconstriction in large [29] and small vessels [30]. Additionally, serotonin released from extravasated platelets is a potent vasoconstrictor [31]. Finally, the blood contains a full array of hemostatic cells such as platelets and proteins such as fibrinogen and thrombin whose function is normally to prevent blood flow through damaged endothelium. The consequences of their presence in the CSF are not well studied.

1.2.3 Animal models of SAH to replicate primary pathology

Animal models of SAH vary depending on the species studied (Figure 2). In non-human primates, SAH is induced via craniotomy and clot placement. This replicates the blood component of SAH but does not replicate the intracranial hypertension and transient global ischemia [32]. Still, clot placement induces large vessel vasospasm in primates at 7 days. In canine models, a double injection of autologous blood into the cisterna magna is the usual approach. The second injection is delayed by 48 hours. This does replicate both primary pathologies in SAH, though the intracranial hypertension can be missed with a slow injection rate. Furthermore, secondary bleeds are a rare occurrence after clinical SAH. Typically, late stage preclinical testing of therapeutic approaches is conducted in these large animals. Early stage preclinical tests are conducted in rats and mice, where two models prevail. The first is a single injection of autologous blood into the cisterna magna or basal cistern, which again replicates both primary pathologies of SAH, depending on the rate of blood injections, which is not always monitored. The second method is induction of SAH via puncture of the Circle of Willis with a nylon monofilament. This latter technique does well in replicating both blood in the subarachnoid space and intracranial hypertension, but has the disadvantage that the amount of blood extravasated during the procedure is uncontrolled [33], leading to high degree of experimental variability

1.3 Physiology and Pathology of the Cerebral Microvasculature

The cerebral microvasculature, defined as those vessels which penetrate and branch inside the brain, represent greater than 400 miles of conduit which is specially

adapted to deliver nutrients and remove waste from the neuropil in a controlled manner. Vessels can be categorized into penetrating and parenchymal arterioles, capillaries, and venules. Study of this vast and diverse network of specialized vessels has been limited by our inability to visualize them *in vivo.* As the technology to do so has increased in the past two decades, so has the number of experimental studies on microvasculature physiology and pathology in SAH. This section will discuss the highly specialized functions of the cerebral microvasculature and current experimental evidence of their dysregulation in SAH.

1.3.2 Microvascular control of Cerebral Blood Flow

Control of blood flow (CBF) by cerebral microvasculature is accomplished primarily through alterations in vessel diameter. Vessel diameter is a powerful determinant of flow rate, as Poiseulle's law dictates that a 20% increase in vessel diameter is capable of doubling blood flow rate through that vessel. The key players in determining vessel diameter are vascular smooth muscle cells, which exist in a single layer on penetrating and parenchymal arterioles and are replaced by analogous pericytes on capillaries. The contractile state of the smooth muscle, and consequently vessel diameter, is largely determined by the myogenic response, a calcium-dependent activation of contractile machinery driven by increases in stretch or transmural pressure of the vessel wall [34]. This autoregulatory mechanism, known as myogenic tone, insures that surges or drops in blood pressure are met by alterations in diameter to maintain constant CBF.

Myogenic tone can be altered to meet the high metabolic demand of the neuropil through a number of mechanisms. The endothelium, a single layer of specialized cells lining the inside layer of the vessel wall, is in direct contact with both blood and the smooth muscle, and can communicate with the latter through release of paracrine factors or through gap junctions. Well characterized factors released from endothelium that counteract myogenic tone include prostaglandin I_2 (PGI_2, prostacyclin), nitric oxide (NO^-), and endothelial-derived hyperpolarization (EDH). PGI_2 causes elevated levels of cyclic-AMP, which inhibits myosin light chain kinase and leads to vasorelaxation [35].

NO^- diffuses into smooth muscle from endothelium and induces production of cyclic-GMP which reduces cytosolic Ca^{2+} to inhibit smooth muscle contraction [36]. There are a number of factors produced by endothelium that cause EDH including epoxyeicosatrienoic acids (EETs), hydrogen peroxide, and hydrogen sulfide [37]. These factors ultimately lead to increased K^+ currents and smooth muscle hyperpolarization, which also reduces Ca^{2+} release in smooth muscle and promotes vasodilation [37]. The endothelium senses changes in shear-stress due to increased downstream flow and releases these factors to dilate in response and maintain CBF [38]. Other well characterized molecules that stimulate release of these factors from endothelium include acetylcholine, bradykinin, and adenosine. It is thought that EDH factors are particularly important among the three pathways in cerebral microvasculature [39] and that this importance increases in disease states such as ischemia [40] and traumatic brain injury [41] where NO^- bioavailability is reduced.

When neurons become active, their metabolic demand increases. Consequently, the need for increased blood flow to specific areas of the brain changes on a minute by minute basis. This temporally and spatially specific alteration of microvascular tone in response to neural activity is known as neurovascular coupling. Neurovascular coupling is not completely understood but is believed to involve vascular smooth muscle's close association with astrocytes [42]. The astrocytes form a continuous layer around the vessel known as the glia limitans perivascularis which can communicate directly with smooth muscle and pericytes via Ca^{2+} dependent release of epoxyeicosatrienoic acids (EETs) or K^+ into the space surrounding smooth muscle to induce hyperpolarization, stimulate vasorelaxation and increased blood flow in response to local neuronal activity [42]. Neurovascular coupling can also be influenced globally through activation of distant ascending brain nuclei such as the locus coeruleus [43].

1.3.3 Altered microvascular tone after SAH

The majority of observational studies in human SAH and experimental models of SAH have documented enhanced vasoconstriction of the cerebral microvasculature. Constriction of arterioles and decreased capillary density were found in patients undergoing surgery for aneurysmal clipping [44]. In large animal models including the

cat and dog, vasoconstriction begins within minutes [45] of SAH induction and persists for as long as 14 days. [46,47]. Small animal models of SAH also document very early vasoconstriction of the microvasculature [48-52]. However, vasoconstriction generally resolves within 72 hours of hemorrhage induction, which suggests some differences between the models. Associated with these vasoconstrictions were decreases in K^+ channel currents [53] and elevated intracellular Ca^{2+} [54] within vascular smooth muscle.

Controlled experimental studies, typically in isolated parenchymal arterioles of the cortex after SAH induction, examined alterations in pathways of endothelial dependent vasodilation. Researchers here found impaired vasodilation induced by some endothelial ligands like ATP, ADP and adenosine [30,55] but not acetylcholine [56] or bradykinin [57]. Several studies tested the response of vascular smooth muscle to endothelial derived vasodilators like K^+ or NO^- by administering these effectors exogenously to bypass the endothelial pathways. The vascular smooth muscle response to both of these effector molecules was found to be impaired as well [56,58,59]. Together, these data indicate that vasoconstriction is occurring both early and late following SAH and is due to both impairments in the ability of the endothelium to release vasoactive factors and the ability of vascular smooth muscle to respond to them.

Recently, two studies have looked at alterations in neurovascular coupling after SAH using acute brain slices with intact astrocytic/smooth muscle pathways. The authors stimulated astrocytic endfeet to release K^+ which normally causes smooth muscle hyperpolarization and vasodilation. After SAH, evoked release of K^+ caused vasoconstriction instead of vasodilation [60,61]. The defect in astrocytically-induced vasodilation was attributed to alterations in extracellular K^+, and indicates that the influence of the endothelium on microvasculature as well as neuronal control of CBF were both impaired after SAH.

While defects in vasodilator pathways have been identified in multiple cell types within the microvasculature after SAH, the end result is the same. After SAH, cerebral microvasculature is unable to maintain adequate CBF through a failure of both autoregulatory and dynamic metabolically driven mechanisms (Figure 3).

1.3.2 Inflammation, Barriers, and Thrombosis

Aside from control of CBF, the microvasculature serves many functions related to protection of neurons and glia from damage. Constituents of the blood plasma that can normally filter out of the circulation and into the parenchyma of peripheral organs are toxic to neurons. To manage this problem, endothelial cells in conjunction with astrocytes form a highly selective semipermeable membrane that restricts movement of these potentially toxic solutes into the brain parenchyma [62]. This is known as the blood-brain barrier (BBB) and is accomplished through formation of tight junctions in brain endothelial cells [63] along with conditioning of the basal lamina by astrocytic end feet [64]. The microvasculature also mediates the interactions between the brain and the immune system. Under normal circumstance the brain is considered an “immune privileged” organ, meaning the innate and adaptive immunity of the periphery does not move as freely into the brain space compared to other organs. However, in response to infection or cell damage, the endothelium will express cell surface proteins that permit the attachment and extravasation of immune cells into the parenchyma [65]. Finally, the cerebral microvasculature participates in hemostasis to prevent pathological bleeding into the parenchyma. Activated or damaged endothelial cells express cell surface receptors which can promote a pro-thrombotic state [66]. In this section I will discuss current experimental research that document pathological alterations of these essential microcirculatory functions after SAH.

1.3.2.1 Vascular Inflammation

Most studies of inflammation after SAH have looked in large vessels, the circulation, or the cerebrospinal fluid, each of which demonstrates increased expression of cell adhesion molecules beginning as early as 24 hours after SAH [67,68]. However, work describing vascular inflammation in microvessels is limited. Existing studies of microvascular inflammation suggests that activation of endothelium and leukocyte recruitment in microvessels occurs rapidly and is sustained following injury [69]. Leukocyte and platelet adhesion begins as early as 10 minutes [70] following SAH

induction and persists for at least 48 hours [71]. Associated with this is increased microvascular expression of p-selectin [72]. Additionally, upregulation of several stress and inflammatory pathways also occurs in microvessels including p-JNK, p53, NF-kB, TNF-a and interleukin-6 [73].

1.3.2.1 Disruption of the Blood-Brain Barrier

Traditionally, disruption of the BBB is documented by extravasation of labelled proteins that are normally excluded from the brain parenchyma. Since movement of these molecules into the parenchymal space must occur at the level of the microvasculature, BBB disruption is one of the most well characterized dysfunctions of the cerebral microvasculature. BBB disruption has been documented as early as 10 minutes following SAH [70], reaching peak disruption by 24 hours [74] and beginning to resolve by 72 hours after SAH [75,76]. Some studies have found this disruption to persist for as long as 7 days. [77,78] Associated with BBB disruption is increased expression of matrix metalloproteinase-9 [74], decreased expression of the tight junction protein zona occludens [76], and alterations in the molecular components of the basal lamina [79].

1.3.2.2 Microthrombosis

Activation or damage of endothelial cells leads to upregulation of p-selectin which can bind to platelets and promote a pro-thrombotic state within the microvasculature [80]. Microthrombi are dense deposits of platelets and fibrin found within parenchymal vessels. These obstructions could block blood flow to local areas and exacerbate brain injury. Several experimental studies of SAH have documented formation of microthrombi within arterioles. The small microthrombi were found as early as 10 minutes after SAH induction [81] but generally peaked 24 or 48 hours after injury [50,82]. One study found they persisted as long as 7 days after SAH induction [83]. Associated with the formation of microthrombi was the uncoupling of endothelial nitric oxide synthase [84] which is thought to enhance free radical production and exacerbate endothelial injury.

1.5 Targeting Multiple Pathways after SAH

Regardless of whether the multiple mechanisms of microvascular dysfunction described after SAH are attributable to global ischemia or blood products in the CSF, a therapeutic approach will likely target more than one of these mechanisms. The work in this thesis will describe two such approaches.

1.5.1 Altered CSF flow and microvascular dysfunction after SAH

A normally functioning CSF system plays two dynamic roles in maintenance of brain homeostasis. The first is to constantly move CSF into and out of the cranium to compensate for alterations in ICP so that adequate CBF can be maintained. The second is to maintain ionic and metabolic homeostasis in the extracellular space of the parenchyma [85]. To accomplish these tasks, CSF is produced constantly at a rate in humans 400 to 500 mL daily [86], leading to complete CSF turnover 3 to 4 times per day. CSF is created in the choroid plexi within the ventricular system before flowing out through the cisterns and along penetrating arterioles in paravascular CSF flow pathways. CSF leaves the cranium through either arachnoid villi, cranial nerve sheathes or through trans-capillary flow in the parenchyma. [87]

When an SAH occurs, blood products enter the CSF system but instead of being cleared out rapidly are trapped in place for up to 14 days, indicating disruption of this clearance pathway [88,89]. This impaired CSF flow system can manifest severely as acute hydrocephalus, which occurs in 20% [9] of individuals but is otherwise untreated if pathological ICP does not develop [26]. Animal studies have documented increased CSF flow resistance after SAH indicating that this normally high- turnover pathway is impaired [90,91]. The consequences of impaired CSF flow are not fully known. Studies in healthy mice with elevated ICP show that microvascular dysfunction, including BBB disruption and impaired CBF develops even at levels not thought to cause cerebral infarct [92]. Further, studies in humans and animals have documented altered levels of waste products [93] and dysregulation of ionic homeostasis [94] in the brain after SAH.

The cause of the latter are unknown, but disruption of normal CSF function is a possible mechanism.

Chapter 2 of this thesis will test the hypothesis that CSF flow impairment forms rapidly after SAH due to blood coagulation products in the extravasated blood. Chapter 2 will further explore this disruption of CSF flow and it's consequence on the cerebral microvasculature, testing the hypothesis that disruption of CSF flow can impair cortical perfusion.

1.5.2 P450 Epoxyeicosanoids to treat microvascular dysfunction after SAH

While some pathology after SAH could be preventable, the transient global ischemia and presence of blood products in the CSF are not, as they occur outside of the clinical setting before the patient reaches clinical care. Therefore, strategies aimed at mitigating vasoconstrictive and inflammatory responses to these pathologies will be needed to prevent further development of secondary disease and improve the outcome of SAH patients.

EETs are vasoactive lipids synthesized from arachidonic acid (AA) by cytochrome P450 enzymes in both endothelium (CYP2J2, CYP 2C8) and astrocytes (CYP2C11) of the brain (Figure 4) [95]. They represent a distinct arm of AA metabolism separate from the well characterized cyclooxygenase and lipoxygenase families. Synthesis begins with the liberation of AA from the cell membrane by phospholipase A_2. The cytochromes then produce four regio-isomers of EETs in varying ratios; 14,15-EETs, 11,12-EETs, 8,9-EETs, and 5,6-EETs. EETs are thought to induce EDH's in cerebral microvessels, which leads to smooth muscle relaxation and vasodilation [96,97]. 11,12-EETs and 8,9-EETs function as anti-inflammatory agents, inhibiting translocation of NF-κB, a master regulator of inflammation, into the nucleus [98]. Less is known about the actions of 5,6-EETs. EETs have also shown to be directly cytoprotective in neurons [99], astrocytes [100] and endothelium [101,102] subjected to

ischemic conditions *in vitro*, though which isoform is responsible is unknown. Finally 14,15-EETs inhibit platelet activation and are considered to be anti-thrombotic [103].

The bioavailability of EETs is largely determined by the enzyme soluble epoxide hydrolase (sEH) which hydrolyzes the epoxide into a vicinal diol creating dihydroxyeicosatrienoic acid (DHETs) [104]. These DHETs are inactive in vivo. Techniques for modifying the activity of sEH in vivo include the use of sEH inhibitors or use of a genetically modified mouse which has deletion of the gene encoding sEH [105]. These sEH knockout mice (sEHKO) have elevated levels of basal EETs within the brain and are protected from models of cerebral ischemia [106,107]. sEHKO mice have also shown reduced expression of vascular inflammatory markers and leukocyte infiltration in a model of renal injury [108]. These effects are consistent with EET's vasodilator and anti-inflammatory actions and provide an ideal model for testing the effects of EETs on microvascular dysfunction in SAH.

Chapter 3 of this thesis includes an observational study of CSF EETs levels in SAH patients who experience DCI and tests the hypothesis that EETs are protective against delayed dysfunction in microvascular cerebral perfusion. Chapter 4 of this thesis will test the hypothesis that elevated levels of EETs are protective against cerebral edema and vascular inflammation after SAH.

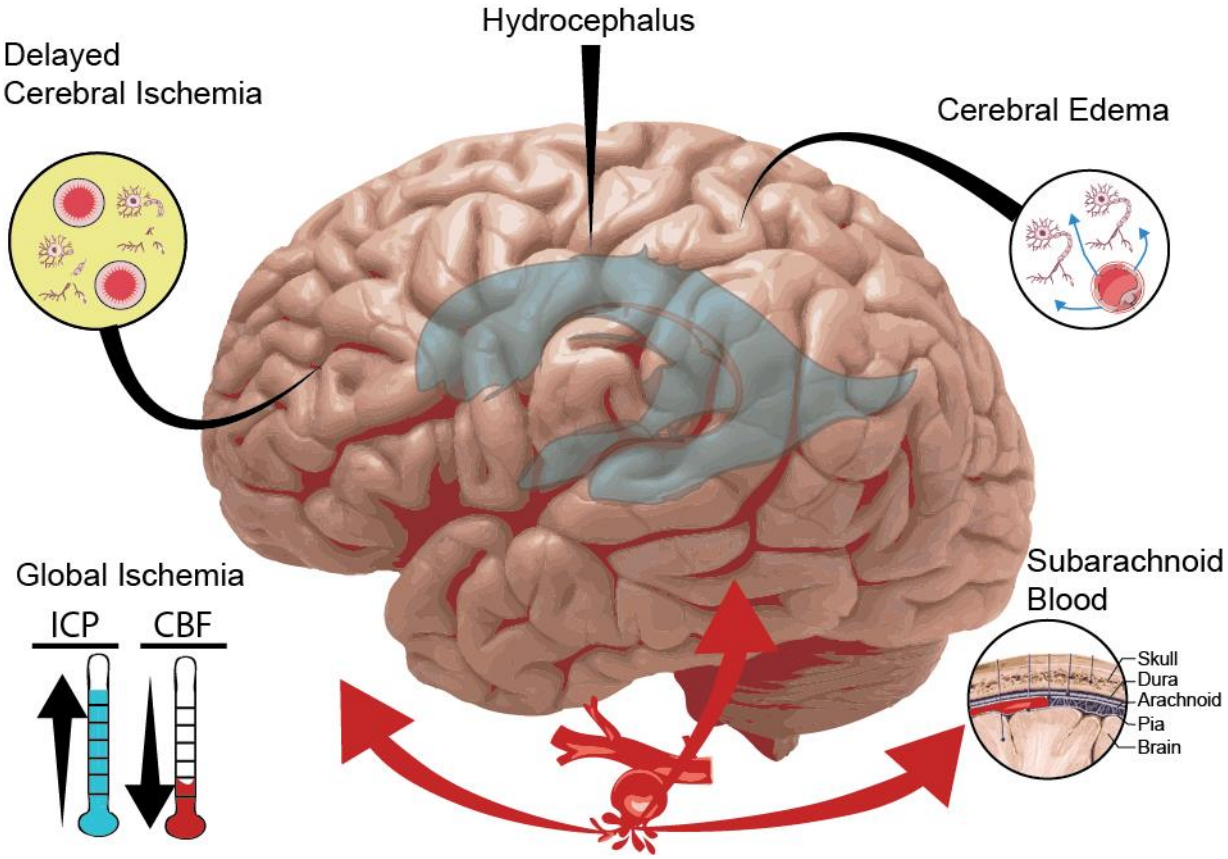

Figure 1. Primary and Secondary Pathology in SAH: Rupture of the large conduit arteries causes immediate release of blood factors into the subarachnoid space. This drives intracranial pressure up which reduces cerebral blood flow (CBF). Sequelae of this double hit include acute hydrocephalus and global cerebral edema. Delayed cerebral ischemia presents 3-14 days after SAH.

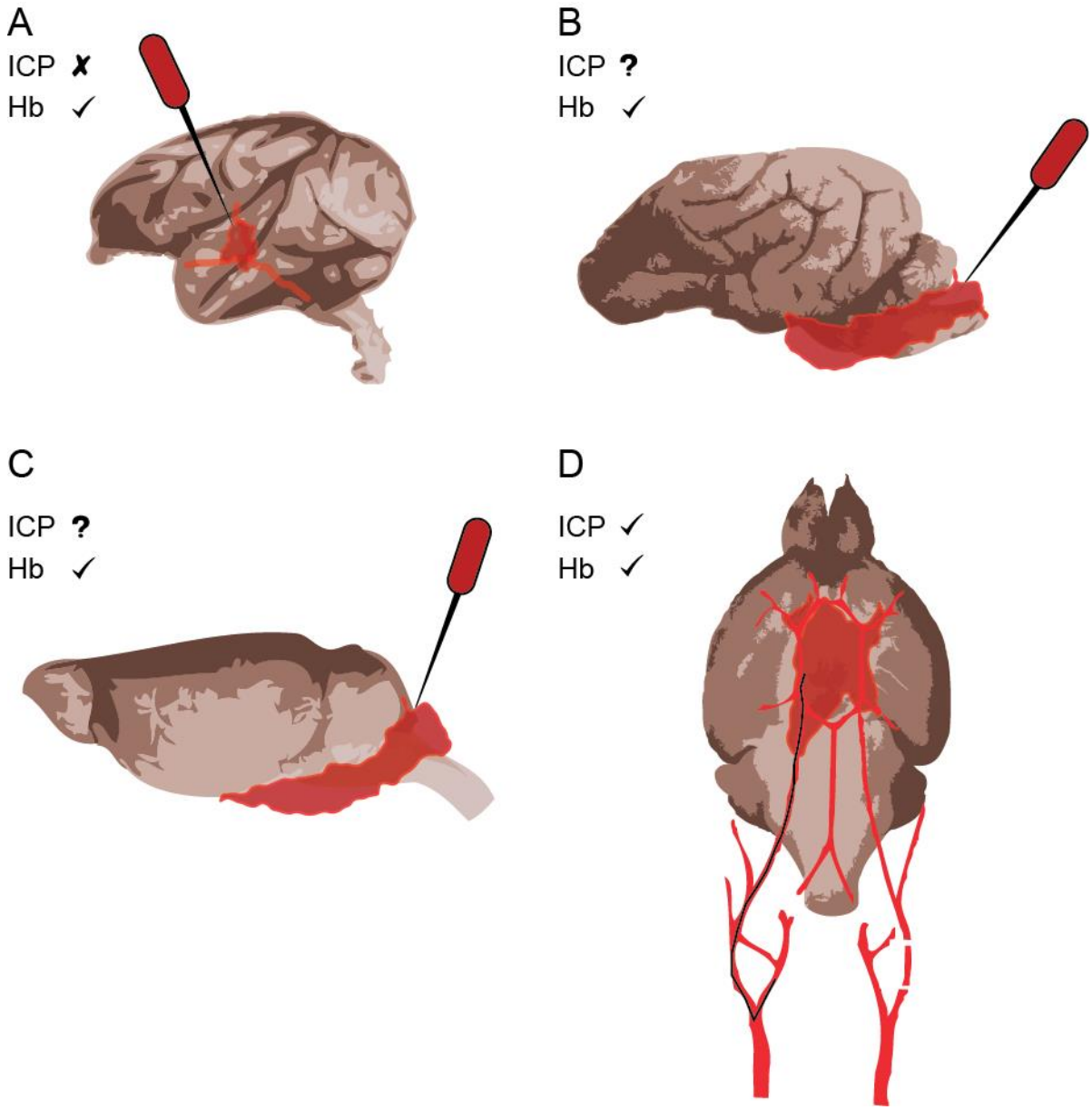

Figure 2. Animal models of SAH: A.) SAH is induced in non-human primates by craniotomy and clot placement near the Carotid/Middle Cerebral Artery bifurcation. Open cranium surgery prevents elevation of ICP. B.) Canine double injection model into the cisterna magna. Elevated ICP is dependent on surgeon technique and is not always noted. C.) Mouse or Rat cisterna magna injection model. Elevated ICP is possible depending on injection rate. D.) Mouse endovascular puncture model. The ICP and blood effects are present but blood volume is highly variable.

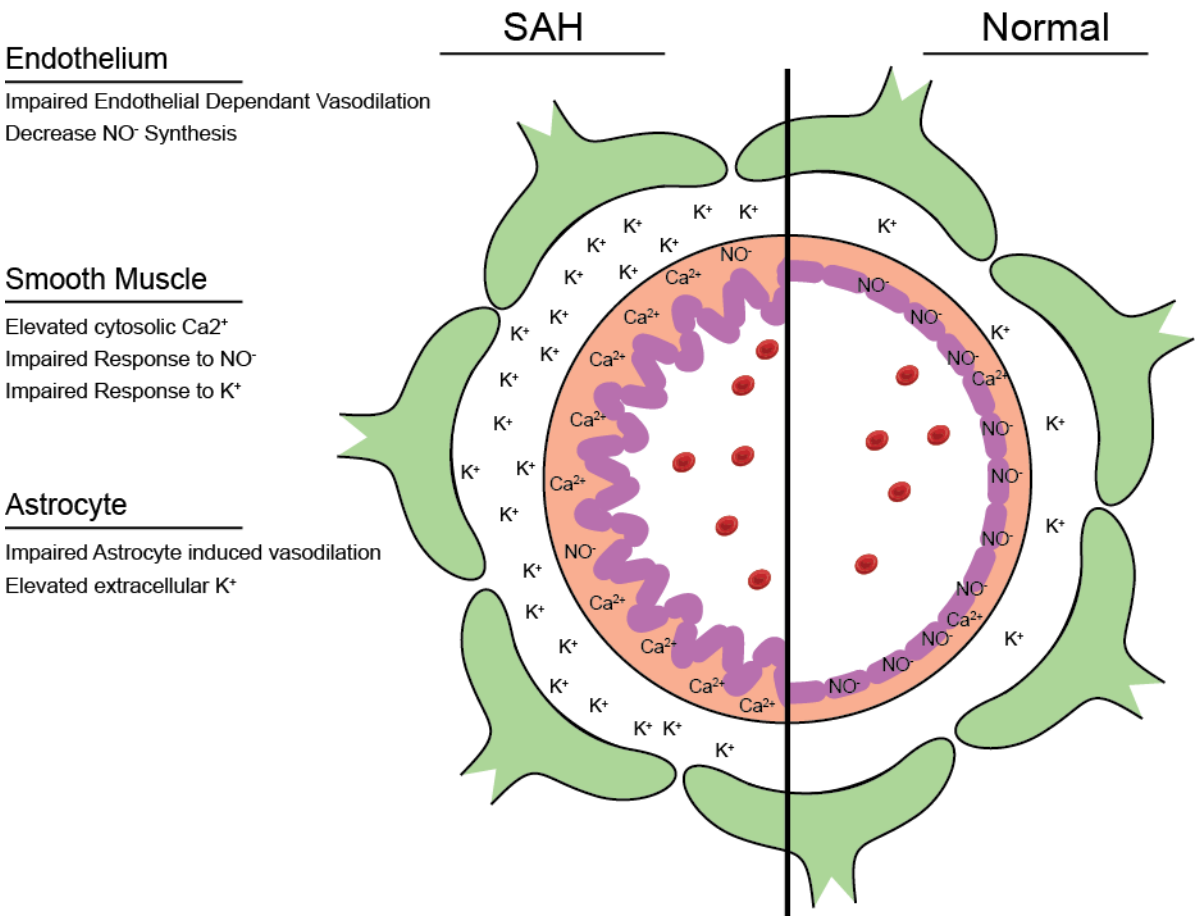

Figure 3. Alterations in microvascular control of CBF after SAH. In normal arterioles (right), myogenic tone is appropriate to the transmural stress placed on the smooth muscle (pink) and mediated by intracellular calcium (Ca^{2+}) levels. Release of endothelial (purple) dependent vasodilators (NO-) modulate this tone. Normally low levels of potassium (K^+) allow astrocytic (green) induction of K^+ release to stimulate hyperpolarization in smooth muscle (pink) in response to neural activity. SAH (left) leads to enhanced vasoconstriction by increasing intracellular Ca^{2+} within smooth muscle and impairing endothelial dependent vasodilation. Elevated levels of K^+ in the perivascular space prevent astrocyte induction of hyperpolarization.

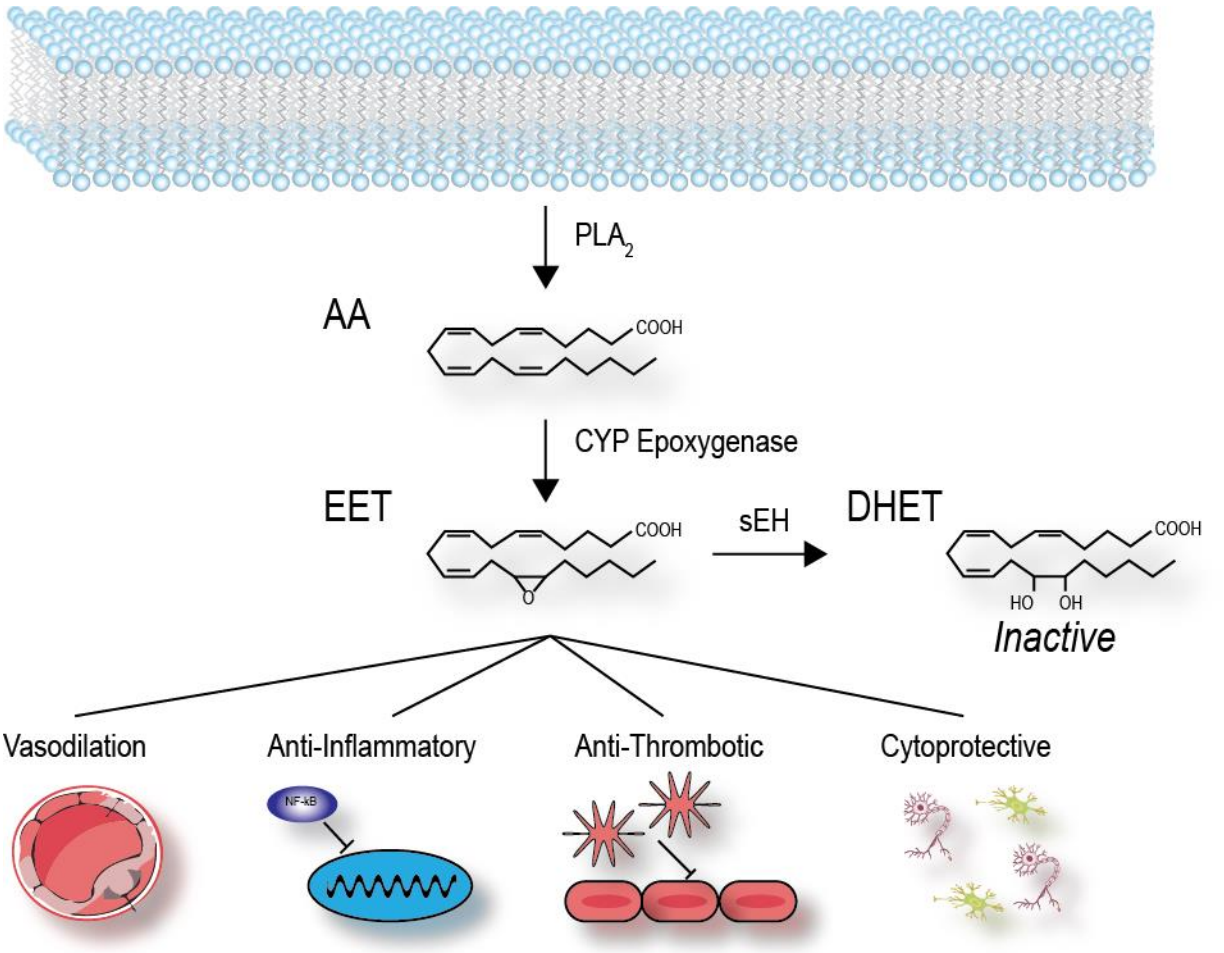

Figure 4. Epoxyeicosatrienoic acid (EETs): Arachidonic acid (AA) is liberated from the cell membrane by phospholipase A_2 (PLA_2). Cytochrome P450 (CYP) epoxygenases convert AA into EETs. EETs effects include: vasodilation, prevention of nuclear translocation of pro-inflammatory Nuclear Factor kappa Beta (NF-kB), decreased platelet-endothelial adhesion, and cytoprotection of neurons and glia. EETs are inactivated by soluble epoxide hydrolase (sEH) via conversion into dihydroxyeicosatrienoic acid (DHET)

Chapter 2

Intracisternal administration of tissue plasminogen activator improves cerebrospinal fluid flow and cortical perfusion after subarachnoid hemorrhage in mice.

2.1 Summary

Early brain injury (EBI) during the first 72 hours after subarachnoid hemorrhage (SAH) is an important determinant of clinical outcome. A hallmark of EBI, global cerebral ischemia, occurs within seconds of SAH and is thought to be related to increased intracranial pressure (ICP). We tested the hypothesis that ICP elevation and cortical hypoperfusion are the result of physical blockade of cerebrospinal fluid (CSF) flow pathways by cisternal microthrombi.

In mice subjected to SAH, we measured cortical blood volume (CBV) using optical imaging, ICP using pressure transducers and patency of CSF flow pathways using intracisternally injected tracer dye. We then assessed the effects of intracisternal injection of recombinant tissue plasminogen activator (tPA).

ICP rose immediately after SAH and remained elevated for 24 hours. This was accompanied by a decrease in CBV and impaired dye movement. Intracisternal administration of tPA immediately after SAH lowered ICP, increased CBV and partially restored CSF flow at 24 hours after SAH. Lowering ICP without tPA, by draining CSF, improved CBV at 1, but not 24 hours. These findings suggest that blockade of CSF flow by microthrombi contributes to the early decline in cortical perfusion in an ICP-dependent and independent manner, and that intracisternal tPA may reduce EBI and improve outcome after SAH.

2.2 Introduction

Cerebrospinal fluid (CSF) resides within the subarachnoid space and plays critical roles in both the regulation of intracranial pressure (ICP) and maintenance of the brain's extracellular environment [109]. Blood leakage into that space, as occurs during subarachnoid hemorrhage (SAH), causes a multitude of complications that contribute to a 50% mortality and even higher morbidity among survivors [8]. These complications are biphasic in nature, with some occurring immediately after ictus and others presenting several days later. The complications occurring within the first 72 hours after SAH are collectively referred to as early brain injury (EBI) [110]. Because early complications are powerful predictors of delayed complications [111]and overall outcome [112], EBI is becoming a major focus of research aimed at improving outcomes of SAH patients.

EBI describes a number of pathological processes, which are likely interrelated and thus are difficult to study in isolation. Broad categories of EBI include blood brain barrier disruption [113], altered metabolic homeostasis [114], cortical spreading depression [115], and neuronal cell death[116,117]. Global cerebral hypoperfusion, which occurs within the first minutes of SAH, is thought to be one of the primary contributors to EBI and is a strong predictor of outcome [112]. Closely associated with hypoperfusion is the rapid elevation of intracranial pressure (ICP) that occurs at the time of hemorrhage [118] and, depending on severity, can remain elevated from hours to days, or even indefinitely [119] following SAH. While elevation of ICP is known to impinge on cerebral perfusion, evidence suggests that hypoperfusion after SAH is multifactorial with both ICP dependent and independent components [120]. A common pathology linking these components has not been established.

CSF moves out of the subarachnoid space and into brain parenchyma alongside penetrating arterioles within the paravascular space [121]. These continuous extensions of the Virchow-Robin space permit movement of CSF through the neuropil and are thought to be integral to extracellular homeostasis. When blood flows out of the vasculature and into these spaces during SAH, the coagulation cascade is initiated, leading to clot formation[122]. This prevents additional bleeding from occurring, but

likely also blocks these CSF flow pathways. Blockade of CSF flow could contribute to the increase in ICP and prevention of normal CSF function. The exact nature of impaired CSF flow within these spaces after SAH and its role in early cortical hypoperfusion is unknown.

The current study was designed to test the hypothesis that early cerebral hypoperfusion is due in part to impaired CSF flow by microthrombi in the subarachnoid and paravascular space and that intra-cisternal administration of tPA restores CSF flow and cortical perfusion in the early phase of SAH. We also sought to determine the relative contribution of ICP to cerebral hypoperfusion.

As a surrogate for tissue perfusion, we used optical microangiography (OMAG), an optical coherence tomography (OCT)-based technique, to quantify blood volume (CBV) in perfused cortical vessels non-invasively through an intact skull [123]. OMAG also allows us to obtain serial measurements of CBV in the same animal over time. The three-dimensional volumetric data produced by OMAG contains blood volume information from actively perfused vessels both on the cortical surface and several hundred microns below the surface and thus is referred to as cortical perfusion. We have previously validated OMAG measurements of perfusion in mouse brain using [^{14}C]-iodoantipyrine autoradiography [106], and have used this approach previously in studies of cerebral ischemia [106] and traumatic brain injury [124].

2.3 Materials and Methods

2.3.1 Animals

Experimental animal procedures performed in this study conform to the guidelines of the US National Institutes of Health, and the animal protocol was approved by the Institutional Animal Care and Use Committee of Oregon Health & Science University, Portland, OR, USA. Mice were housed in a room with a light:dark every 12 hours, and given free access to standard rodent chow and water. Studies were performed on 8 - 12 weeks old wild-type (WT) C57BL/6J male mice obtained from Jackson Laboratories.

2.3.2 Induction of SAH

SAH was induced in mice using the endovascular perforation technique adapted from Sozen et al [125]. Briefly, mice were anesthetized with isoflurane (1.5 to 2% in O_2-enriched air by face mask), and maintained at 37±0.5°C rectal temperature using warm water pads. Two small laser-Doppler probes (Moor Instruments) were affixed bilaterally over the parietal bones to monitor cerebrocortical perfusion and confirm vascular rupture. To induce hemorrhage, a nylon suture (5-0) was introduced into the internal carotid artery via the external carotid artery and advanced ~10mm beyond the carotid bifurcation and into the Circle of Willis. The suture was then advanced slightly further to induce a hemorrhage, and then removed. The common carotid artery was maintained patent at all times to maximize flow to the ruptured artery immediately following arterial perforation. Mortality throughout the study was < 10% and most often occurred immediately following SAH induction. Only mice who survived the initial surgery were included in this study. In sham operated animals, the suture was advanced into the internal carotid artery and then removed without arterial perforation.

2.3.3 Optical Microangiography (OMAG)

To monitor changes in CBV *in vivo*, we used OCT-based OMAG [123]. Briefly, at baseline and after SAH or sham surgery, mice were anesthetized with isoflurane (1.5 to 2% in O2-enriched air by face mask). The skin over the skull was reflected, the cortex illuminated through the skull with a 1,310 nm light source, and the resulting backscattered and reference light detected to produce spectral interferograms. Volumetric imaging data were collected by scanning the probe beam through a 1,000 x 500 x 512-voxel cube, representing 2.5 x 2.5 x 2 mm3 (*x-y-z*) of tissue. After scanning, the skin over the skull was closed and the animal allowed to recover. CBV images within the scanned tissue volume were rendered in 3-D (AMIRA, Visual Imaging GmbH), then thresholded and analyzed for mean pixel intensity changes over time using Image-J software. The 72h time-course study presented in figure 1 is a combination of six scans covering the entire surface of the mouse cortex. Subsequent time sensitive

studies focused on a single scan over the MCA territory ipsilateral to the hemorrhage site.

2.3.4 Experimental manipulation of ICP

Following SAH, mice were mounted on a stereotaxic frame and the skull was exposed. For simultaneous measurement and manipulation of ICP, burr holes were placed bilaterally 0.5 mm rostral to bregma and 1 mm lateral to midline over the lateral ventricles. The dura mater was removed, and custom-made 21-gauge steel guide tubes with dummy cannulas were placed 1.5 mm below the skull and sealed using dental cement and cyanoacrylate glue. One tube served as the experimental cannula for drainage, and the opposite tube served as a port for measurement of ICP using a closed system pressure transducer connected to a pressure monitor (Hewlett Packard). The dummy was removed (0 min time) from the experimental tube in the “open” group and CSF was allowed to drain freely. In the “closed” group, the dummy cannula remained in place. After ICP measurements, the PE catheter was removed from the measurement tube, and the dummy was replaced to prevent further drainage of CSF. The skin was replaced around the cannulas and the animal was allowed to recover. 24 hours following SAH, the animals were again anesthetized, and ICP was measured again. Cannula flow in the open group was assessed at 24h and only animals with freely flowing cannulas at 24h were included in the study. For studies looking at manipulation of ICP and its effect on cortical perfusion, a single tube was placed in the left lateral ventricle as the experimental cannula and the right hemisphere was left untouched for OMAG image acquisition.

2.3.5 CSF flow and hemorrhage assessment

At 30 minutes (figure 4) or 24 hours (figure 5) after SAH or sham surgery, animals were anesthetized using isoflurane (1.5-2%) and placed on a stereotaxic apparatus. Mice received 10 µl of dye (0.4 % Evan’s Blue (Fisher) and 0.1% bovine serum albumin (Fisher) in saline) injected into the cisterna magna at a rate of 2ul/min over 5 minutes. The dye was allowed to circulate for 30 minutes after injection. The animals were then deeply anesthetized and perfused in cold heparinized saline before

the brains were removed and taken for imaging. Images of the ventral surface were obtained using a Nikon digital camera and capture software (ACT-1 Nikon). The images were normalized to background and the red channel or blue channel isolated and thresholded for analysis of blood or dye present in the basal cisterns respectively. Dye movement was used as a surrogate for CSF flow, which was assessed by a blinded investigator in two ways. The first was a categorical 6 point distribution score that described the distribution of tracer over the ventral surface of the brain. To generate the score, the ventral surface image was divided into 6 regions and given a score of 0 for no dye present or 1 for dye present in each region. This was then summed (figure 3B). The second method was a quantification of total pixel area that reached beyond the brainstem (the site of injection and dye pooling) and into the basal cisterns. Blood in the basal cisterns was also quantified by a blinded investigator as total pixel area beyond the brainstem. For immunolabelling of fibrin strand deposition, mice were deeply anesthetized with isoflurane (5%) and transcardialy perfused with cold heparinized saline, followed by 4% paraformaldehyde, and post-fixed overnight. The whole brain was removed and blocked in 4% normal goat serum for 3h at room temperature, then incubated in primary antibody overnight at 4ºC (chicken anti-mouse fibrinogen, 1:200; immunology consultants laboratory). Secondary detection was with Alexa Fluor ® 594 conjugated goat anti-chicken secondary antibody (1:800, Invitrogen) incubated for 3h at room temperature. After washing, whole brains were imaged using a fluorescent dissecting microscope (leica microsystems) equipped with camera and imaging software (LAS EZ, Leica).

2.3.6 Intracisternal Injections of tPA and ICP measurement

Following SAH or sham surgery, animals were mounted on a stereotaxic frame under isoflurane anesthesia (1.5-2%). An incision was made above the occipital bone and the posterior neck musculature was partially reflected to reveal the atlanto-occipital membrane. A custom made 30-gauge cannula connected to PE-10 tubing (B-D) was then inserted into the cisterna magna and affixed to the skull using dental cement (Lang Dental) and cyanoacrylate glue. ICP was assessed through the cannula using a pressure transducer connected to a pressure monitor (Hewlett Packard). After the

monitor was connected, ICP was recorded after 15 minutes of equilibration. Following ICP measurements, 10 µl of CSF was drained out of the cisterna magna to accommodate subsequent infusion of 10 µl solution containing either 15 µg recombinant tissue plasminogen activator (tPA) in sterile water (Cathflo, Alteplase, Genentech), aCSF (containing NaCl 73.05 mg/ml, KCl 1.86 mg/ml, MgCl2-6H2O 2.03 mg/ml, CaCl2-2H2O 2.94 mg/ml, NaH2PO4-H2O 1.73 mg/ml, NaHCO3 21 mg/ml, glucose 4.5 mg/ml) or vehicle (L-arginine 52.5mg/ml, H3PO4 15mg/ml, polysorbate 80 0.17 mg/ml in sterile water). Intracisternal injection was performed using an infusion pump (Harvard Apparatus) at a rate of 2µl/min in 5 minutes. Sham-operated animals also received tPA injections. After injection, the tubing was heat-sealed to prevent backflow, the muscle and skin sutured and the animal allowed to recover 24h. After 24h, this same cannula was used for the final ICP measurement and dye injection.

2.3.7 Statistics

Comparison of CBV and ICP changes between treatment groups and over time was made using a two-way within-between ANOVA. Comparison of CBV and ICP changes over time were made using a one-way repeated measures ANOVA. Comparison of cisternal blood between groups was made using one-way ANOVA. All post-hoc comparisons were made using Bonferroni's correction. Comparison of dye region data between groups was made using a Kruskal-Wallis test with Dunn's post-hoc comparison. All data analysis was performed using Prism 5.0 (Graphpad). Data are expressed as mean ± SEM unless otherwise noted. Statistical significance was set at $p < 0.05$.

2.4 Results

2.4.1 Blood distribution in the endovascular perforation model

By perfusing the mice with saline immediately after the hemorrhage, we were able to observe where extravasated blood from the endovascular puncture model distributes immediately following induction of the hemorrhage. Within 30 minutes of the

endovascular puncture, blood has moved into the basal cistern and along paravascular spaces on the outside of the Middle Cerebral artery (MCA) (figure 5a). We confirmed induction of the hemorrhage using CBF measured by laser-Doppler probes placed against the skull over the MCA territory during the surgery. We found that at the time of the hemorrhage, an abrupt drop in CBF occurs bilaterally and slowly returns to ~65-75% of baseline by ten minutes. The contralateral side experiences a less severe drop than the ipsilateral side to the hemorrhage ($P<0.05$ at 1-8 minutes, $n = 31$) but CBF values ultimately converge by the end of the ten minute period (figure 5b).

2.4.2 Cortical perfusion is impaired following subarachnoid hemorrhage

To study changes in cortical perfusion over days after SAH, we scanned a large area of the cortical surface using OMAG (larger box in figure 6a) at baseline before animals were subjected to SAH or sham surgery. Following a 6-hour recovery period, animals were rescanned at 6, 12, 24 and 72 hours following SAH. Cortical perfusion was decreased compared to sham animals at 6h (figure 6b, 73.0 ± 3.3% vs 99.3 ± 2.1%, n = 5 for sham and 10 for SAH), 12h (79.1 ± 3.1% vs 103.4 ± 2.2%), 24h (80.0 ± 2.5% vs 102.2 ± 1.4%) and 72h (87.8 ± 3.3% vs 102.1 ± 3.0%) after SAH. Cortical perfusion was reduced bilaterally across middle cerebral and anterior cerebral flow territories indicating the effect was global (figure 6c). Further studies using OMAG were limited to the scan area indicated by the smaller box in figure 6a.

2.4.3 Cortical perfusion deficits are due in part to elevated ICP

There is evidence to suggest that early hypoperfusion following SAH is independent of ICP [126]. To test whether ICP contributes to the hypoperfusion seen in our model, we developed single- and double-cannula methods for measuring CBV and ICP respectively before and after ventricular drainage. At the 1h time point following SAH induction, we measured ICP in one lateral ventricle and drained CSF out of the other. ICP immediately decreased when the cannula was opened and CSF allowed to drain (from 34.8 ± 1.36 to 25.4 ± 1.8 mmHg, n = 5, figure 7b). In another group of animals, CSF was drained from one cannula while OMAG scans were performed over the MCA territory on the opposing side without a cannula. Figure 7c shows that CBV

was also increased from 45.7 ± 4.9% to 66.0 ± 7.1% of baseline (n =5) when the cannula was opened and CSF was allowed to drain. This finding suggests that the decrease in CBV present 1h after SAH is at least in part due to increased ICP.

2.4.4 CSF flow is impaired immediately following SAH

Impaired CSF flow is a likely cause of increased ICP, so we sought to determine whether CSF flow is impaired immediately following SAH. 30 minutes after SAH induction, we assessed CSF flow by tracking tracer dye injected into the cisterna magna. In sham operated mice, the tracer dye moves into the basal cistern and out along paravascular routes alongside the MCA (figure 8 a, b). In the SAH mice, tracer dye pools around the brainstem and does not enter into the basal cistern or paravascular spaces which are occupied by blood (figure 8 a, b). The third most abundant protein in the plasma is fibrinogen, which is rapidly converted into insoluble fibrin strands upon extravasation. To determine if paravascular fibrin deposition takes place after SAH, we fixed whole brains 30 minutes after SAH and labeled the surface using a fibrinogen antibody. Labeling shows fibrin strand deposition in the paravascular spaces of the MCA (figure 8c). This finding suggests that CSF flow is blocked immediately following SAH, and that fibrin deposition is occurring in the paravascular space.

2.4.5 tPA partially restores CSF flow pathways blocked by subarachnoid thrombi

To determine if CSF movement was impeded by microthrombi obstructing CSF flow pathways, we examined the effect of intracisternally injected tPA on tracer dye movement 24h after SAH or sham surgery. 1h after SAH, mice received an injection of 10 µl of either aCSF or 1.5 mg/ml tPA into the cisterna magna. Sham-operated mice also received tPA to rule out effects of tPA unrelated to SAH. The mice were recovered until 24h later, when all mice received injections of tracer dye into the cisterna magna (figure 9a). Movement of dye was assessed semi-quantitatively by subdividing the ventral surface into six regions and assigning a value of 1 or 0 for the presence or absence of dye in any given region (figure 9b). In sham-operated mice, the dye moved freely from the cisterna magna into the basal cisterns and out along major paravascular

routes (figure 9c, n=3 with all three animals scoring 6, suggesting free dye movement and presence of the dye in all regions). In aCSF-injected SAH mice, the tracer dye pooled around the brainstem and did not enter into the basal cisterns or along paravascular routes, resulting in dye absence from most areas and a median score of 1, suggesting restricted dye movement (figure 9c, n = 10). Finally, SAH mice injected with tPA showed partial restoration of dye movement into the basal cisterns and out along paravascular routes, resulting in a median score of 3 (figure 9c, n = 10). This observation suggests that CSF flow impairment after SAH is in part due to clot formation, which can be partially reversed with tPA.

2.4.6 tPA reduces ICP and improves cortical perfusion after SAH

Because impaired CSF flow may increase ICP, which decreases cortical perfusion, we determined if intracisternal tPA, which improves CSF flow dynamics, can also decrease ICP and increase cortical perfusion after SAH. We used OMAG to measure perfused CBV over the MCA territory at baseline and at 1 hour after SAH (before tPA injection). Mice were then injected with tPA, and survived for 24h, when CBV was measured again before sacrifice (figure 10a). ICP was measured using a cannula inserted prior to injection at 1h after SAH, and the measurement repeated at 24h after SAH. Prior to treatment (1 h after SAH), both tPA and aCSF groups had similarly elevated ICP (figure 10b, 28.7 ± 3.2 and 28.5 ± 4.8 mmHg in aCSF (n=5) and tPA (n=6) groups, respectively). Both groups also had equally decreased CBV (figure 10c, 35.0 ± 5% in aCSF (n=5) and 32.2 ± 5% in tPA group (n=6)) at 1h after SAH prior to treatment. 24h after SAH, tPA-treated animals had significantly higher CBV than aCSF-treated mice (figure 10c, 80.0 ± 4.7% (n=6) vs. 51.7 ± 9%, n = 5, respectively). Mice treated with tPA also had lower ICP than aCSF-treated mice (figure 10b, 17.5 ± 3.0 (n=6) vs. 34.8 ± 3.7 mmHg n = 5, respectively). Because L-arginine is required for stability of tPA in solution, and may serve as a precursor for nitric oxide synthesis and subsequent vasodilation, we included an additional vehicle group containing the equivalent dosage of l-arginine. We found no differences in CBV between this vehicle group or the aCSF group 24h after SAH (figure 10c (n = 4)). We additionally measured ICP in 3 vehicle treated animals and found no difference from aCSF treated animals

24h after SAH. There was no effect of tPA injections alone on ICP or CBV in sham-operated mice (figure 10b, c).

2.4.7 Management of ICP alone does not improve cortical perfusion at 24h

Since there are other functions of CSF besides ICP regulation [109], and there is evidence of ICP independent contributors to impaired cortical hypoperfusion, we asked the question of whether the ICP reduction by tPA was sufficient in itself to explain the improvement in cortical perfusion at 24h. To answer this question, we extended the time of CSF drainage through the ventricular cannula to the 24h time point. We first measured ICP before CSF drainage, then immediately after, and again at 24h after opening the cannula. As a control, we included a group with an inserted cannula that was kept closed. Prior to cannula manipulation, both “open cannula” and “closed cannula” groups had similarly elevated ICP (figure 11b, 37.3 ± 3.0 vs. 37.0 ± 2.3 mmHg in open vs. closed groups, respectively, n = 4 per group). Both groups also had similar reductions in perfused CBV after SAH (figure 11c, 34.2 ± 4.2% in open- (n=8) vs. 28.3 ± 3.3% in closed-cannula (n=6) groups). Consistent with figure 3 above, immediately after cannula manipulation, ICP was decreased (from 37.3 ± 2.4 to 26.2 ± 1.9 mmHg, n = 4, figure 11b) and CBV over the MCA territory was increased (from 31.5 ± 4% (n=8) to 49.6 ± 5.5% (n=8) of baseline, figure 11c) in the open- compared to the closed-cannula group. Interestingly, at 24h after SAH, while ICP remained lower in the open compared to the closed group (13.5 ± 4.3 vs. 26 ± 1 mmHg, n =4 figure11b), there was no significant difference in CBV between the open- and closed-cannula groups (96.1 ± 7.1% (n=8) vs. 79 ±2.1% (n = 6, figure 11c). This observation suggests that the improvement in cortical perfusion by tPA treatment is only partly due to reduced ICP, and that improved CSF flow contributes to cortical perfusion improvement by an additional mechanism unrelated to ICP.

2.6 Discussion

2.6.1 Review of findings

In the current study, we demonstrated that SAH in the mouse induces rapid and sustained decrease in cortical perfusion, associated with increased ICP and impaired CSF dynamics. Furthermore, intra-cisternal injection of tPA reduced ICP and restored CSF flow and cortical perfusion. However, when we drained CSF through a ventricular cannula to decrease ICP without tPA treatment, we were able to improve perfusion at 1h, but not 24h after SAH. These findings suggest that the early decrease in cortical perfusion after SAH is in part due to impaired CSF flow by blood clots, and that intracisternal administration of tPA improves CSF flow and cortical perfusion which cannot fully be explained by decreased ICP.

2.6.2 Relationship between ICP and CBV

In our model, elevated ICP is an important contributor to early hypoperfusion within the first hours of SAH, but our results suggest that this role diminishes over 24h. Despite that finding, restoration of CSF flow with tPA can improve cortical perfusion 24h after SAH in a manner that must be separate or additive to its effect on ICP. The mechanism by which restoration of CSF flow can improve cortical perfusion remains to be determined, especially given that the consequences of impaired CSF function, aside from elevated ICP, are unknown.

2.6.3 Impaired CSF flow and early brain injury

The brain parenchyma lacks a traditional lymphatic system for the clearance of interstitial solutes. It has been long suggested that the CSF system serves that role by clearing interstitial fluid by bulk flow along preferential pathways, especially paravascular spaces and axon tracts[127]. More recently, a specific paravascular pathway has been described in detail[121]. Once CSF is produced in the choroid plexus, it moves from within the ventricles through the cisterns and out over the surface of the brain along peri-arterial pathways [128]. CSF then penetrates brain parenchymal tissue via a continuous extension of the Virchow-Robin space along the penetrating arterioles known as the paravascular space [121]. Once it passes through the parenchyma and equilibrates with the extracellular space, CSF then drains from the cranium through three known pathways [109]: 1) the cervical lymphatic pathway, 2) the arachnoid

granulations, and finally 3) across postcapillary venules in the paravascular space. If we make the assumption that these flow pathways must be patent for the proper maintenance of extracellular homeostasis by CSF, we can infer from our findings in this study that this function is also impaired following SAH. Clinical and animal studies that have shown a build-up of metabolic waste products, decreased available glucose, and altered ionic concentrations [114,120,129] – all hallmarks of EBI – support this idea. We also cannot ignore that a functional and patent CSF system is likely critical to the clearance of toxic blood products from the initial hemorrhage itself. Any or all of these perturbations of normal physiology could contribute to the early ICP-independent vascular dysfunction that is documented in both animal[118] and clinical studies [126,129]. Further, as we gain a better understanding of the importance of CSF function, coupled with our finding that blockade of CSF flow occurs within minutes of an SAH, we are obliged to examine how disruption of normal CSF function could contribute to the wide range of pathologies collectively referred to as EBI[110].

2.6.4 Previous work studying thrombolytic therapy after SAH

Both thrombolytic and anti-thrombolytic drugs are still actively being studied for treatment of SAH. While these would seem to be contradictory, there is rationale and evidence for both. Specifically, intrathecal thrombolytic therapy has been shown to reduce delayed vasospasm in dogs[130], non-human primates[131-133] and rabbits[134,135]. However, these studies did not examine the effect of tPA on early injury after SAH, and did not link the beneficial effect of tPA to CSF dynamics. Other studies showed improved CSF flow after SAH in cats by tPA, but did not link these changes to early changes in cortical perfusion [91,136]. In clinical studies, intrathecal thrombolysis has been shown to improve outcome and reduce the need for shunt placement [137-142]. In contrast to tPA, anti-thrombolytic therapy has been shown to increase the incidence of cerebral ischemia and worsen outcome after SAH[143]. More recent work suggests that anti-thrombolytic in the ultra-early stage of SAH may be beneficial in preventing re-bleeding[144], yet detrimental in the later stages when clot clearance and restoration of CSF flow become more important [145]. Together, these

studies are consistent with our findings in support of a beneficial role for disrupting subarachnoid thrombi and improving CSF flow in the early stages following SAH.

2.6.5 Risk of aneurysmal re-rupture after thrombolytic therapy

The intended scope of this study is limited to improving our understanding of mechanisms behind early cortical hypoperfusion and impaired CSF flow in the early stages of SAH. Nevertheless, we will consider the implications of an early intervention involving a thrombolytic agent. The most dangerous perceived complication of intrathecal thrombolytic therapy after SAH is secondary bleeding, which, even without thrombolytic therapy, is a major cause of death after SAH [8]. However, our understanding of the physical forces that affect the action of thrombolytic agents do not support the idea that intrathecal tPA would cause substantial clot lysis at the aneurysm site, in contrast to intravenous administration which is strongly contraindicated in SAH. This is due to the effect of pressure driven permeation, where the pressure gradient across the clot is the major determinant of the rate at which clot lysis occurs [146]. Intravenously, tPA is most effective in the arterial circulation where the pressure gradient across a given clot is high, and much less effective for venous thrombi where low pressure gradients exist [147]. At the site of an aneurysm clot, the pressure gradient is in the completely opposite direction to support pressure driven permeation of tPA from the subarachnoid space and would substantially impair the rate of clot lysis. This idea is supported by clinical evidence, which to date have found no increase in the incidence of aneurysm re-rupture following thrombolytic therapy [137,139,141]. Experiments designed to address the question of whether substantial clot lysis can occur at the aneurysm site from intrathecal tPA administration are warranted.

2.6.6 Conclusion

Blood clots within the subarachnoid space impair CSF flow, which contributes to increased ICP and impaired cortical perfusion during the early phase (24 hours) after SAH. Intracisternal tPA administration immediately after SAH partially restores CSF flow, reduces ICP and improves cortical perfusion. Improvement of CSF flow dynamics may serve as an important therapeutic target for SAH.

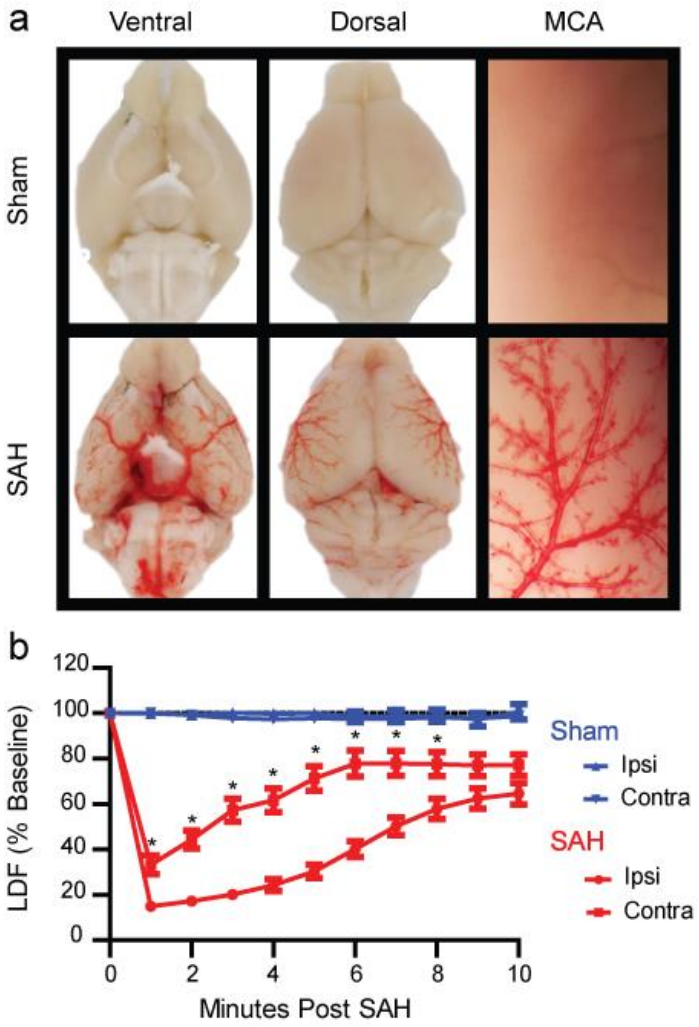

Figure 5. Validation of endovascular puncture model. a.) Mouse brains were perfused with heparinized saline to clear any intravascular blood and imaged 30 minutes after endovascular puncture. SAH mice show a wide distribution of extravasated blood throughout ventral (lower left) and dorsal (lower middle) brain surfaces. The magnified image of a perfused MCA (lower right) shows movement of extravasated blood along the paravascular pathway. b.) CBF measured by laser Doppler in both the ipsilateral (ipsi) and contralateral (contra) MCA territories of sham (blue) and SAH (red) mice. SAH mice (n = 31) experience a rapid drop in CBF following puncture. Contralateral CBF recovers more rapidly than ipsilateral CBF but both reach 65-75% of baseline by 10 minutes (* = $p < 0.05$ contralateral different from ipsilateral)

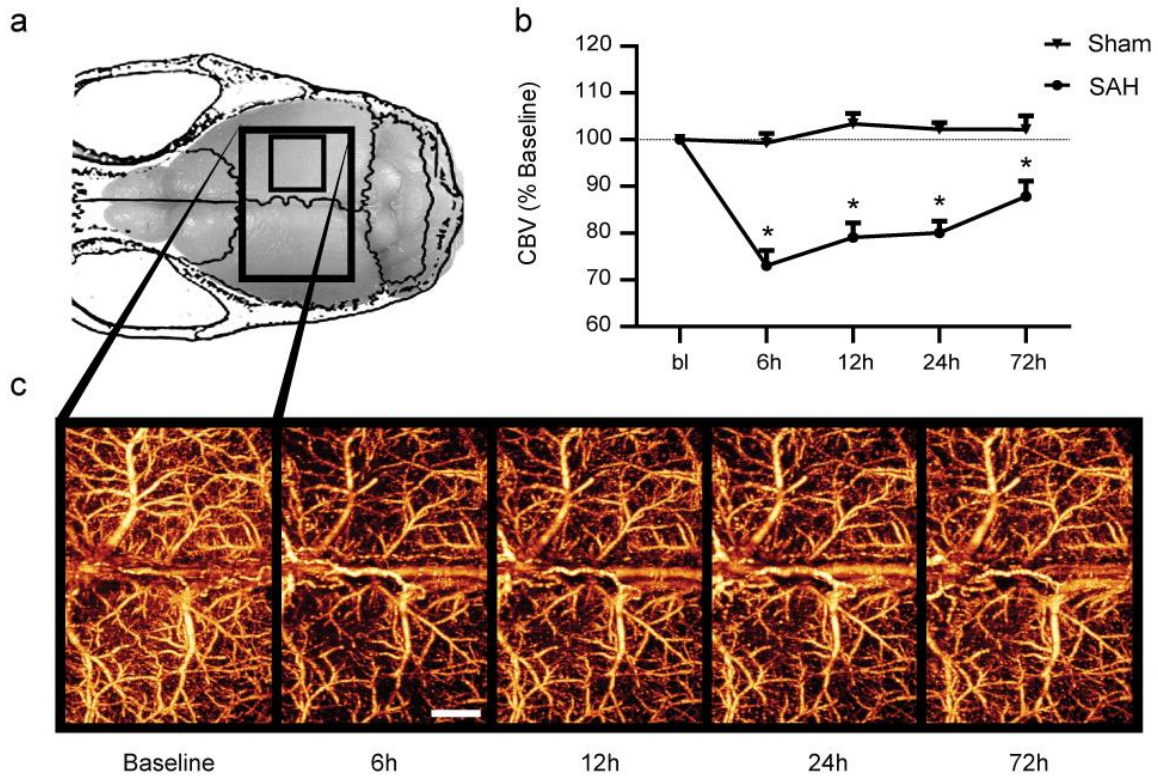

Figure. 6 Cortical perfusion is impaired globally early after SAH. a.) Changes in perfused CBV were tracked in mice for several days following SAH or sham surgery using OMAG. The scan area of the dorsal cortex was 5 mm X 7.5 mm (large box). The smaller box indicates the scan area for all subsequent studies. b.) Cortical perfusion was reduced in SAH animals as early as 6 hours after SAH and persisting for at least 72 hours. c.) Representative OMAG images of SAH mouse showing changes in perfused CBV over time. Decreased intensity corresponds to a reduction in perfused CBV. Values are mean ± sem. SAH (n = 10), sham (n = 5), * P<0.01. scale bar = 1 mm

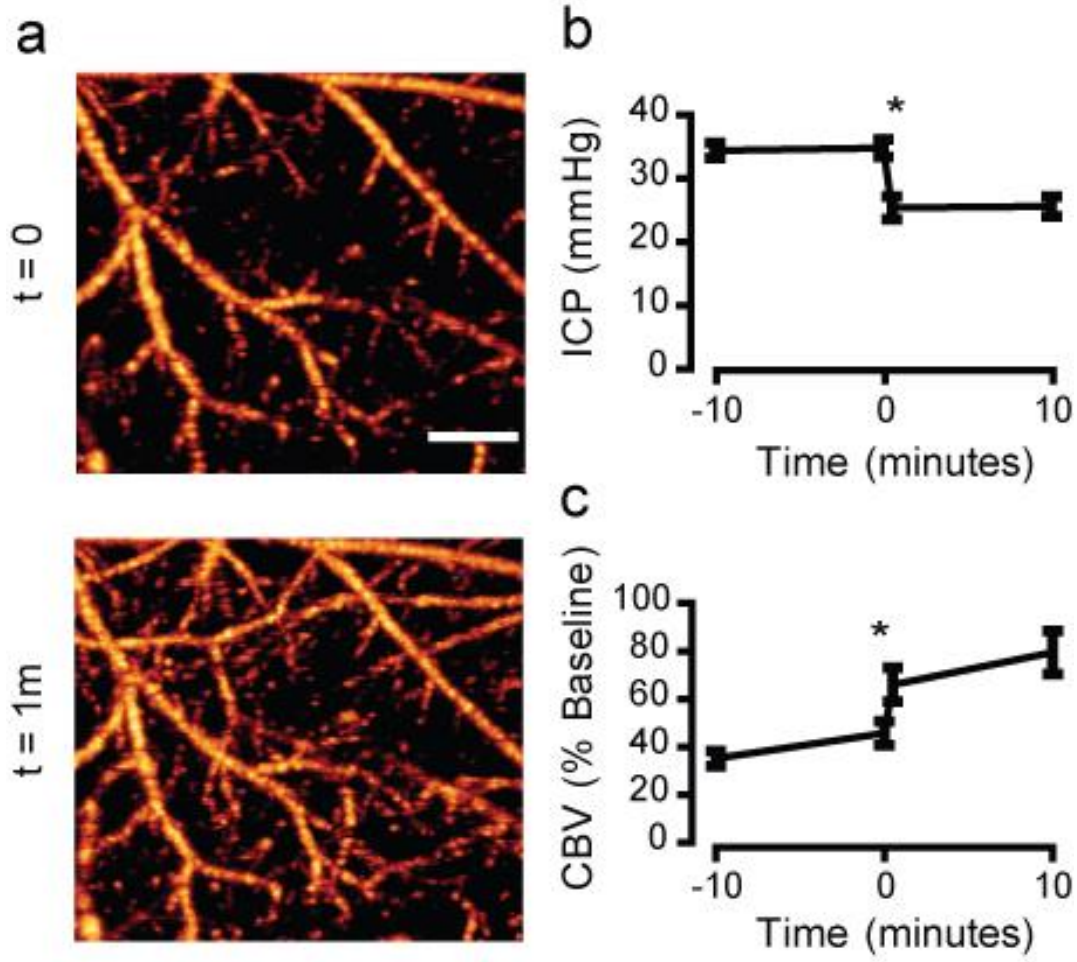

Figure. 7 Elevated ICP contributes to the early decrease in cortical perfusion after SAH a.) Representative OMAG scans of the cortex within the MCA territory 1h after SAH. A ventricular cannula was placed on the contralateral side and opened to drain CSF, leading to an immediate improvement of cortical perfusion. b.) ICP measurements 1h post SAH. Cannula was opened to allow CSF drainage at time = 0. n = 5, * = P <0.05. C.) Quantification of perfused CBV 1h post SAH. Cannula was opened at time = 0. n = 5, * P <0.05 . scale bar = 500 um

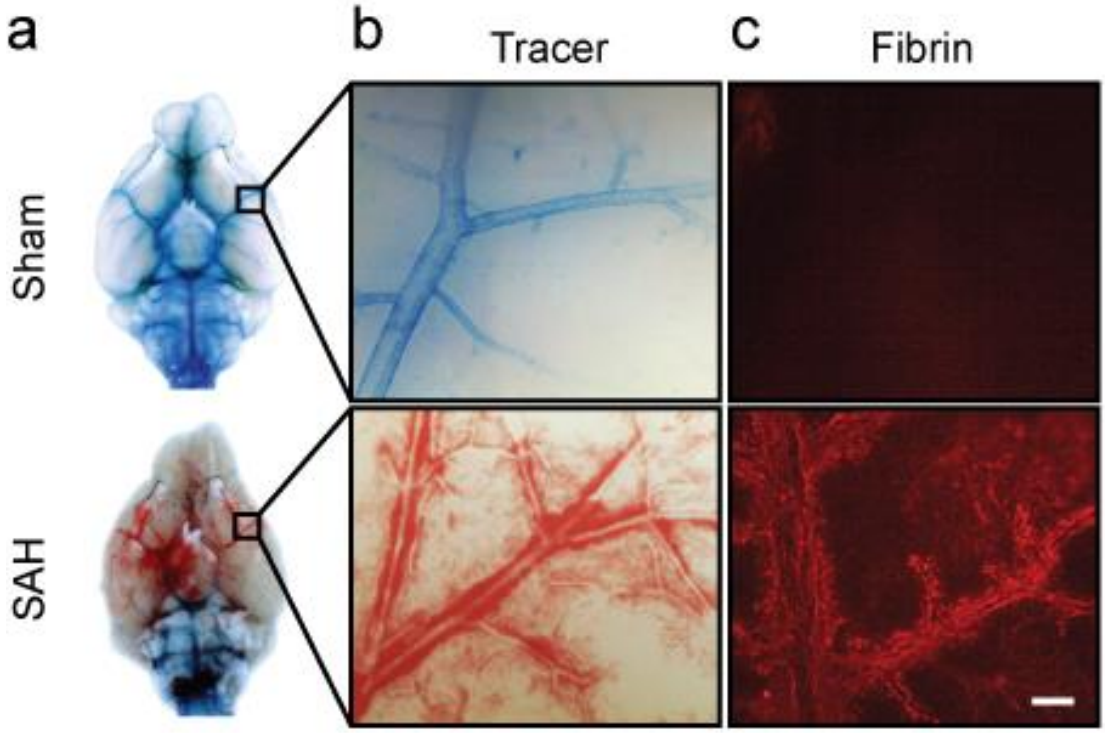

Figure. 8 CSF flow is blocked immediately following SAH a.) Images were taken of the ventral surface of the perfused mouse brain 1h after SAH or sham surgery and 30 minutes after intracisternal tracer dye injection. In sham mice, tracer dye distributes throughout the basal cistern and paravascular routes. In SAH mice, tracer dye pools around the brainstem and does not enter paravascular routes. b.) High magnification images of MCA branches showing tracer dye movement into paravascular spaces. In sham animals, tracer dye moves along MCA branches and out to penetrating vessels. In SAH animals this space is occupied by blood and no tracer dye is present. c.) Fibrinogen staining showing fibrin strand formation in paravascular spaces following SAH but not sham surgery. Scale bar = 100um

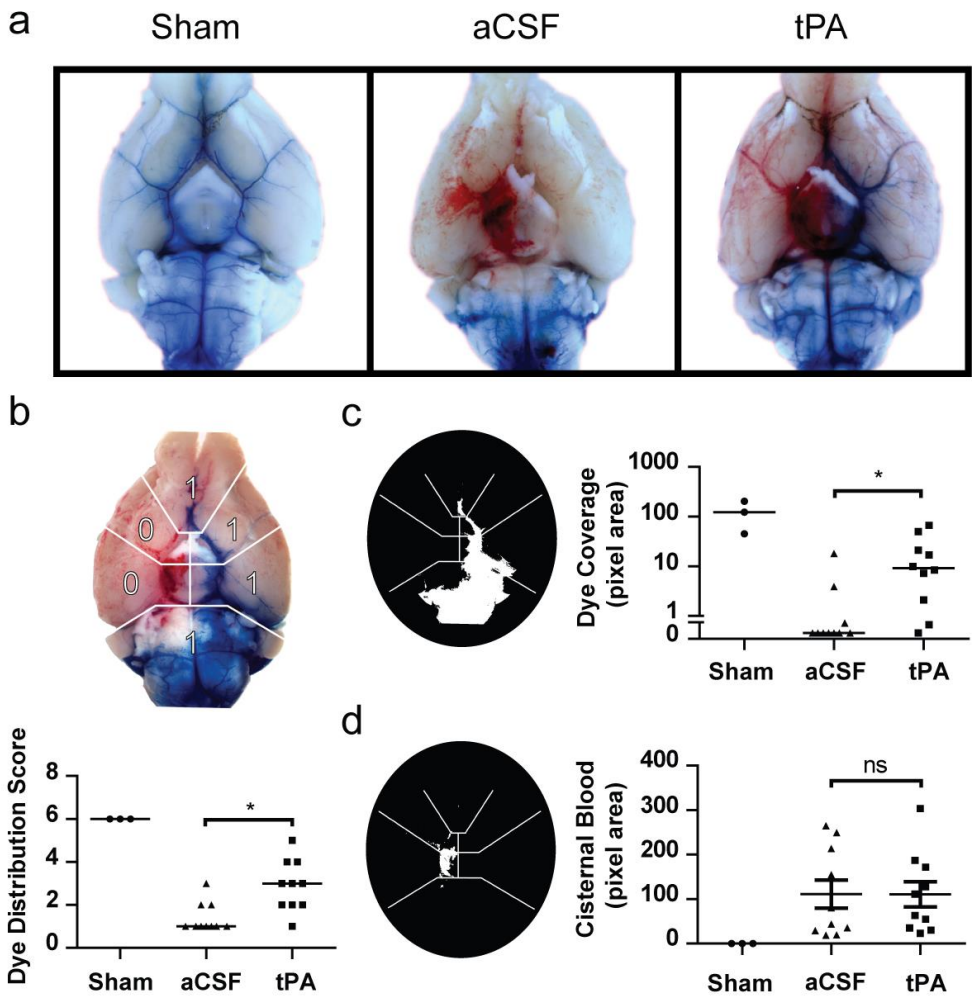

Figure. 9 Intracisternal tPA can restore CSF flow within 24h a.) Images were taken of the ventral surface of the perfused mouse brain 24h after SAH or sham surgery and 30 minutes after intracisternal dye injection. Dye moves freely in sham animals but not aCSF treated SAH animals. Intracisternally injected tPA 1h after SAH partially restores CSF flow to the basal cistern and paravascular routes by 24h. b.)To assess effect of tPA dye movement within the basal cisterns, the blue channel was isolated and thresholded for categorical quantification of dye distribution over the ventral surface of the brain and c.) quantification of pixel area coverage of dye beyond the brainstem. Data are expressed as medians. d.) To assess the effect of tPA on hemorrhage size, the red channel was isolated and thresholded for quantification of pixel area of blood beyond the brainstem. Sham (n = 3), SAH aCSF (n = 10)SAH tPA (n = 10) * = P<0.05

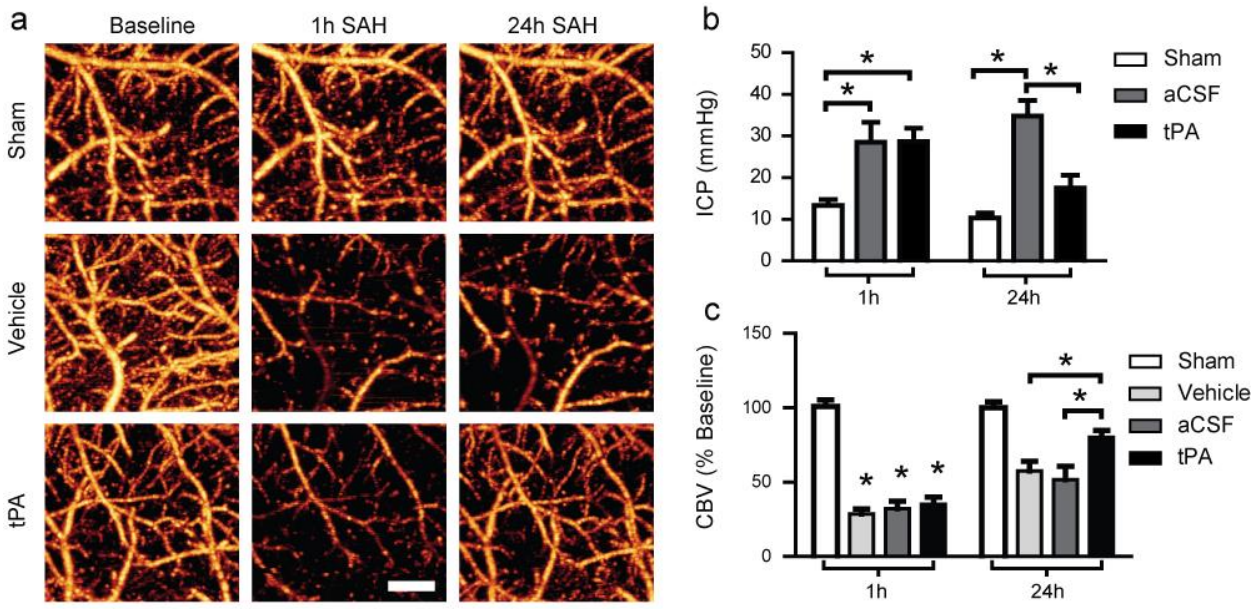

Figure.10 tPA reduces ICP and improves cortical perfusion 24 hours after SAH. a.) Representative OMAG images of the cortex within the MCA territory at baseline, 1h post SAH/sham (pre-treatment), and 24h post-SAH/Sham (post-treatment). b.) ICP measured at the cisterna magna 1h post SAH/sham (pre-treatment) and 24h post SAH/sham (post-treatment). Intracisternal tPA reduced ICP 24h after SAH compared to aCSF treated mice. c.) Quantification of perfused CBV 1h post SAH/Sham (pre-treatment) and 24h post SAH (post-treatment). Intracisternal tPA increased perfused CBV compared to aCSF or vehicle treated mice. Sham (n =3), SAH aCSF (n =5), SAH vehicle (n=4) SAH tPA (n = 6) * = P <0.05. Scale bar = 500 um

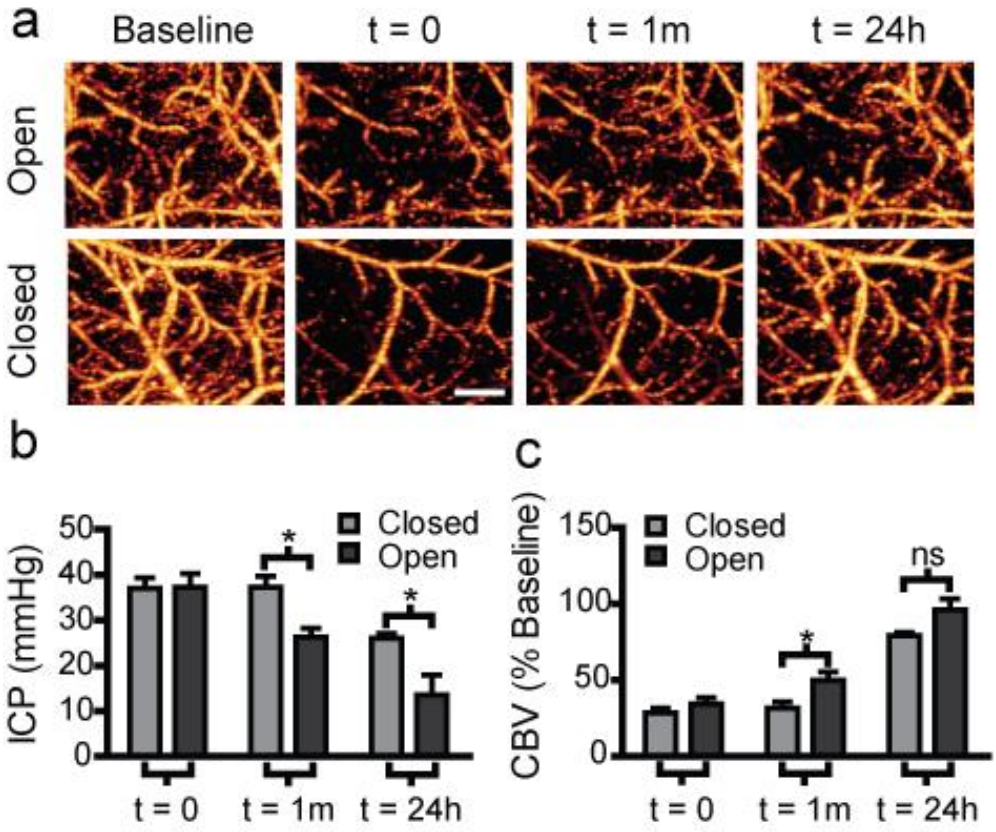

Figure. 11 CSF drainage without tPA does not improve cortical perfusion at 24h a.) Representative OMAG images showing changes in perfused CBV. A ventricular cannula was placed on the contralateral side and opened 1h after SAH then allowed to drain for 24h. Scans were taken at baseline, 1h post-SAH before cannula manipulation (time = 0), immediately after cannula manipulation (time = 1m), and 24h later (time = 24h). b.) Quantification of ICP 1h post-SAH before cannula manipulation (time = 0), immediately after cannula manipulation (time = 1m), and 24h later (time = 24h). Open cannula reduced ICP at both the 1h and 24h timepoints after SAH. Closed (n =4) Open (n = 4), * = P<0.05. c.) Quantification of perfused CBV changes expressed as percent of baseline. Open cannula increased perfused CBV over closed group at 1h but not 24h after SAH. Closed (n = 6), Open (n = 8), * = P< 0.05, ns = no significance. scale bar = 500 um

Chapter 3

Protective Role of P450 Epoxyeicosanoids in Subarachnoid Hemorrhage

3.1 Summary

Background: Patients recovering from aneurysmal subarachnoid hemorrhage (SAH) are at risk for developing delayed cerebral ischemia (DCI). Experimental and human studies implicate the vasoconstrictor P450 eicosanoid 20-hydroxyeicosatetraenoic acid (20-HETE) in the pathogenesis of DCI. To date, no studies have evaluated the role of vasodilator epoxyeicosatrienoic acids (EETs) in DCI.

Methods Using mass spectrometry, we measured P450 eicosanoids in cerebrospinal fluid (CSF) from 34 SAH patients from 1 to 14 days after admission. CSF eicosanoid levels were compared in patients who experienced DCI versus those who did not. We then studied the effect of EETs in a model of SAH using mice lacking the enzyme soluble epoxide hydrolase, which catabolizes EETs into their inactive diol. To assess changes in vessel morphology and cortical perfusion in the mouse brain we used optical microangiography, a non-invasive coherence based imaging technique.

Results Along with increases in 20-HETE, we found that CSF levels of 14,15-EET were elevated in SAH patients compared to control CSF, and levels were significantly higher in patients who experienced DCI compared to those who did not. Mice lacking sEH had elevated 14,15-EET and were protected from the delayed decrease in microvascular cortical perfusion after SAH, compared to wild type mice.

Conclusions Our findings suggest that P450 eicosanoids play an important role in the pathogenesis of DCI. While 20-HETE may contribute to the development of DCI, 14,15-EET may afford protection against DCI. Strategies to enhance 14,15-EET, including sEH inhibition, should be considered as part of a comprehensive approach to preventing DCI.

3.2 Introduction

An estimated 33,000 patients suffer from aneurysmal subarachnoid hemorrhage (SAH) in the US annually, which has a mortality rate of 20-40% and a very high rate of disability among survivors [4,5], primarily attributed to delayed cerebral ischemia (DCI). DCI occurs in 30% of survivors [11], usually between 3 and 14 days after the initial hemorrhage [12]. Current monitoring and treatment strategies require prolonged intensive care unit stays, at high institutional and patient cost. There are few known risk factors, no reliable predictive test, and few preventative treatments for the development of DCI.

The best characterized pathological feature associated with DCI is severe constriction of cerebral arteries, or vasospasm, which leads to hypoperfusion and ischemia in dependent brain regions [12]. These constrictions occur at several places along the vascular tree, from large conduit arteries, which are easily detectable by angiography, down to the smallest penetrating arterioles detectable only by perfusion computed tomography [148]. Different vasoactive molecular mediators exert varying levels of influence on vessel tone along the branches of the vascular tree [39]. While large vessel vasospasm has been largely attributed to alterations in endothelin-1 and nitric oxide signaling [149], less is understood about microvascular vasospasm despite its significant contribution to DCI [150].

Cytochrome P450 eicosanoids are produced by microvascular endothelium and astrocytes [95]. These lipid effector molecules were first implicated in DCI with the discovery of elevated CSF levels of 20-hydroxyeicosatetraenoic acid (20-HETE) in human SAH patients [151] and in animal models of SAH [152]. It is not known if other P450 eicosanoids with vasodilator properties play a potentially opposing role in SAH. Namely, 14,15-epoxyeicosatrienoic acids (14,15-EET) has been shown to preferentially dilate cerebral microvessels [96] and act as a neuroprotectant in models of cerebral ischemia [153]. Levels of 14,15-EET in brain are regulated by their synthesis via cytochrome P450 epoxygenases in endothelium and astrocytes [154], and their metabolism primarily by the enzyme soluble epoxide hydrolase (sEH) [95].

To investigate if 14,15-EET is altered after SAH in humans, we sampled the CSF in a cohort of SAH patients at high risk for DCI, whose neurologic status on admission necessitated the placement of an external ventricular drain. Along with the already documented increase in 20-HETE we also found that 14,15-EET is elevated in SAH patients compared to non-hemorrhage controls. Patients with the highest levels of both eicosanoids were more likely to go on to experience DCI. To determine if increased 14,15-EET plays a protective role against the development of vasospasm after SAH, we subjected mice with genetic deletion of sEH, which has higher 14,15-EET, to experimental SAH and found that these mice were protected from the decrease in microvascular perfusion after SAH compared to WT mice.

3.3 Methods

3.3.1 Approval statement.

The clinical study was approved by the Institutional Review Board, and informed consent was obtained. All experimental animal procedures performed in this study conform to the guidelines of the US National Institutes of Health. The laboratory animal protocols were approved by the Animal Care and Use Committee of Oregon Health & Science University (Portland, OR, USA).

3.3.2 Patient population.

Adult patients with aneurysmal subarachnoid hemorrhage confirmed with digital subtraction cerebral angiography between December 1, 2008 and August 1, 2013 were recruited from the Neurosciences Intensive Care Unit at Oregon Health & Science University (OHSU) – a stroke referral center in Portland, OR. All patients had ventriculostomies placed for hydrocephalus.

3.3.3 Clinical Data and Outcomes.

Baseline demographic and physiologic data were collected from electronic medical records. Hunt Hess grade, modified fisher score and aneurysm location were collected from the admission history and physical and based on first CT scan or angiogram. Development of delayed cerebral ischemia (DCI) was also determined using patient records including clinical notes, laboratory data, and imaging studies. The primary outcomes of interest were the development of DCI and mortality. We defined DCI as an acute decline in neurologic status documented by a decrease in Glasgow coma scale of at least 2 points, depressed level of consciousness or new focal neurologic sign lasting at least 1 hour, and not explained by other disease processes such as hydrocephalus, electrolyte abnormalities or infection, that was concomitant with evidence of vasospasm by cerebral angiography or transcranial Doppler. The secondary outcome measured was patient disposition. We dichotomized disposition into those who went home (either to live independently or with assistance) and those who were discharged to rehabilitation centers, skilled nursing facilities, or who died.

3.3.4 CSF

3.3.4.1 Collection and Processing

Cerebrospinal fluid (CSF) was obtained at intervals while the ventriculostomy was in place. CSF was obtained on day 1, and every other day after that up to day 14. The number of samples collected from each patient ranged from 1-7 depending on the availability of CSF with a median of 3 samples collected per patient. Samples were sorted into two-day bins with n = 22, 23, 23, 13, 19, 13, 8 for days 1-2, 3-4, 5-6, 7-8, 9-10, 11-12, and 13-14 respectively. Sample numbers were higher at earlier time-points because this is when ventricular drains were most likely to still be in place. A volume of 3 mL of CSF was collected directly from the ventricle using standard sterile procedure, placed immediately on ice and spun in a chilled centrifuge at 10,000 RPM for 10 minutes. The supernatant was collected and 15 µl of 1% butylated hydroxytoluene was added as an anti-oxidant agent to prevent EETs oxidation. Samples were stored at -80° C until analyzed by LC-MS/MS.

3.3.4.2 Control CSF

CSF samples from healthy age and sex matched controls (n = 10) were obtained from the Oregon Alzheimer Center and were collected as part of an unrelated aging study [155]. Participants in this study had no clinically significant pathologies. Specifically, patients were excluded from the study if they had a history of stroke, TIA, myocardial infarction, diabetes, or a body mass index ≥30. Additionally, the participants had no evidence or history of cognitive dysfunction and a mini mental status score of ≥ 26. CSF was collected via lumbar puncture, flash frozen and stored at -80º C until analyzed by LC-MS/MS.

3.3.4.2 Preparation of Samples and Calibrators.

CSF sample preparation was a slight modification of Poloyac et al. [151]. CSF samples were thawed on ice, 10 µl of 10 mg/ml butylated hydroxytoluene (BHT) was added to each sample along with internal standard mix consisting of 1 ng of each of the following, d_8-15 HETE, d_6-20 HETE, d_8 14,15 EET, and d_{11}-14,15 DHET. The samples were vortex mixed briefly and then spun at 2000xg for 5 minutes to pellet any solid debris. The samples were gravity loaded onto Oasis HLB 30 mg solid phase extraction (SPE) cartridges which had been pre-equilibrated with 1 ml of methanol, followed by 1 ml of water. Following loading the SPE were washed with 3 mls of 5% methanol. SPE were then dried for 15 minutes at maximum house vacuum of 5-15 Hg before being eluted with 3 mL of methanol. A brief application of vacuum finished the elution, and then the samples were dried under vacuum at for 1 hour 20 minutes at 35°C. The tube walls were washed with 1 ml of hexane, immediately re-dried and then brought up in 50 µl of start solvent which consisted of 45:55 (vol:vol) acetonitrile:water with 0.2 mg/ml triphenylphosphine (TPP), 0.01% BHT and 0.01% formic acid and placed in sample vials with inserts and analyzed by LC-MS/MS. The injection volume was 20 µl. An un-extracted standard curve was used for the majority of the studies after an initial experiment comparing spiked CSF to un-extracted samples showed similar values. Area ratios were plotted and unknown determined using the slopes. U-extracted standard curves were always prepared and compared to a spiked CSF sample because of the difficulty of obtaining blank CSF in sufficient volumes to prepare full standard curves.

3.3.4.3 LC-MS/MS Analysis of Eicosanoid Metabolites.

DHETs, HETEs and EETs levels were analyzed using a 5500 Q-TRAP hybrid/triple quadrupole linear ion trap mass spectrometer (Applied Biosystems) with electrospray ionization (ESI) in negative mode as described previously [156]. The mass spectrometer was interfaced to a Shimadzu (Columbia, MD) SIL-20AC XR auto-sampler followed by 2 LC-20AD XR LC pumps and analysis on an Applied Biosystems/SCIEX Q5500 instrument (Foster City, CA). The instrument was operated with the following settings: source voltage -4000 kV, GS1 40, GS2 40, CUR 35, TEM 450 and CAD gas HIGH. The scheduled MRM transitions monitored with a 1.5 minutes window are presented in Table 1. Compounds were infused individually and instrument parameters optimized for each MRM transition. The gradient mobile phase was delivered at a flow rate of 0.5 ml per min, and consisted of two solvents, A: 0.05% acetic acid in water and B: acetonitrile. Initial concentration of solvent B was 45%, this was held for 0.1 minutes before being increased to 60% over 5 minutes, then increased to 61.5% over 5 minutes, followed by an increase to 95% over 1.1 minutes, held at 95% for 2 minutes, decreased to start conditions of 45% B over 0.4 minutes and then equilibrated for 5 minutes. The Betabasic-18 100x2, 3µ column was kept at 40 °C using a Shimadzu CTO-20AC column oven. Data were acquired and analyzed using Analyst 1.5.1 software. The standard curves were from 0-1000 pg/sample and the limit of quantification was 10 pg per sample except for 19-HETE and 20-HETE where the limit of quantification was 25 pg per sample where the relative standard deviation was less than 20%. Values that were above detection thresholds but below quantification thresholds were assigned a value of 4pg/ml.

3.3.5 Animals.

All mice were housed on a 12:12-h light:dark cycle and given free access to standard rodent chow and water. Homozygous sEHKO mice were generated in-house by breeding homozygous sEHKO mice. Homozygous mice are viable, fertile, normal in size and do not display any gross physical or behavioral abnormalities. Genotype was confirmed by PCR, as previously described [107]. Homozygous sEHKO mice have been

backcrossed to C57BL/6J for at least 7 generations. Therefore, sEHKO mice were compared to wild-type (WT) C57BL/6J mice obtained from Jackson Laboratories. All experiments were conducted with male mice 8 -12 weeks of age. Animals underwent either survival or non-survival, as described below. Both surgeries were performed identically, differing only in that non-survival animals had a femoral artery catheter inserted for arterial blood pressure monitoring, and that animals were culled for hemorrhage size measurements after thirty minutes. Animals in the survival study had no femoral artery catheter and were survived for imaging studies.

3.3.6 Mouse SAH model.

For both acute and longitudinal studies, SAH was induced in mice using the endovascular perforation technique [157] [125]. Briefly, mice were anesthetized with isoflurane (1.5 to 2% in O_2-enriched air by face mask), and maintained at 37±0.5°C via rectal temperature monitoring and warm water pads. A small laser-Doppler probe (Moor Instruments) was affixed to the skull to monitor cortical perfusion and confirm vascular rupture. To induce hemorrhages, a sharpened nylon suture (5-0) was introduced into the internal carotid artery via the external carotid artery and advanced ~10mm into the Circle of Willis. The suture was then advance slightly further to induce a hemorrhage and removed immediately. The common carotid artery was maintained patent at all times to maximize flow to the ruptured artery immediately following arterial perforation. In sham-operated animals, the suture was advanced into the internal carotid artery and then removed without arterial perforation.

3.3.7 Acute SAH studies.

WT and sEHKO mice were subjected to SAH while simultaneously being monitored for mean arterial blood pressure (MAP) (n = 4 all groups) and cortical perfusion (n = 4 all groups) for 30 minutes after SAH in a non-survival surgery. Arterial blood pressure was monitored via femoral artery catheter. Laser Doppler measurements were collected from a probe affixed to the skull above the middle cerebral artery (MCA). Thirty minutes after SAH induction, the animals were perfused transcardially with heparinized cold saline and the brains analyzed for hemorrhage

grade (n = 8 all groups) using a system adapted from Sugawara et al [158]. Briefly, an image of the ventral surface of the perfused brain was obtained using a Nikon Coolpix camera. Images were subdivided into 6 sections (Fig. 2C) and each section given a score of 0-3 by a blinded investigator according to the amount of blood present. A score of 0 was assigned to sections with no visible blood, while a score of 3 was assigned to sections with thick blood clots that blocked visualization of underlying vasculature.

3.3.8 Longitudinal studies using optical microangiography (OMAG).

To monitor changes in vessel diameters and CBV *in vivo*, we used the OCT-based imaging technique OMAG [106,123,159]. Briefly, at baseline and on days 1 and 3 after SAH (sEHKO n = 4, WT n = 6) or sham (n = 6) surgery, mice were anesthetized with isoflurane (1.5 to 2% in O2-enriched air by face mask). The skin over the skull was reflected, the cortex illuminated through the skull at 1,310 nm, and the resulting backscattered and reference light detected to produce spectral interferograms. Volumetric imaging data were collected by scanning the probe beam through a 1,000 x 500 x 512-voxel cube, representing 2.5 x 2.5 x 2 mm3 (*x-y-z*) of tissue (Fig.1). After scanning, the skin over the skull is closed and the animal is allowed to recover. Global CBV images were rendered in the 3-D software AMIRA (Visual Imaging GmbH) and analyzed for mean pixel intensity changes over time using Image-J [160]. Pixel intensity histograms were generated in Image-J. For vessel diameter measurements, the same data was rendered in IMARIS (Bitplane) software. Using the filament tracing function and the mean diameter calculator, average vessel diameters were calculated at each branching segment of the MCA within the scan area (n = 198, 98, and 154 vessel segments for WT, sEHKO and sham respectively). Vessels were chosen for analysis based on baseline scans by an individual blinded to 24h and 72h outcomes.

3.3.9 Whole brain mouse eicosanoid measurements

All samples (n = 10 all groups) were kept on dry ice until homogenization. Each sample was placed into 1.5 mls of PBS with with 15 µl of an anti-oxidant mix consisting of 0.2mg/ml BHT, 2 mg/ml TPP, and 2 mg/ml indomethacin. They were then homogenized on ice using a polytron, setting 2-3 for 20-30 seconds till homogenous.

Samples were prepared in batches of 15 samples, kept on dry ice prior to homogenization and wet ice at all times thereafter. The samples were immediately re-frozen on dry ice methanol after the aliquot was removed for analysis. 1 ml of 15% KOH was added to each tube, and an aliquot corresponding to 10 mg of brain tissue was added, the tube was briefly vortexed, capped tightly and then hydrolyzed at 40°C for 1 hour. Samples were cooled briefly (<=5 minutes) and then spiked with internal standard mix consisting of 1 ng of each of the following, d_8-15 HETE, d_6-20 HETE, d_8 14,15 EET, and d_{11}-14,15 DHET. Samples were acidified with 200 µl of glacial acetic acid, and the pH checked using pH paper for a desired range of 3-4. Samples were extracted with 3 ml of ethyl acetate, followed by 3 ml of hexane:ethyl acetate 1:1, followed by 2 ml of hexane. The extracts were combined and dried under vacuum for 35 minutes at 35 °C. 150 µl of 0.1N HCl was added to residue in each tube, followed by the addition of 1 ml of hexane. Samples were vortexed for 2x 20 sec, spun at 2000xg for 5 minutes and then hexane was transferred to a fresh tube. Samples were then dried under vacuum for approximately 7 minutes till dry and immediately brought up in 100 µl of start solvent which consisted of 45:55 (vol:vol) acetonitrile:water with 0.2 mg/ml TPP, 0.01% BHT and 0.01% formic acid and filtered through 0.22 micron placed in sample vials with inserts and analyzed immediately by LC-MS/MS. The injection volume was 20 µl. An un-extracted standard curve was used for these studies.

3.3.10 Western blot.

sEH protein expression was measured as previously described [161]. In brief, mice were perfused with ice-cold heparinized saline to remove blood, and brains were collected. Brains were homogenized in lysis buffer, centrifuged, and supernatant collected. Protein samples (40 µg) were separated by gel electrophoresis and then transferred to Polyvinylidene Difluoride (PVDF) membranes. Blots were blocked in 5% dry milk, and incubated at 4°C overnight with a primary rabbit polyclonal antibody against murine sEH (1:500; Cayman Chemical, Ann Arbor, MI). The signal was visualized using a horseradish peroxidase-linked (HRP) rabbit secondary antibody (1:1,000; GE Healthcare, Piscataway, NJ) followed by detection using Supersignal chemiluminescent reagents (Thermo Fisher Scientific, Waltham, MA) with a FluorChem

FC2 (Protein Simple, Santa Clara, CA). Blots were stripped using Restore Western Blot Stripping Buffer (Thermo Fisher Scientific) and re-probed for beta actin (1:2,000; Sigma-Aldrich) and followed by HRP mouse secondary antibody (1:1,000; GE Healthcare) and re-imaged.

3.3.11 Statistical analysis

Human CSF eicosanoid data followed a non-normal distribution and are displayed either as whisker box plots with the line representing the median, the box representing the interquartile range and error bars of traditional Tukey whiskers (Figure 1) or as median with error bars of interquartile range (figure 2,3). Error reported with median values in the text and tables is the absolute deviation around the median. Multiple comparisons were made using the Kruskall-Wallis test with Dunn's Multiple Comparison test for post-hoc analysis. Single comparisons were made using the Mann-Whitney U test. To determine the threshold CSF eicosanoid value for relative risk analysis a receiver-operator curve was generated and the value with the highest likelihood ration was chosen. Relative risk was calculated using Fisher's exact test. For animal studies, data are expressed as means ± SD. Protein and eicosanoid concentrations were compared using Student's t-test. For acute studies of MAP and CBF, as well as longitudinal studies of CBV, comparisons of sEHKO and WT mice were conducted using a two-way mixed effects ANOVA followed by Bonferroni post-hoc tests for pairwise comparisons. Hemorrhage grades were compared using a Mann-Whitney test. OMAG vessel diameters were compared within groups using a repeated measures ANOVA followed by a Tukey's multiple comparison test for pair-wise comparisons. For diameter change comparisons between groups, we used a Kruskal-Wallis test with Dunn's multiple comparison test for pairwise comparison. A value of $p < 0.05$ was considered statistically significant. All statistical tests were made using Prism 5.0 (Graphpad).

3.4 Results

3.4.1 Time course of CSF 14,15-EET and 20-HETE following SAH

We enrolled 34 SAH patients, who required external ventricular drainage on admission into the study along with 10 healthy control patients who received lumber puncture. All but one SAH patient had a modified Fisher score of 3 or above (median of 4), indicating severe bleeding and high risk of developing DCI [162]. As shown in Figure 12 (and supplementary Fig 1), all eicosanoids measured were elevated in CSF from SAH patients compared to control CSF, where eicosanoids were undetectable. Median CSF values of 20-HETE were highest on days 1-2 (88.4 ± 74.4 pg/ml), which by days 13-14 decreased by more than 80% (17.3 ± 3.9 pg/ml) (Fig 12a). This finding confirms other studies that measured 20-HETE in SAH patients CSF [163]. A similar pattern was also observed for 12-HETE (supplementary Fig 1). Conversely, median CSF values of 14,15-EETs were low on days 1-2 (6.3 ± 4.3 pg/ml), which rose over the course of the study by more than 6 fold on days 13-14 (38.7 ± 22.9 pg/ml). A similar pattern was also found for CSF levels of other EETs regio-isomers 8,9-EETs and 11,12-EETs (supplementary Fig 1). No discernable patterns were detected for 11-HETE or 15-HETE (supplementary Fig 1).

3.4.2 CSF 14,15-EET and 20-HETE correlate with DCI

We next sought to determine if CSF concentrations of 14,15-EET and 20-HETE correlate with the development of DCI. To do this, we used the peak, nadir, and mean CSF concentrations for 14,15-EET and 20-HETE over the course of the study for each patient (Table 1). Levels were correlated with DCI or mortality as primary outcomes, and with the disposition of the patient at time of discharge (i.e., discharged to home, inpatient care, expired, etc.) as the secondary outcome. We found no difference in 14,15-EET or 20-HETE levels in patients who died compared to survivors. Peak and mean 14,15-EET and 20-HETE levels were elevated in patients who experienced DCI versus those who did not. Nadir, mean and peak 20-HETE CSF concentrations were elevated in patients with a worse disposition compared to those discharged to home.

Before making further comparisons between the non-DCI and DCI groups, we excluded three patients from additional analysis. These patients were considered “neurologically devastated” on admission and care was withdrawn, making assessment of DCI in these patients impossible. Admission characteristics of the remaining patients were similar between groups. Specifically, there was no difference in Hunt and Hess clinical score or modified Fisher score between non-DCI and DCI groups (Table 3).

We then compared the time course of 20-HETE and 14,15-EET levels between DCI (n= 13) and non-DCI (n =18) patients (Fig. 13). We found the greatest differences occurring in the first four days for both 20-HETE (Fig. 13a) and 14,15-EET (Fig. 13b) as well as the final 4 days for 14,15-EET. A comparison of all values collected in the first four days between DCI and non-DCI patients revealed a significant increase in both 20-HETE (170.3 ± 114.0 pg/ml vs. 19.9 ± 9.0 pg/ml, $p < 0.01$, Fig 13c) and 14,15-EET (14.8 ± 10.8 pg/ml vs. 4.9 ± 1.6 pg/ml, $p < 0.05$, Fig 13d) in the DCI vs. non-DCI group. There were no differences between groups in the final four days of the study in either 20-HETE or 14,15-EET CSF levels.

3.4.3 CSF 14,15-EET and 20-HETE as predictive biomarkers of DCI

Because the major difference in CSF levels between groups occurred early after admission, we tested the value of early 14,15-EET and 20-HETE CSF concentrations (in the first 96 hours) as predictive biomarkers of DCI occurring later in the clinical course of the disease. We included only patients who had at least one CSF sample collected within the first 96 hours following SAH. For those patients with multiple CSF samples collected during this period, the highest value was used in the analysis. We compared 20-HETE and 14,15-EET concentrations (Fig. 14a) between DCI (n =12) and non-DCI (n = 15) groups, and found that the DCI group had elevated levels of both 20-HETE (218.2 ± 101.1 pg/ml vs. 23.4 ± 8.9 pg/ml, $p<0.01$) and 14,15-EET (22.3 ±15.3 pg/ml vs. 6.4 ± 2.4 pg/ml, $p<0.05$). To determine the ideal threshold values for a predictive test for DCI that was both sensitive and specific, we calculated the receiver operator characteristics (ROC), which plot the range of sensitivity and specificity over several different threshold values (Fig. 14b). As a comparison with a clinically used test,

we also included the peak Lindegaard Ratio (LR) values for each patient within the same time frame (96 hours). The LR is calculated as the ratio of blood flow velocity in the middle cerebral artery (MCA) to the velocity in the internal carotid artery using Transcranial Doppler Ultrasound. LR is routinely used to assess large vessel vasospasm in SAH patients.

The area under the curve (AUC) in Fig 14b is a rough estimate of the “clinical usefulness” of a given test. 20-HETE had the highest AUC (0.93) followed by 14,15-EET (0.79). The AUC of the LR (0.58) fell closest to the zero discrimination line indicating limited clinical usefulness. Using the sensitivity and specificity calculated from the ROC, we selected the threshold values with the highest likelihood ratios (sensitivity/1-specificity) for 20-HETE (148.6 pg/ml, likelihood ratio = 11.3) and 14,15-EET (23.9 pg/ml, likelihood ratio = 7.5) to assess relative risk of DCI(Fig. 14c). We included additional metrics for comparison including Hunt & Hess clinical grading score greater than or equal to 3, which has been reported to be associated with DCI. We also included early peak LR greater than 3 (days 1-4) and late peak LR greater than 3 (days 7-10), the latter considered part of the diagnostic criteria for DCI during most “at-risk” time points following SAH. Neither H&H ≥ 3 nor LR > 3 at any time point was significantly associated with increased relative risk of DCI. However, CSF 20-HETE levels above 148.9 pg/ml were associated with a greater than five-fold increase in the risk of DCI (5.1, 95% CI 1.8-14.5, $p<0.01$). CSF 14,15-EET levels above 23.9 pg/ml were also associated with a significant increase in the risk of DCI (2.9, 95% CI 1.4-5.6, $p<0.05$).

3.4.4 14,15-EET is elevated in sEHKO mice

While a significant body of work exists documenting the negative effects of 20-HETE in SAH and other diseases, it is counterintuitive that elevated levels of 14,15-EETs would confer greater risk of DCI. Previous work has shown 14,15-EET to be protective in both cerebral and cardiac ischemia, in part due to its vasodilator and anti-inflammatory properties. To study the effects of elevated 14,15-EET on DCI, we studied mice with sEH gene deletion (sEH knockout, sEHKO).The enzyme sEH hydrolyzes

14,15-EET molecule into its vicinal diol 14,15-DHET. Western blot analysis of sEH in whole brain showed no expression in the brains of sEHKO compared to WT mice (Fig 15a). Consequently, these mice had elevated basal levels of 14,15-EETs (Fig. 15b) and lower levels of 14,15-DHET (Fig. 15c) in brain tissue. As a negative control, we measured the levels of 20-HETE, which is not known to interact with sEH, and found no difference in basal brain 20-HETE between sEHKO and WT mice (Fig. 15d).

We then subjected the mice to the endovascular perforation model of SAH which involves perforation of the Circle of Willis with a stiff filament inserted into the internal carotid artery at the neck. To insure that WT and sEHKO mice received a similar insult, we measured changes in laser Doppler flux (Fig. 16a) over the MCA ipsilateral to the hemorrhage site as well as mean arterial blood pressure (Fig. 16b). We found no differences in the initial response to SAH between groups. We additionally measured the hemorrhage grade based on the amount of blood in the brainstem and basal cisterns and found no differences between in WT and sEHKO in severity and extent of hemorrhage (Fig 16c).

3.4.5 Early decrease in arterial vessel diameters after SAH

Optical Microangiography (OMAG) is an interferometry-based imaging technique, where scans show both perfusion and 3-D morphological information of mouse cortical surface vasculature through an intact skull. OMAG scans can be repeated non-invasively many times to measure changes in the same vessels over time. Using OMAG, we first looked for signs of vasospasm by measuring the diameters of terminal branches of the MCA in sham, WT SAH and sEHKO SAH mice (Fig 17a). Diameters of MCA surface branches within the scanned area ranged from 35 to 120 μm at baseline. Induction of SAH caused a decrease in vessel diameters in both WT and sEHKO mice within 24h which persisted for up to 72h (Fig 17b). There were no further changes in vessel diameters between 24h and 72h after SAH, nor were there differences in the degree of vessel diameter change between WT and sEHKO mice at any time point after SAH (Fig 17c).

3.4.6 sEHKO mice are protected from delayed decreases in microvascular perfusion after SAH

Since OMAG scans are based upon the Doppler shift caused by flow of RBCs, changes in velocity or flux can be determined in parallel with vessel diameter. This information was used to look at relative changes in cortical perfusion in the same animals over time (Fig 18a). Although surface vessel diameters decreased 24h after SAH, microvascular cortical tissue perfusion was preserved in these same animals at this time point. However, 72h after SAH, WT mice experienced a significant drop in mean pixel intensity (-16.93 ± 5.6% from baseline, $p < 0.05$), indicating a decrease in microvascular perfusion compared to baseline, whereas sEHKO mice had no change in perfusion between 24 and 72 hours after SAH. Since signal intensity reflects RBC velocity, which is slower in capillary beds, we were able to broadly differentiate between high-velocity, high-throughput vessels (such as large surface arteries or veins) and microvascular flow beds based on pixel intensity histograms of our scans. As shown in Figure 18c, we found that low-intensity signals corresponding to microvascular flow (Fig 18c shaded box) made up the bulk of our scan information and were shifted lower in WT SAH but not sEHKO mice at 72h. This observation suggests that sEHKO mice are protected from delayed reduction in microvascular perfusion after SAH.

3.5 Discussion

In the current study we provide both clinical and laboratory evidence for the role of P450 eicosanoids in the pathogenesis of DCI after aneurysmal SAH. We found that both 14,15-EET and 20-HETE were elevated in CSF of aneurysmal SAH patients at high risk for DCI up to 14 days following admission. The degree to which these eicosanoids were elevated predicted DCI with higher sensitivity and specificity than traditional predictors, such as admission modified Fisher score, Hunt & Hess score, and early or delayed trans-cranial Doppler. We found that sEHKO mice, which have elevated 14,15-EET, were protected from delayed reductions in perfusion seen in WT mice, and protection was specific to the microcirculation. To our knowledge this is the

first study to identify elevated levels of P450 eicosanoids other than 20-HETE in the CSF of SAH patients, and to provide evidence in support of a protective role for EETs.

There are several important findings in the clinical arm of this study. First, the greatest differences in CSF eicosanoid levels between DCI and non-DCI patients occurred within the first 96h after admission. This is promising in that an early CSF eicosanoid test, which would be the most useful time point for clinical decision making, may be valuable for stratifying risk of DCI. This finding should guide future studies testing eicosanoid biomarkers to focus on early time points following SAH. Additionally, other eicosanoids are elevated after SAH besides 20-HETE and 14,15-EET, including 11-HETE, 12-HETE, 15-HETE, 8,9-EET and 11,12-EET. One explanation is that these eicosanoids are only present in the CSF due to the extravasated blood itself, as plasma contains measurable levels of all of these eicosanoids [164]. However, this is unlikely given that levels of EETs increase from day 1 to day 14, while 20-HETE decreases, suggesting that active production and secretion into the CSF is occurring. It is more likely that these eicosanoids are part of the ever-growing list of neuro-inflammatory mediators that are produced by cells residing inside the brain in response to injury [165]. In support of this idea, we have previously shown that brief, transient ischemia is sufficient to induce sustained up-regulation of the EETs synthetic enzyme P450 2C11 in rat brain tissue [166]. Similar work has shown brain tissue increases in 20-HETE synthetic enzymes, CYP4A/4F, for as long as 10 days following ischemia [167]. While 20-HETE has pro-inflammatory and vasoconstricting effects, which likely contribute to and exacerbate DCI, 14,15-EET is a vasodilator and anti-inflammatory, and likely increases as an endogenous protective response against DCI. This is supported by our findings that individuals harboring a mutation in the gene encoding sEH, which could lead to elevated basal levels of 14,15-EETs, have improved outcomes after SAH compared to those harboring the common polymorphism [168]. Overall, this view suggests there exists a balance between protective and injurious eicosanoids in regulating the response to injury.

Injury mechanisms that lead to elevated levels of these eicosanoids in the *early* time-points after SAH are collectively referred to as “early brain injury” [169]. Early

pathogenetic mechanisms after SAH include global cerebral ischemia, blood brain barrier disruption, inflammation and hydrocephalus, among others. The occurrence of some of these early pathologies is associated with the development of DCI. Specifically, early ischemia in the first sixty hours of SAH, size of the initial hemorrhage, and neurologic status at admission all have been shown to predict DCI [170] [111]. We demonstrate in our study that elevated levels of these eicosanoids can also predict DCI, providing further support for the idea that early brain injury is an important determinant of DCI. It is worth noting that 94% of the patients enrolled in this study were classified as “high-risk” for DCI based upon assessment of modified Fisher score on admission. This means that an early CSF eicosanoid test has the potential to stratify DCI risk beyond conventional tests and allow the identification of those most likely to develop DCI. It is important to note that patients were prospectively enrolled in this study, but analysis of CSF eicosanoids and selection of test thresholds were retrospective. Confirming the predictive value and potential clinical utility of early eicosanoid testing to quantify EBI and predict DCI requires confirmation of our results in a blinded prospective study on a different patient population.

Another interesting finding from this study is that 14,15-EET levels, while elevated above controls at the onset of SAH, rise even further in the late stages of recovery. While this rise in EETs over time coincides with the timeframe for likely DCI, we are hesitant to make any conclusions about cause and effect on clinical observation alone. Our data from the experimental model of SAH support our hypothesis that the rise in EETs may play a protective role against DCI. Further, because our previous work has shown that EETs synthesis is driven by ischemia [166], we speculate that this elevation could be in response to a secondary brain insult such as DCI. However, EETs levels rise late in both the non-DCI and DCI groups, suggesting that if this is indicative of a secondary insult, that insult is clinically silent in a large subset of these patients. Clinically silent ischemia is not uncommon in SAH, and multiple studies find that 10-23% of new infarcts attributable to DCI are clinically silent [171] [172]. Since 94% of the patients in our cohort have large SAH as determined by CT we do not know what the time course of CSF 14,15-EETs would be for an individual with a less severe SAH. A study cohort that includes “low-risk” SAH patients and sensitive markers of ischemia is

needed to test whether 14,15-EET is a sensitive marker for asymptomatic and symptomatic DCI.

Our work in the mouse model of SAH provides an important insight into the mechanism of DCI. We found that pial branches of the MCA constrict early in the mouse, but do not lead to loss of microvascular perfusion. This is reminiscent of recent work questioning the relationship between proximal large-vessel vasospasm and DCI [173]. When delayed microvascular perfusion reductions do develop in WT mice, they are not accompanied by additional reductions in pial artery vessel diameter. This suggests that proximal vessel vasospasm and microvascular dysfunction do not share the same mechanisms. One characteristic of the microvasculature that sets it apart from larger vessels is a greater sensitivity to endothelial derived hyperpolarizing factors (EDHF), which 14,15-EET behaves similarly to in the cerebral circulation [96]. As arterial branches diminish in size along the vascular tree, their sensitivity to EDHF increases [39]. This is one possible explanation for our finding that sEHKO mice, which have elevated 14,15-EET, have the same reduction in pial MCA artery diameter as WT mice yet are protected from the delayed microvascular dysfunction 72h after SAH. Other mechanisms of microvascular dysfunction that could be affected by elevated 14,15-EETs include the formation of microthrombosis which is an increasingly understood contributor to microvascular dysfunction. Thrombi are generated within the inflamed microvasculature and become trapped within constricted arterioles [71] leading to blockade of poorly collateralized capillary beds and ischemia. EETs have a potent anti-inflammatory effect through inhibition of NF-κB [174] and direct effects on thrombosis [175] both of which could reduce the formation of microthrombi. Other mechanisms of dysfunction such as pericyte dysfunction and swelling of astrocytic end-feet [176] could be affected by EETs which are capable of directly protecting endothelial (16), neuronal [99]' and glial cells from death [100].

In conclusion, our data indicate that early CSF monitoring of P450 eicosanoids after SAH may be a useful tool in predicting the incidence of DCI. P450 eicosanoids have differential effects on DCI. Whereas 20-HETE has been shown to be detrimental, 14,15-EET may be protective. In experimental SAH, the microvascular component of

DCI is sensitive to enhanced 14,15-EET due to genetic deletion of sEH. The findings suggest that strategies aimed at enhancing EETs synthesis and inhibiting their metabolism may protect against the development of DCI in SAH patients.

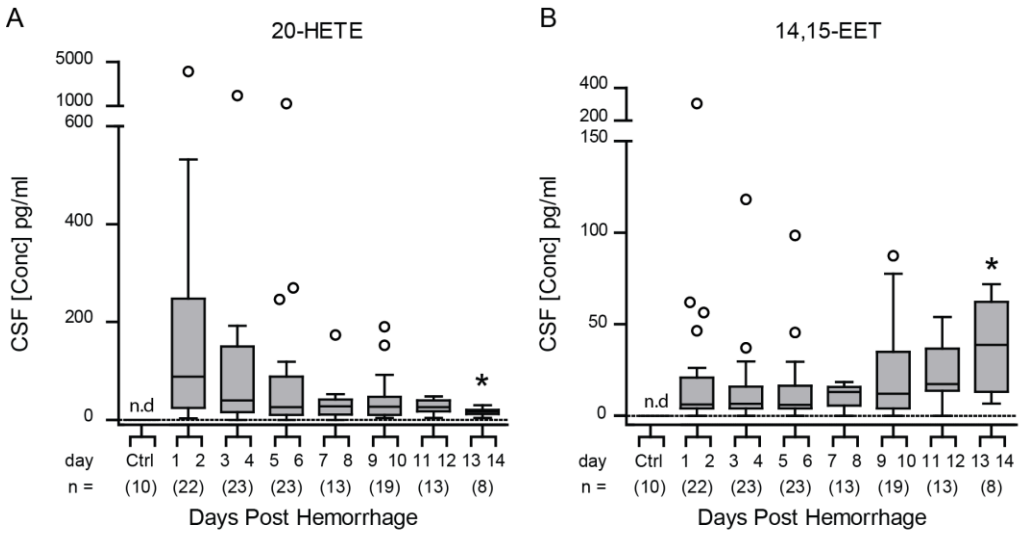

Figure 12. Eicosanoid levels following SAH. Concentration of A) 20-HETE and B) 14,15-EET in picograms per milliliter of CSF in an age/sex matched control group (Ctrl n =10) and in SAH patients (n = 34) up to fourteen days following SAH. $p < 0.05$ compared to days 1-2.

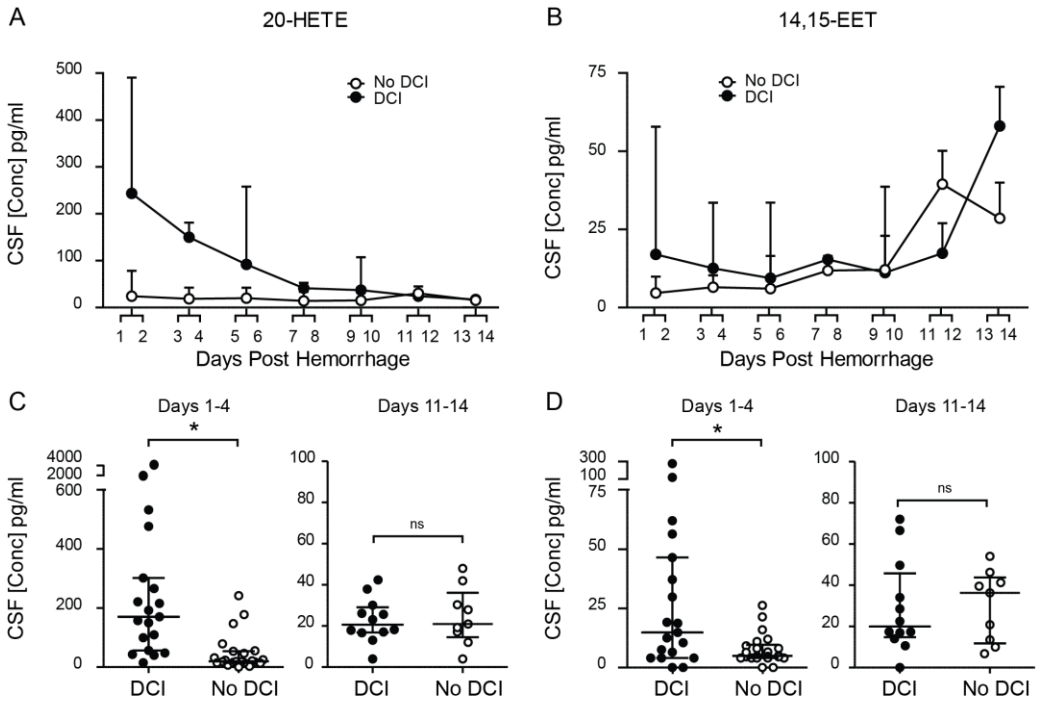

Figure 13. 20-HETE and 14,15-EET are elevated early in SAH patients who go on to experience DCI. (A,B) Time course of CSF 20-HETE (A) and 14,15-EET (B) levels in patients with DCI and without DCI. (C,D) Comparison of samples gathered in the first 4 days after admission and the last four days between DCI and non DCI patients. Both CSF 20-HETE (C) and 14,15-EET (D) levels are elevated early but not late after SAH in patients who go on to develop DCI.

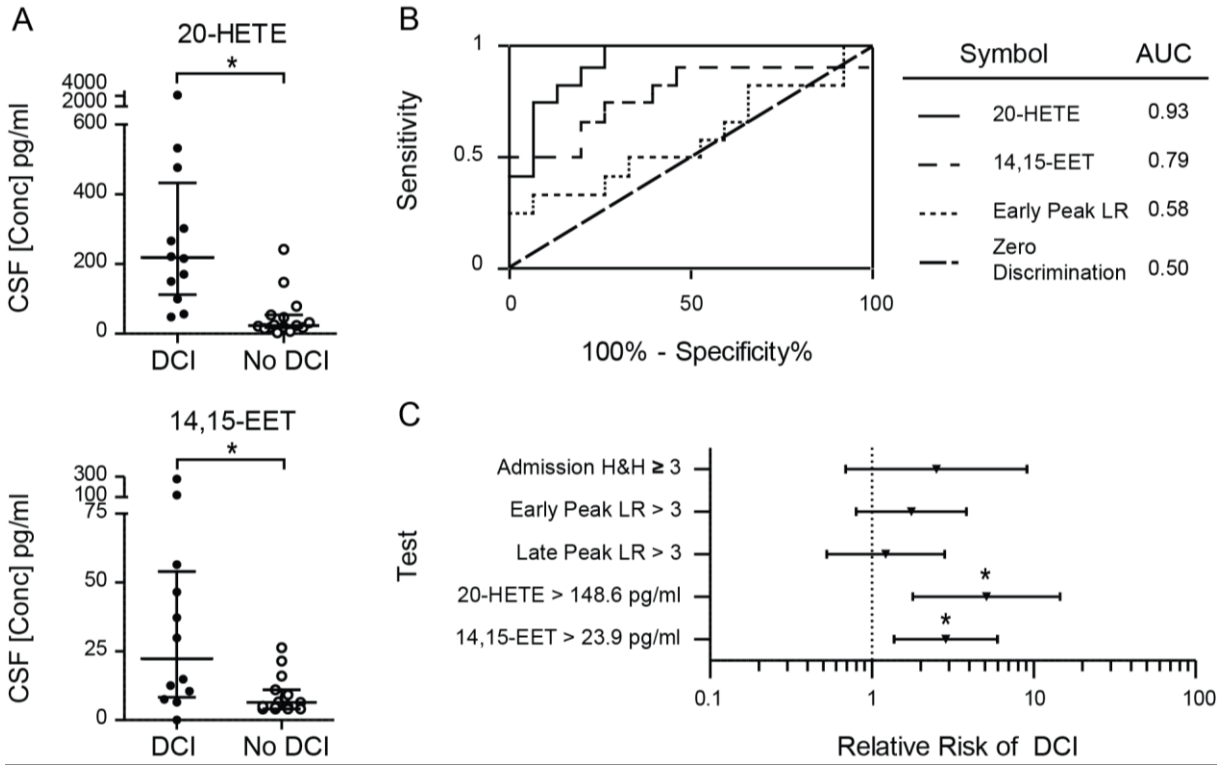

Figure 14. Peak 96h eicosanoid levels predict DCI (A) Peak single sample CSF 20-HETE and 14,15-EET levels within the first 96h after admission in DCI (n = 12) and non-DCI (n =15) patients. * = $p < 0.05$ (B) Receiver operator characteristic (ROC) for predicting DCI using CSF 20-HETE, 14,15-EET, or transcranial Doppler Lindegaard ratio (LR) measured within the first 96 h. Both 20-HETE and 14,15-EET have an AUC well above zero discrimination. (C) Relative risk of DCI is elevated in patients with CSF 20-HETE or 14,15-EET above threshold. Thresholds were chosen based on data from ROC. Included for comparison are admission Hunt & Hess (H&H) score above 3, early peak LR above 3 (first 96 h), and late peak LR (days 7-10) above 3. Data are expressed as relative risk with 95% CI error bars. * = $p < 0.05$.

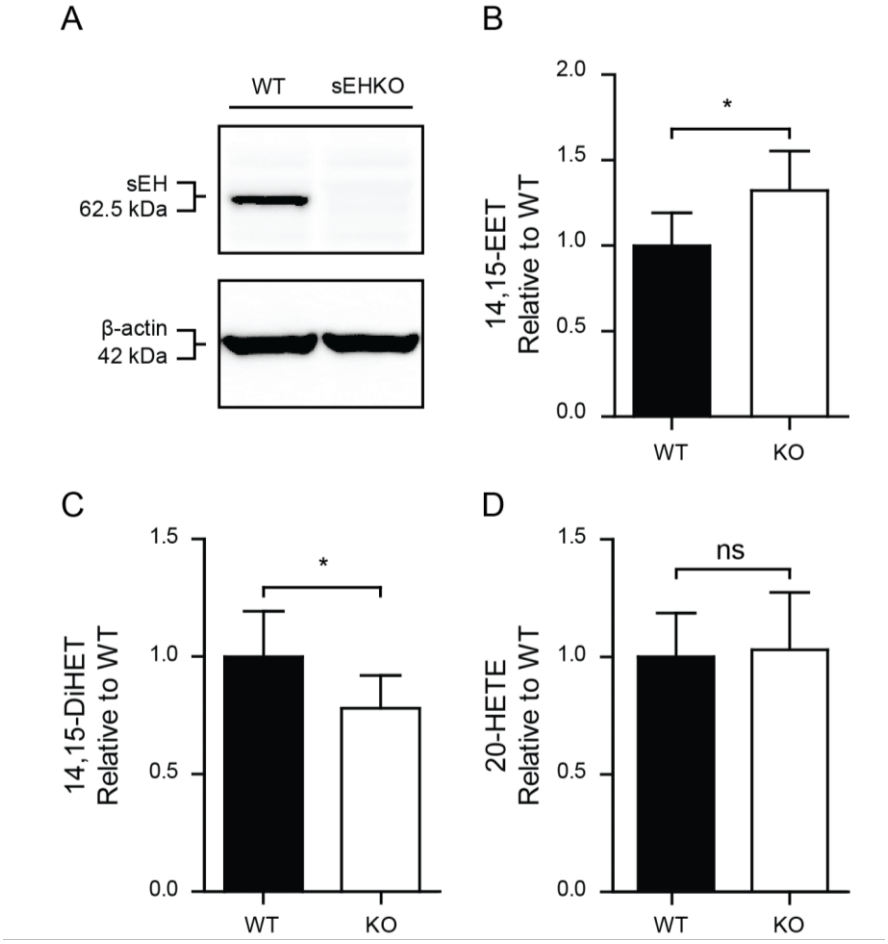

Figure 15. 14,15-EETs are elevated in sEHKO mice. (A) Representative western blot of sEH protein showing no expression in sEHKO mice. (B) Concentration of 14,15-EETs measured by LC-MS/MS is elevated in whole brain of sEHKO mice relative to WT mice. (C) Whole brain 14,15-DHET, the product of sEH hydrolysis, is lower in sEHKO mice compared to WT. (D) Whole brain 20-HETE is unchanged in sEHKO mice. n = 10 per group. * = $p < 0.05$. ns =no significance.

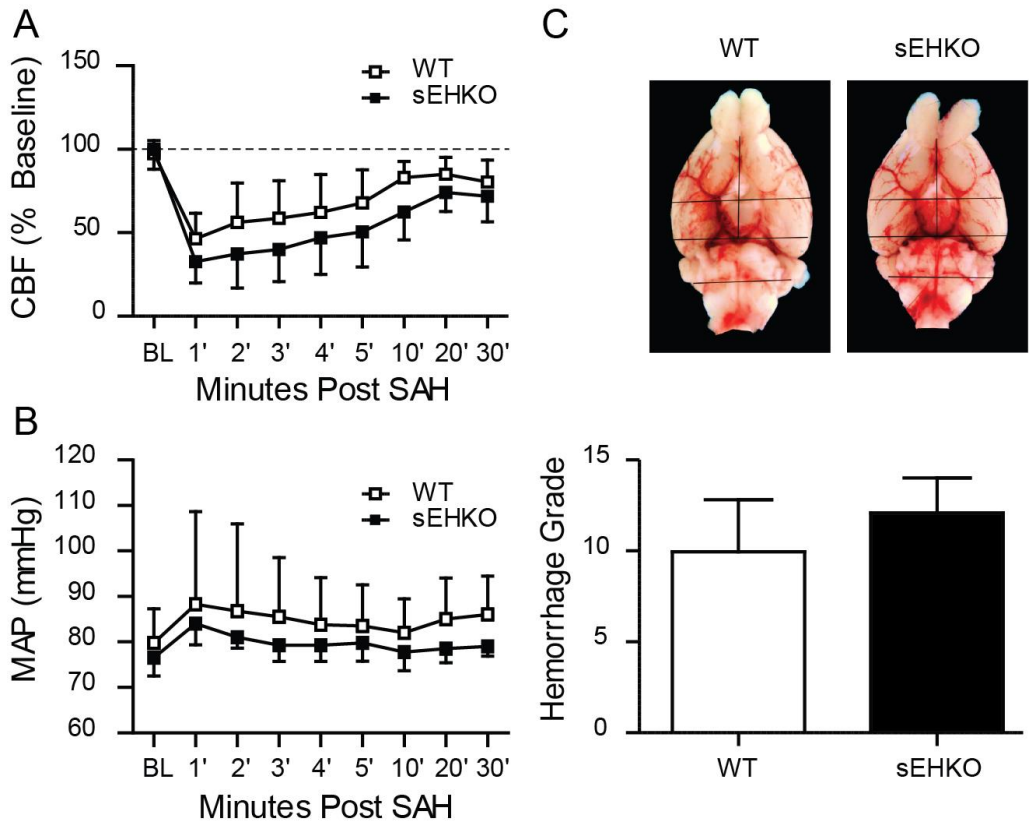

Figure 16. WT and sEHKO mice respond identically to SAH. (A) Laser doppler flowmetry of the ipsilateral MCA in WT (n = 8) and sEHKO(n = 8) mice in the first 30 minutes following SAH. (B.) Mean arterial pressure in WT (n =4) and sEHKO (n = 4) in the same time frame. (C.) Hemorrhage grade measured by blood in the brainstem and basal cisterns in WT (n = 8) and sEHKO (n = 8).

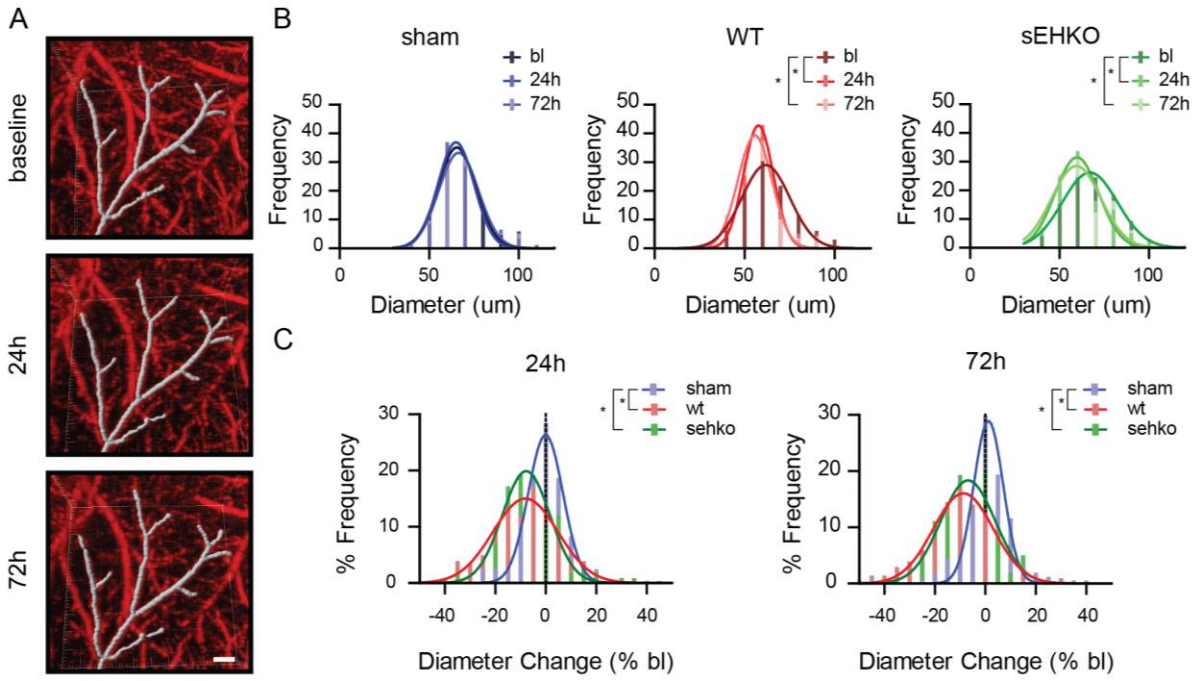

Figure 17. Arterial diameter changes following SAH: A.) Representative images of vessel diameter analysis using OMAG scans and IMARIS software in a WT mouse at baseline, 24h and 72h following SAH. Average diameters were measured in each segment separated by a branch point along the middle cerebral artery up to the point of penetration into the cortex. Scale bar = 50 um. B.) Frequency distribution of vessel diameters within groups, over time for sham, wild-type SAH mice (WT), and sEHKO SAH mice (sEHKO). SAH causes modest vessel diameter narrowing in both sEHKO and WT mice at 24h and up to 72h after SAH. Data are expressed in percent frequency of absolute vessel diameters within 10um bins. * = different from baseline $p < 0.05$. C.) Frequency distribution of changes in vessel diameter between groups for the 24h and 72h time points. Vessel diameters decrease in a similar manner in both WT and sEHKO mice at 24h and 72h. Data are expressed in percent frequency of percent change from baseline in 5% bins. * = different from sham $p < 0.05$. n = 198, 98, and 154 vessel segments for WT, sEHKO and sham respectively.

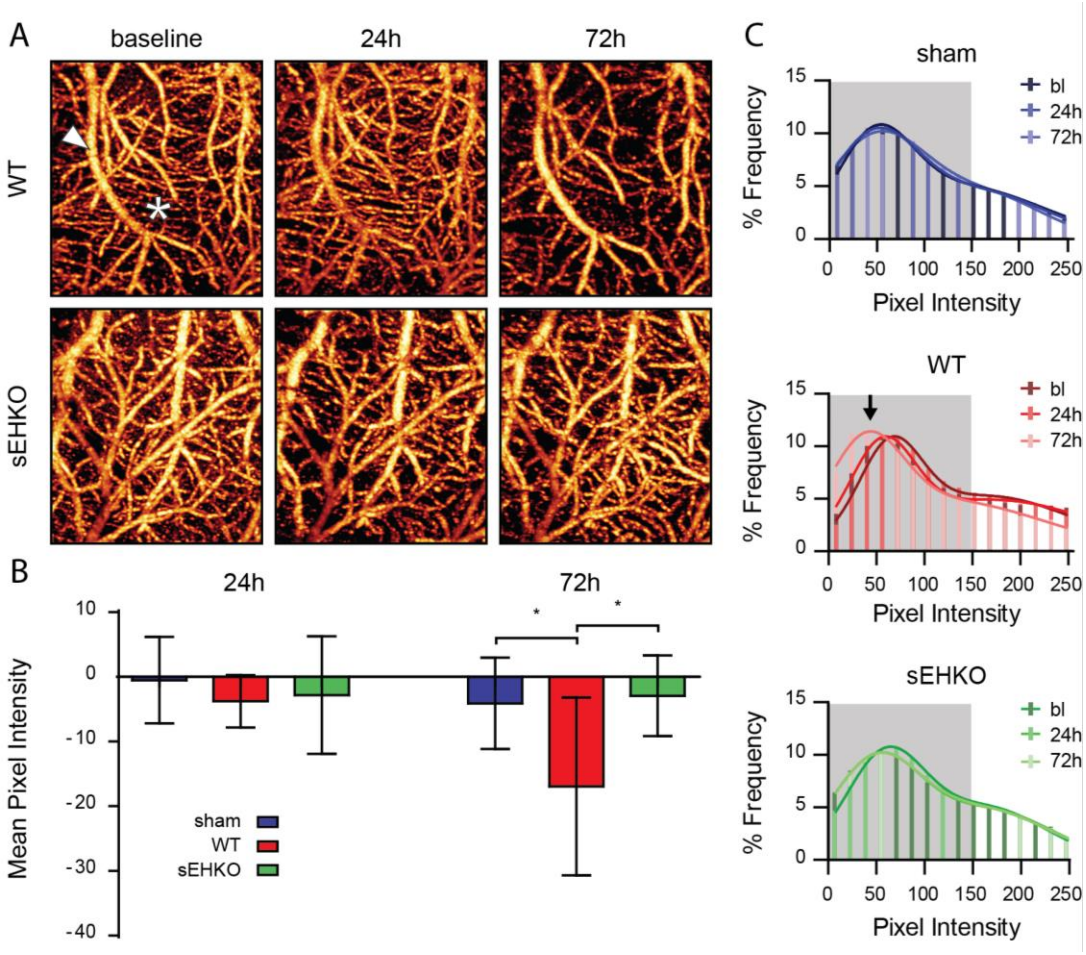

Figure 18. Microvascular perfusion changes following SAH: A.) OMAG scans are sensitive to blood velocity and RBC flux; high throughput vessels (arrowhead) will have a higher intensity than low throughput microvasculature (asterisk). Representative images of OMAG scans at baseline, 24h and 72h following SAH in WT (upper) and sEHKO (lower) cortical surface vasculature showing a decrease in perfusion from baseline scans in WT but not sEHKO mice 72h after SAH B.) Quantification of mean pixel intensity in sham (n = 6) , WT (n = 6), and sEHKO (n = 4) mice following SAH. * = different from WT, $p < 0.05$. C.) Average pixel intensity histograms fitted with a double gaussian model. Low intensity (< 150 shaded in grey) microvasculature makes up the bulk of the histogram. Arrow in WT histogram indicates a shift in low intensity pixels 72h after SAH in WT mice representing a decrease in microvascular perfusion that does not occur in sEHKO mice.

Table 1
Admission Characteristics

	Ctrl	SAH
N	10	34
Demographics		
Average Age, years	63.0	56.8
Male, n (%)	3(30.0)	10(29.4)
Aneurysm Location, n (%)		
ACOM	-	10 (29.4)
ICA/MCA	-	13(38.2)
PCOM	-	8(23.5)
Vertebrobasilar	-	3(8.8)
Admission Status, n (%)		
Hunt Hess Score ≥ 3	-	23 (67.6)
WFNS ≥ 4	-	19 (55.9)
Fisher Score ≥ 3	-	32 (94.1)

Table 2
CSF Eicosanoid Levels and Outcome

	Nadir Levels		Mean Levels		Peak Levels	
	20-HETE	14,15-EET	20-HETE	14,15-EET	20-HETE	14,15-EET
Mortality						
Alive (27)	13.2 ± 9.2	4.0 ± 4.0	43.0 ± 26.2	11.7 ± 7.2	56.3 ± 41.9	20.8 ± 14.3
Dead (7)	18.2 ± 4.7	4.0 ± 0.0	43.5 ± 21.8	5.8 ± 1.8	67.2 ± 42.4	8.8 ± 4.8
Disposition						
Home (16)	**9.4 ± 8.1****	4.0 ± 2.4	**19.4 ± 8.7*****	12.1 ± 7.2	**40.9 ± 24.3****	23.6 ± 16.2
SNF,Rehab,Dead (18)	**69.7 ± 38.6**	4.0 ± 0.0	**69.7 ± 38.6**	9.3 ± 5.3	**133.1 ± 88.5**	15.4 ± 11.4
Delayed Cerebral Ischemia						
No DCI (21)	13.2 ± 5.5	4.0 ± 0.75	**28.5 ± 14.4*****	**7.2 ± 3.2***	**42.6 ± 21.5*****	**10.8 ± 6.8***
DCI (13)	18.2 ± 4.7	4.0 ± 4.0	**95.5 ± 40.8**	**20.9 ± 12.1**	**221.0 ± 121.4**	**46.5 ± 31.7**

Table 3
No DCI vs. DCI Admission Characteristics

	No DCI	DCI
N	18	13
Demographics		
Average Age, years	57.4	55.2
Male, n (%)	5 (27)	2 (15.4)
Aneurysm Location, n (%)		
ACOM	7 (38.9)	3 (23.1)
ICA/MCA	4 (22.2)	7 (53.8)
PCOM	5 (27.8)	2 (15.0)
Vertebrobasilar	2 (11.1)	1 (8.0)
Admission Status, n (%)		
Hunt Hess Score ≥ 3	9 (50.0)	11 (85.0)
WFNS ≥ 4	7 (38.9)	9 (69.2)
Fisher Score ≥ 3	17 (94.4)	12 (92.0)

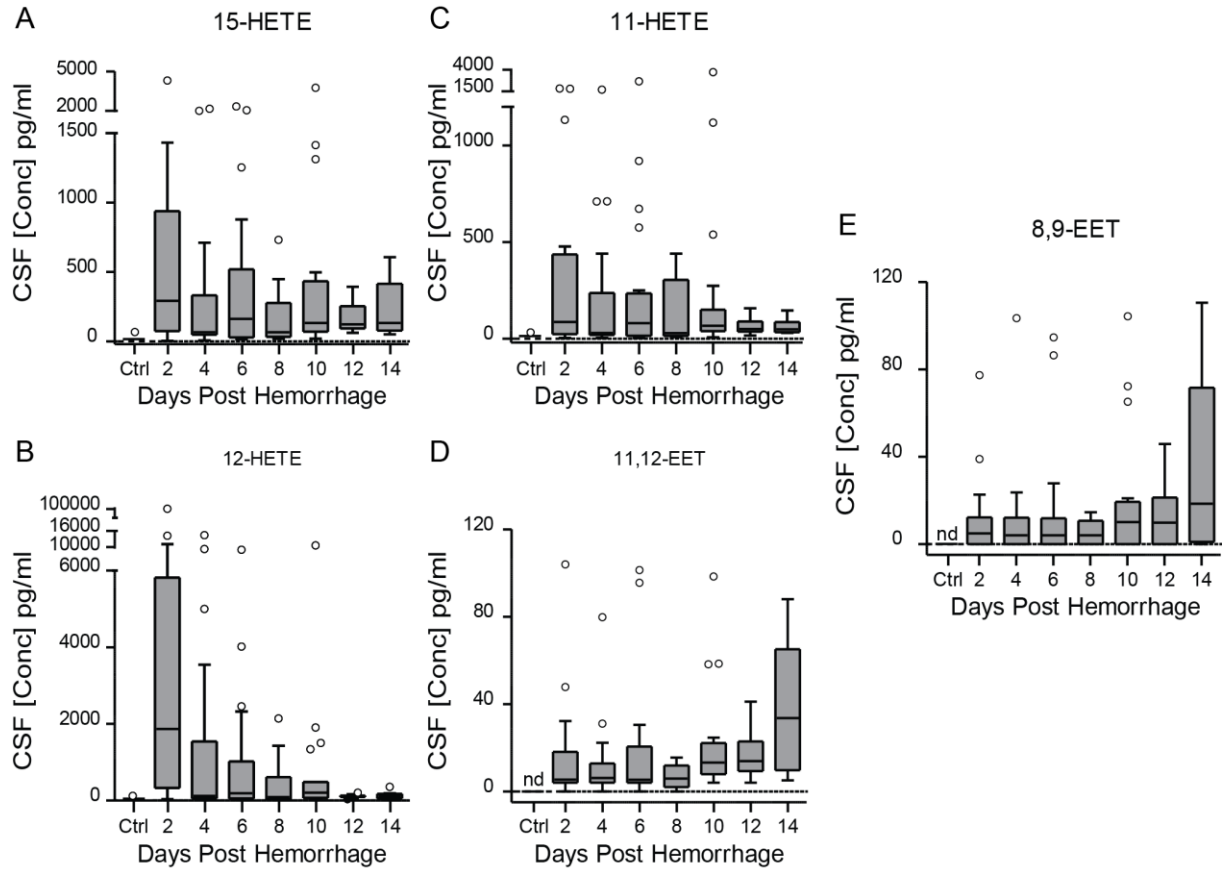

Supplemental Figure 1 . Eicosanoid levels following SAH. Concentration of A) 15-HETE, B) 12-HETE, C) 11-HETE, D) 11,12-EET and E.) 8,9-EET in picograms per milliliter of CSF in an age/sex matched control group (Ctrl n =10) and in SAH patients (n = 34) up to fourteen days following SAH. nd= not detected

Chapter 4

Role of Soluble Epoxide Hydrolase in Communicating Hydrocephalus, Cerebral Edema and Vascular Inflammation after Subarachnoid Hemorrhage.

4.1 Summary

Background and Purpose - Acute communicating hydrocephalus and global cerebral edema are common and serious complications of subarachnoid hemorrhage (SAH), whose etiologies are poorly understood. Using a mouse model of SAH, we determined if soluble epoxide hydrolase (sEH) gene deletion protects against SAH-induced hydrocephalus and edema by increased levels of vasoprotective eicosanoids and suppressing vascular inflammation.

Methods - SAH was induced via endovascular puncture in WT and soluble epoxide hydrolase knockout (sEHKO) mice. Hydrocephalus and tissue edema were assessed by T_2-weighted MR imaging. Endothelial activation was assessed in vivo using T_2-star weighted MR images after intravenous administration of iron oxide particles linked to anti-vascular cell adhesion molecule-1 (VCAM-1) antibody 24h after SAH. Behavioral outcome was assessed at 96h after SAH with the open field and accelerated rotarod tests.

Results – SAH induced an acute and sustained communicating hydrocephalus within 6h of endovascular puncture in both WT and sEHKO mice. This was followed by tissue edema, which peaked at 24h after SAH and was limited to white-matter fiber tracts. sEHKO mice had reduced edema, less VCAM-1 uptake and improved outcome compared to WT mice.

Conclusions - Genetic deletion of sEH reduces vascular inflammation and edema, and improves outcome after SAH. sEH inhibition may serve as a novel therapy for SAH.

4.2 Introduction

Acute communicating hydrocephalus and global cerebral edema are common life-threatening complications of subarachnoid hemorrhage (SAH), which occur in 20% of patients [9,10,177] and are independent risk factors for poor outcome [10,23]. They can occur together in the same patient, but are often present separately. Thus, while both represent a dysfunction in water handling within the cranium, their etiologies are likely different and possibly unrelated. Current treatments for hydrocephalus and cerebral edema are largely supportive and do not target the underlying pathologies. This is especially the case for hydrocephalus, which leaves some patients requiring permanent ventricular shunts due to unremitting disease [178,179]. Clearly, a better understanding of the mechanisms underlying these complications is needed to identify viable therapeutic targets.

Mouse models of SAH have been employed to study mechanisms of cerebral edema [180,181], but have not taken into account the potential contribution of hydrocephalus to brain water content [182]. To date, there are no studies describing hydrocephalus in mouse models of SAH. In the current study, we employ high-field magnetic resonance imaging (MRI) to study the timing, severity, and localization of acute communicating hydrocephalus as well as cerebral edema occurring simultaneously in the mouse endovascular puncture model of SAH.

One form of cerebral edema, vasogenic edema, is caused by extravasation of ions and proteins through a disrupted blood-brain barrier and is often preceded by activation of the vascular inflammatory cascade [183]. Epoxyeicosatrienoic acids (EETs) are anti-inflammatory eicosanoids formed by cytochrome P450 enzymes in brain glia and endothelium [95] and oppose inflammation through inhibition of the NF-κB master pathway [184]. We have previously demonstrated that mice with elevated levels of EETs due to genetic deletion of their metabolizing enzyme soluble epoxide hydrolase (sEH knockout, sEHKO mice) are protected from both experimental cerebral ischemia [107] and delayed microvascular dysfunction after experimental SAH. We hypothesized that the beneficial effects of EETs extend to alter early brain injury by modulating inflammation and edema formation. Our findings demonstrate that sEHKO mice have

reduced edema, decreased cerebrovascular inflammation and improved outcome after SAH, although the extent of hydrocephalus was similar to WT mice.

4.3 Methods:

4.3.1 Animals

Experimental animal procedures performed in this study conform to the guidelines of the US National Institutes of Health, and the animal protocol was approved by the Institutional Animal Care and Use Committee of Oregon Health & Science University, Portland, OR, USA. All mice were housed on a 12:12-h light:dark cycle and given free access to standard rodent chow and water. Homozygous sEHKO mice were generated in-house by breeding homozygous sEHKO mice. Homozygous mice are viable, fertile, normal in size and do not display any gross physical abnormalities. Genotype was confirmed by PCR, as previously described [107]. Homozygous sEHKO mice have been backcrossed to C57BL/6J for at least 7 generations. Therefore, sEHKO mice were compared to wild-type (WT) C57BL/6J mice obtained from Jackson Laboratories. All experiments were conducted with male mice 8 - 12 weeks of age.

4.3.1 Endovascular Puncture

SAH was induced in mice using the endovascular perforation technique adapted from Sozen et al [181]. Briefly, mice were anesthetized with isoflurane (1.5 to 2% in O2-enriched air by face mask), and maintained at 37±0.5°C rectal temperature using warm water pads. Two small laser-Doppler probes (Moor Instruments) were affixed bilaterally over the dorsolateral parietal cortex to monitor cerebrocortical perfusion and confirm vascular rupture. To induce hemorrhage, a nylon suture (5-0) was introduced into the internal carotid artery via the external carotid artery and advanced ~10mm beyond the carotid bifurcation and into the Circle of Willis. The suture was then advanced slightly further to induce a hemorrhage, and then removed. The common carotid artery was maintained patent at all times to maximize flow to the ruptured artery immediately following arterial perforation. After endovascular puncture, the filament was

removed, the wound closed and the animal was allowed to recover. Mortality throughout the study was less than 10% and most often occurred immediately following SAH induction. Only mice which survived the initial surgery were included in this study. In sham-operated animals, the suture was advanced into the internal carotid artery and then removed without arterial perforation.

4.3.3 Physiological Monitoring

In a subset of non-survival surgeries, animals were monitored for intra-cranial pressure (ICP), systemic arterial blood pressure (BP) and cerebral blood flow (CBF) for thirty minutes following induction of the hemorrhage. For ICP measurements, a small burr hole (<0.5mm) was made into the left parietal bone and a micro-tip catheter transducer (Millar) 0.33 mm in diameter was placed into the parenchyma. The transducer was connected to a PCU-200 ICP monitor (Millar). For blood pressure recording, the femoral artery was catheterized and connected to a BP-1 monitor (World precision Instruments). For cerebral blood flow monitoring, a single laser-Doppler probe (Moor Instruments) was placed over the right parietal bone. All three monitoring devices were connected to a Digi-data 1440 digital-to-analog converter (Molecular Devices) and recorded using pCLAMP (Molecular Devices). After all devices were connected, SAH was induced as described above and the mouse was monitored for thirty minutes. All probes were then removed and the mice were deeply anesthetized with isoflurane, then cardiac perfused with cold heparinized saline and the brain examined to confirm hemorrhage.

4.3.4 Vascular Cell Adhesion Molecule-1 (VCAM-1)-bound micro particles of iron oxide (MPIO)

We conjugated monoclonal rat anti-mouse CD106 (VCAM-1; 1510-01 Southern Biotech) with a monoclonal mouse IgG1 (0102-01 Southern Biotech) covalently bound to Dynabeads MyOne Tosylactivated MPIOs (Invitrogen) per manufacturer's instructions. Briefly, MPIOs were washed with sodium borate buffer (0.1 M, pH 9.5) and combined with antibodies (40ug antibody/1mg MPIO) and 3 M ammonium sulfate to give a final

concentration of 6mg/ml MPIO. The solution was incubated on a rotating platform at 37°C overnight. We then collected MPIO by using a magnet and discarded the supernatant. We added PBS plus 0.5% BSA and 0.05% Tween 20 (pH 7.4) as a blocking agent and incubated MPIO at 37 °C overnight again. We washed MPIO with PBS plus 0.1% BSA and 0.05% Tween-20 before storing at a final concentration of 5mg MPIO per ml in PBS plus 0.1% BSA and 0.05% Tween 20 at 4 °C.

4.3.5 MRI

MR imaging employed a Bruker-Biospin 11.75T small animal MR system with a Paravision 4.0 software platform, 9 cm inner diameter gradient set (750 mT/m), and a mouse head (20 mm ID) quadrature RF transceiver coil (M2M Imaging Corp.) The mice were positioned with their heads immobilized in a specially designed head holder with adjustable ear pieces. Body temperature was monitored and maintained at 37°C using a warm air temperature control system (SA instruments). Isoflurane (0.5–2%) in 100% oxygen was administered and adjusted while monitoring respiration.

To quantify brain size, ventricle size and white matter edema, a coronal 25-slice T_2-weighted image set (Paravision spin echo RARE, 256×256 matrix, 98 μm in-plane resolution, 0.5 mm slice width, TR 4000 msec, $TE_{effective}$ 32 msec, RARE factor 8, 4 averages, acquisition time 8.5 min) was obtained at baseline, 6h, 12h, 24h and 72h after SAH or sham surgery to assess brain anatomy. Images were processed using JIM (Xinapse). Images from +3.00 mm bregma to -6.00 mm bregma were manually edited to remove voxels representing non-brain tissue and used for further analysis. Brain volume was calculated using these images and quantified as percent change from baseline scans to normalize for variations in brain volume between animals. To measure ventricular volume and edema, images were thresholded to the intensity of grey matter to isolate hyperintensities representing ventricles and edematous tissue. Areas of edema were defined as areas of hyperintensity that were located within brain parenchyma. The total volume of voxels identified as ventricles and edematous tissue were quantified. To normalize for variation in baseline ventricular volume, percent changes from baseline scans were calculated. To normalize for variation in brain size, edema volume was calculated as percent of total brain volume.

To quantify nanoparticle uptake 25 h after SAH or sham surgery, we employed a 3D T_2* weighted sequence (Paravision 3D FLASH, TE 9ms, FOV 3.5 x 1.75 x1.75 cm, 256x128x128 matrix, 137 μm isotropic resolution, TR 25 msec, FA 15º, acquisition time 6.8 min). Mice were first imaged without injection of MPIOs. Mice were then injected with VCAM-1 MPIO or IgG MPIO at 4.5 mg Fe/kg body weight and rescanned at the 80 minute time point. We chose to image the mice at the 80 minute time point after MPIO injection based upon previous work [185,186]. Following the scans, mice were deeply anesthetized and transcardially perfused with cold heparinized saline followed by 4% paraformaldehyde before being prepared for histological analysis. All image processing was done using tools from FSL [187-189] and JIM (Xinapse). Images were manually edited to remove voxels representing areas of non-brain tissue. The resulting brain extracted images were scaled and normalized based on the intensity of the upper 70th percentile of nonzero voxels. Baseline images were brought into a common space using linear rigid-body registration and averaged to create a study template [188,189]. Baseline and post-iron images were then registered to this template and smoothed with a 3D Gaussian kernel (sigma = 50 microns). Maps of the decrease in normalized signal were calculated by dividing the post-iron images by the baseline images. The percentage of voxels with intensity decreases greater than 60% were quantified.

4.3.6 Histology

72h after SAH, mice were deeply anesthetized with isoflurane (5%) and perfused transcardially first with cold heparinized saline followed by 4% paraformaldehyde as a fixative. Brains were then incubated in 4% paraformaldehyde for 48h at 4ºC before being embedded in paraffin. Brains were then cut into 8um sections and stained with hematoxilin and eosin. Images were collected on a BX40 microscope (Olympus) using a Micropublisher 5.0 camera (Qimaging). Images of the corpus callosum were obtained and converted to greyscale then thresholded. Vacuolization at the corpus callosum was quantified by taking the mean pixel intensity of the thresholded images.

4.3.7 Behavioral Assessment

Mice were allowed to recover for 96 h after SAH or sham surgery before being assessed for behavior. To test general locomotor activity, mice were first placed in an open field apparatus (Columbus instruments) and allowed to roam freely for ten minutes. Total distance travelled was recorded. On the same day, to test sensorimotor function, mice were placed on the accelerated rotarod (Columbus Instruments) with speeds increasing by one rpm every three seconds in three consecutive “time to fall” trials. Mice were tested again on the rotarod in the same manner for two additional days to reach a total of nine “time to fall” trials. Time to fall was then averaged over the nine trials for each mouse.

4.3.8 Statistics

Group data are expressed as mean ± sem unless otherwise stated. LDF, ICP, MAP, ventricular volume, brain size, and edema percentage were compared between groups using a repeated measures two-way ANOVA with Holm-Sidak post-hoc tests. Vacuolization data was log transformed and compared using one-way ANOVA with Holm-Sidak post-hoc tests. VCAM-1 uptake was compared using one-way ANOVA with Holm-Sidak post-hoc tests. Finally, behavioral comparisons were made using two-way ANOVA with Holm-Sidak post-hoc tests.

4.4 Results:

4.4.1 SAH induces immediate and sustained rise in ICP

Endovascular puncture caused blood to fill the basal cisterns and subarachnoid space of the mouse within minutes. T2-weighted MRI scans within 30 minutes showed blood flowing retrogradely as far as the 4th ventricle (Figure 19a; note the change in T2 signal in CSF spaces from white to black). We monitored ICP, MAP and CBF in a cohort

of WT and sEHKO mice for thirty minutes following vessel puncture. At the moment of hemorrhage, ICP spiked as CBF decreased (figure 19b). Arterial pressure also increased. The ICP waveform changed after hemorrhage to increased pressure fluctuations during systole indicating reduced CSF compliance (Figure 19b inset). In both sEHKO and WT mice, ICP rose considerably at the time of hemorrhage (WT 60.2 ± 9.9 mmHg vs sEHKO 69.2 ± 6.0 mmHg) and returned to an elevated set point by thirty minutes (WT 33.0 ± 3.2 mmHg vs sEHKO 30.4 ± 1.1 mmHg). Laser Doppler flow also decreased substantially at the time of SAH (WT 55.2 ± 19.2 % vs sEHKO 37.3 ± 6.8 % of baseline) and returned to a point below baseline by 30 minutes (WT 80.9 ± 28.2 % of baseline vs sEHKO 77.9 ± 20.7 % of baseline). Baseline MAP appeared lower in sEHKO mice but was not statistically significant (WT 74.3 ± 1.0 mmHg vs sEHKO 60.8 ± 2.3 mmHg) and rose to similar levels after hemorrhage (WT 83.6 ± 8.6 mmHg vs sEHKO (85.4 ± 6.8 mmHg) before returning back towards baseline by thirty minutes (WT 74.2 ± 1.8 mmHg vs sEHKO 70.2 ± 2.1 mmHg). There were no significant differences between WT and sEHKO mice at any time point.

4.4.2 Acute communicating hydrocephalus forms rapidly and persists after SAH

Before and at several time points after (6h, 12h, 24h, and 72h) inducing SAH, we obtained T2 weighted coronal sections to look for signs of hydrocephalus. Within 6 h of SAH, ventricular volume had increased substantially (Figure 20a). Signs of brain swelling in the form of central sulcus effacement were also evident at 6h (figure 20a arrowheads). To ascertain whether the hydrocephalus was obstructive or communicating in nature, we looked for signs of uneven enlargement of the ventricular system or large blood clots within the cerebral aqueduct that could block CSF flow. In all scans, the enlargement of the ventricular system was uniform from the anterior horns of the lateral ventricles to the cisterna magna. We found ventricular blood in some of the animals scanned, but a continuous patent flow pathway could be traced in all animals imaged. Additionally, we found enlargement of the CSF spaces outside of the ventricular system including the intrathecal space around the spinal cord and the subarachnoid space separating the cortex from midbrain structures (figure 20a arrows). WT and sEHKO mice had a similar increase in ventricular volume at each time points

beginning as early as 6 h (WT 181.3 ± 4.9 % of baseline vs sEHKO 185.4 ± 17.5 % of baseline) and persisting the length of the study at 72 h (WT 206.2 ± 13.2 % of baseline vs sEHKO 208.2 ± 23.9 % of baseline) (figure 20b). Brain swelling also occurred in both groups beginning at 6 h (WT 0.67 ± 0.5 % vs sEHKO 1.7 ± 0.8 % change from baseline) persisting to 72 h (WT 3.0 ± 0.5 vs sEHKO 2.2 ± 0.6 % change from baseline) (figure 20c). There were no differences between WT and sEHKO mice at any time point.

4.4.3 sEHKO mice have reduced periventricular white matter edema after SAH

Edema, visualized by hyperintensities on T2 weighted images, began to form specifically in the periventricular white matter of SAH mice within 6 h then peaked at 24 h before beginning to recede at 72 h (figure 21a). The white matter structures affected included the corpus callosum and the dorsal hippocampal commissures (figure 21a arrows). Histological sections of the corpus callosum showed substantial vacuolization of the white matter in WT mice. sEHKO mice had significantly less edema at 24 h (WT 3.1 ± 0.5 % brain volume vs sEHKO 1.7 ± 0.4 % brain volume $p < 0.05$) and 72h (WT 2.7 ± 0.5 % brain volume vs sEHKO 0.7 ± 0.2 % brain volume $p < 0.05$) compared to WT mice (figure 21b). Vacuolization found in histological sections of the corpus callosum was also significantly reduced in sEHKO mice compared to WT mice (WT 1.6 ± 0.4 a.u. vs sEHKO 1.2 ± 0.09 a.u. $p < 0.05$) (figure 21c).

4.4.4 sEHKO mice may have reduced expression VCAM-1 following SAH.

As a measure of vascular inflammation in vivo, we studied the expression of VCAM-1 on brain endothelium using VCAM-1 tagged micrometer-sized iron oxide (VCAM-1 MPIO). 24 h after SAH or sham surgery, we injected the labelled particles into the vasculature and imaged the animals via T2-star weighted MRI. VCAM-1 MPIO uptake, showed as hypointensities on the scans, and was greatest in the vasculature along the midline and surrounding the midbrain of the mice (figure 22a). We found very little uptake in the IgG-tagged MPIO mice as well as the sham-operated mice. sEHKO mice had reduced overall VCAM-1 uptake in the whole brain compared to WT mice (WT 0.3 ± 0.05 % bv vs sEHKO 0.19 ± 0.07 % bv) although this was not statistically significant (figure 22c).

4.4.5 sEHKO mice have improved outcome after SAH

To assess behavioral outcome after SAH, the open field test and the accelerated rotarod were performed 96 h after SAH or sham was induced. Sham operated sEHKO mice performed differently on the open field test than sham operated WT mice (WT 6944.4 ± 433.9 cm vs sEHKO 5675.9 ± 418.2 cm) (figure 23a), which complicated the comparison. Comparing within genotype, we found that SAH caused a reduction in total movement on the open field in WT(sham 6944.4 ± 433.9 cm vs SAH 5106.9 ± 525.1 cm $p < 0.05$) but not sEHKO mice (sham 5675.9 ± 418.2 cm vs SAH 4663.2 ± 589.4 cm). On the accelerated rotarod, WT and sEHKO sham mice remained on the rotating rod for similar amounts of time (WT 42.5 ± 3.0 s vs sEHKO 43.1 ± 3.5 s), (figure 23b) allowing a direct comparison between genotypes after SAH. At 96 h after SAH, sEHKO mice remained on the accelerating rotarod longer compared to WT mice (WT 36.5 ± 2.7 s vs sEHKO 47.3 ± 2.5 s $p < 0.05$).

4.5 Discussion

The present study shows that acute communicating hydrocephalus and cerebral edema occur simultaneously in the mouse endovascular puncture model of SAH. The onset of hydrocephalus was rapid and sustained, occurring within 6 h of SAH and remaining present for at least 72 h. Cerebral edema formed primarily in the white matter fiber tracts and followed a time course that was distinct from that of the hydrocephalus. Specifically, edema formation was gradual, peaked at 24 h and began to recede by 72 h after SAH, while hydrocephalus persisted. Mice with genetic deletion of sEH, which have elevated basal levels of EETs, had a similar severity of hydrocephalus and brain swelling compared to WT mice, but significantly less edema formation within the white matter. We tested one potential mechanism of this edema formation, vascular inflammation indicated by expression of VCAM-1, which was reduced in sEHKO mice compared to WT. However, this result was not statistically significant. Finally, sEHKO mice have improved behavioral outcome after SAH.

We have identified additional features of the endovascular puncture model that mimics human disease seen clinically. Specifically, a substantial number of SAH patients present with acute hydrocephalus at admission [190] and our model replicates this rapid time scale, a feature not found in other rodent models of hydrocephalus [182,191,192]. While we see the hydrocephalus lasting at least 72h in our model, we do not know the time frame at which hydrocephalus resolves, so whether our model represents the 10-20% of those chronically hydrocephalic patients that require implantation of semi-permanent shunts to manage unremitting disease [178,179] remains to be determined. Edema formation in our model shares similarities with the human condition as well. While human brains have a substantially larger percentage of white matter than mice [193], edema forms preferentially within white matter, sparing the grey matter [10,194], in both species. Both vasogenic and interstitial edema, the two most likely forms of the edema we see, develop preferentially in the white matter [195] and distinguishing between the two using our imaging modality is not possible. In future studies, we plan to use diffusion weighted imaging, which can distinguish between these two types of edema [195].

The anti-inflammatory effects of EETs are well documented in mice [174,184,196,197] and inform us about the etiology of hydrocephalus and edema after SAH. First, the rate of formation, severity, and persistence of hydrocephalus are not altered in sEHKO mice which have elevated levels of basal EETs. This supports our hypothesis that hydrocephalus is likely mechanical in nature and not inflammatory. We have previously shown that CSF flow is blocked within minutes of SAH by fibrin deposition within the CSF pathways [198]. We hypothesize that fibrin deposition within these CSF flow pathways is necessary and sufficient to induce acute communicating hydrocephalus after SAH. Additionally, while hydrocephalus is unchanged in the sEHKO mice, edema is significantly reduced in association with the reduction in vascular inflammation as measured by reduced VCAM-1 expression in the cerebrovasculature. However, it is important to note that VCAM-1 expression were not statistically different between groups. VCAM-1 is a cell adhesion molecule expressed by damaged or activated endothelium and important to the trans-migration of infiltrating inflammatory cells [65]. Elevated levels of VCAM-1 have been detected in the plasma and CSF of

SAH patients [67,68]. Its activation is generally accepted to be a part of the brain inflammatory response [65] [199] and has been associated with breakdown of the blood-brain barrier in other models of disease [185,200,201]. In this context, we interpret our finding to mean that vasogenic edema, brought on by the inflammatory response to SAH, is responsible in part for cerebral edema after SAH and that modulation of sEH to increase levels of EETs is protective.

Though we have shown that sEHKO mice have less vascular inflammation and cerebral edema associated with improved outcome after SAH, genetic deletion or inhibition of sEH to increase levels of EETs has shown to be protective in several models of disease by several different mechanisms [175]. The effect of EETs within the brain is broad and includes anti-inflammatory, anti-thrombotic [103], cytoprotective [202] and vasodilator effects [203]. Additionally, we have previously shown that delayed microvascular perfusion deficits, which are affected by sEH gene deletion, occur in this model of SAH. Thus, it is unlikely that the beneficial effects of sEH deletion are due to a single mechanism of action by EETs in this model. Despite this limitation, our findings here complement our previous work and support the hypothesis that sEH inhibition may be a viable therapeutic strategy in SAH through more than one mechanism.

In conclusion, the endovascular puncture model in the mouse is a reasonable model to study the etiology of acute communicating hydrocephalus and cerebral edema after SAH. Genetic deletion of sEH reduces vascular inflammation and edema formation in this model as well as improving outcome. This finding adds to the body of literature supporting further investigation of sEH inhibition as a therapeutic target in SAH.

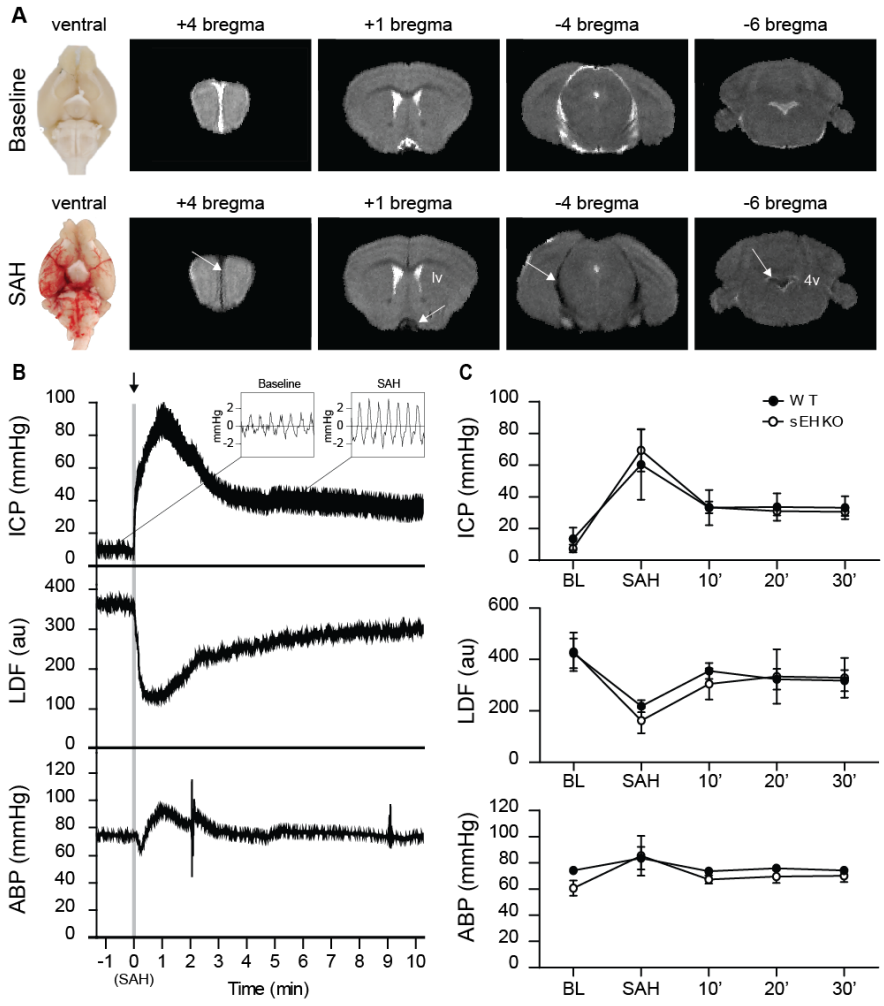

Figure 19. SAH causes similar changes to physiology in both WT and sEHKO mice. A.) Representative gross images (left) and T2 weighted MRI (right) of naïve (top) and SAH (bottom) mice 30 minutes after induction. Blood within CSF space causes the T2 weighted signal to change from white to black (arrows). Blood fills the subarachnoid space and retrogradely flows into the 4th ventricle. B.) Representative tracing of ICP, LDF and ABP in a WT SAH mouse. ICP rises to match ABP within the first minute of SAH before returning to a pressure above baseline. The ICP waveform (inset) fluctuates with systole to a greater degree after SAH indicating reduced CSF compliance. LDF decrease steeply at the time of hemorrhage before slowly returning toward baseline. C.) Average changes in ICP, LDF, and MAP in WT(n =5) and sEHKO(n = 5) mice after SAH. There were no significant differences between groups.

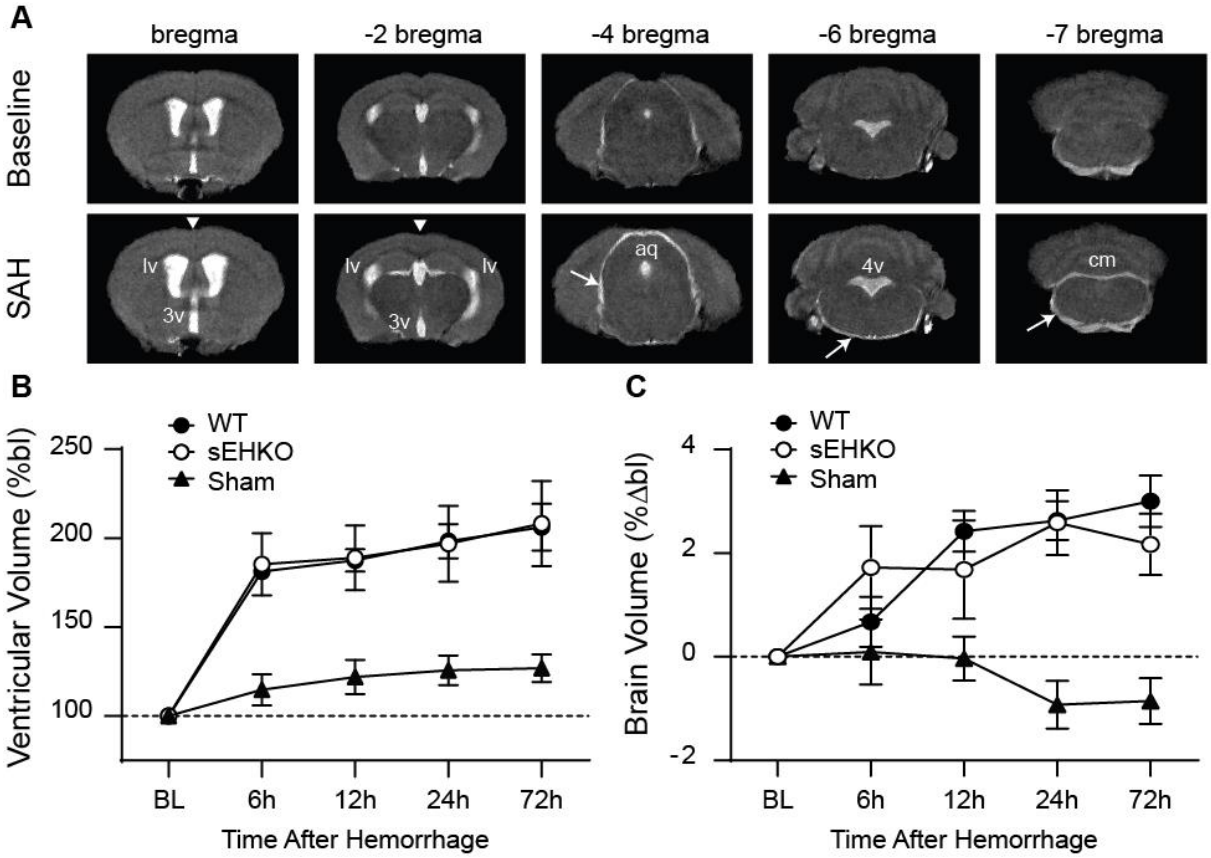

Figure 20. SAH induces acute communicating hydrocephalus in both WT and sEHKO mice. A.) representative T2 weight MRI images at baseline (top) and 6h after SAH (bottom). Expansion of the CSF space occurs at all levels including lateral ventricles (lv), third ventricle (3v), cerebral aqueduct (aq), fourth ventricle (4v), cisterna magna (cm) and the subarachnoid space (arrows). Effacement of the central sulcus is also apparent at 6h after SAH (arrowheads). B.) Ventricular volume changes WT (n = 10), sEHKO (n = 7) SAH animals and sham(n = 5). There is no significant difference between WT and sEHKO SAH mice. C.) Brain size changes WT (n = 10, sEHKO (n = 10) SAH animals and sham (n =5). There is no significant difference between WT and sEHKO SAH mice.

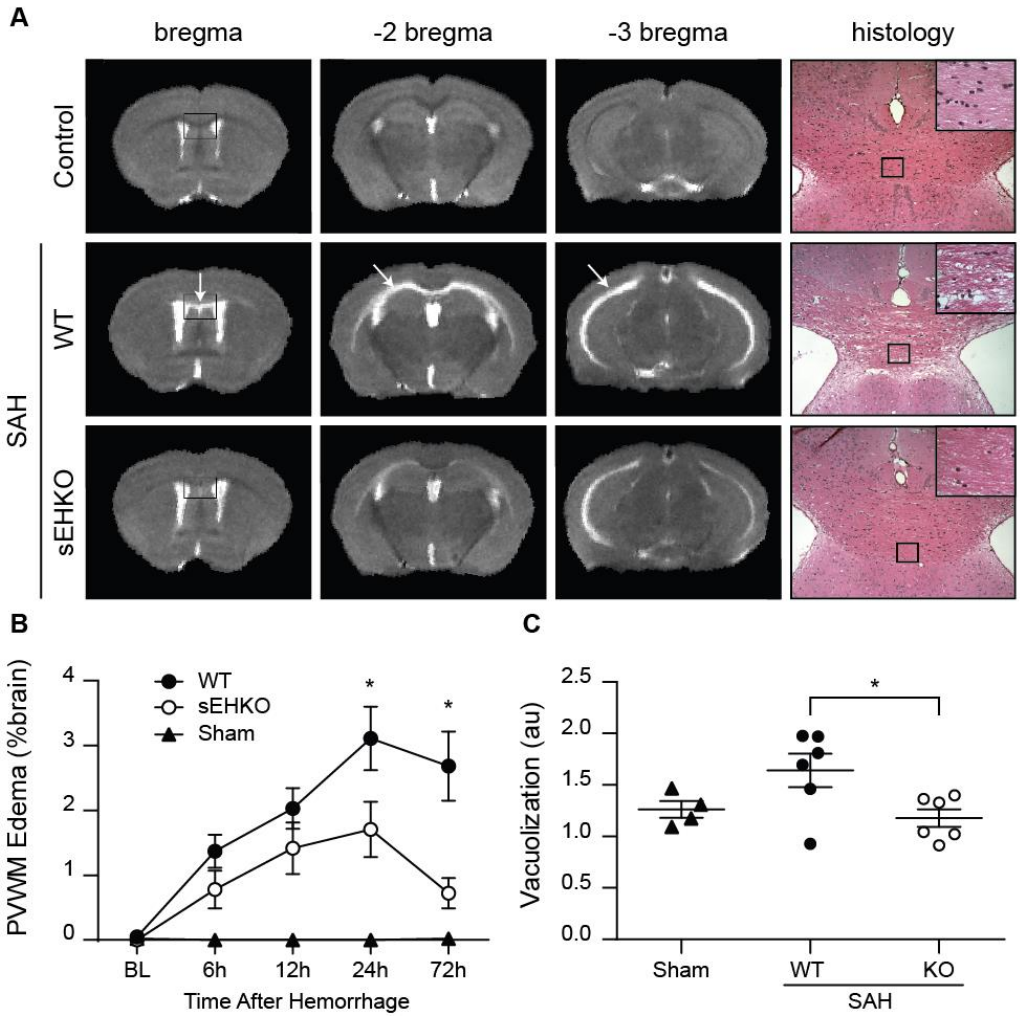

Figure 21. sEHKO mice have less edema than WT mice. A.) representative T2 weighted MRI images in sham (top) WT SAH (middle) and sEHKO SAH (bottom) at 24h after SAH. Edema forms in the specifically within the white matter of the corpus callosum and dorsal hippocampal commissures (arrows). Histological sections (right) of the corpus callosum 72h after SAH show vacuolization within the white matter of SAH mice. B.) Perventricular white matter edema formation as a percent of brain volume in WT (n =10), sEHKO (n = 7) and sham (n = 5) mice. sEHKO mice have less edema at 24h and 72h after SAH (* = $p<0.05$). C.) Vacuolization determined by changes in mean pixel intensity of the corpus callosum in WT SAH (n = 6), sEHKO SAH (n = 6) and sham (n =4) mice 72h after SAH. sEHKO mice have less vacuolization than WT mice (* = $p<0.05$).

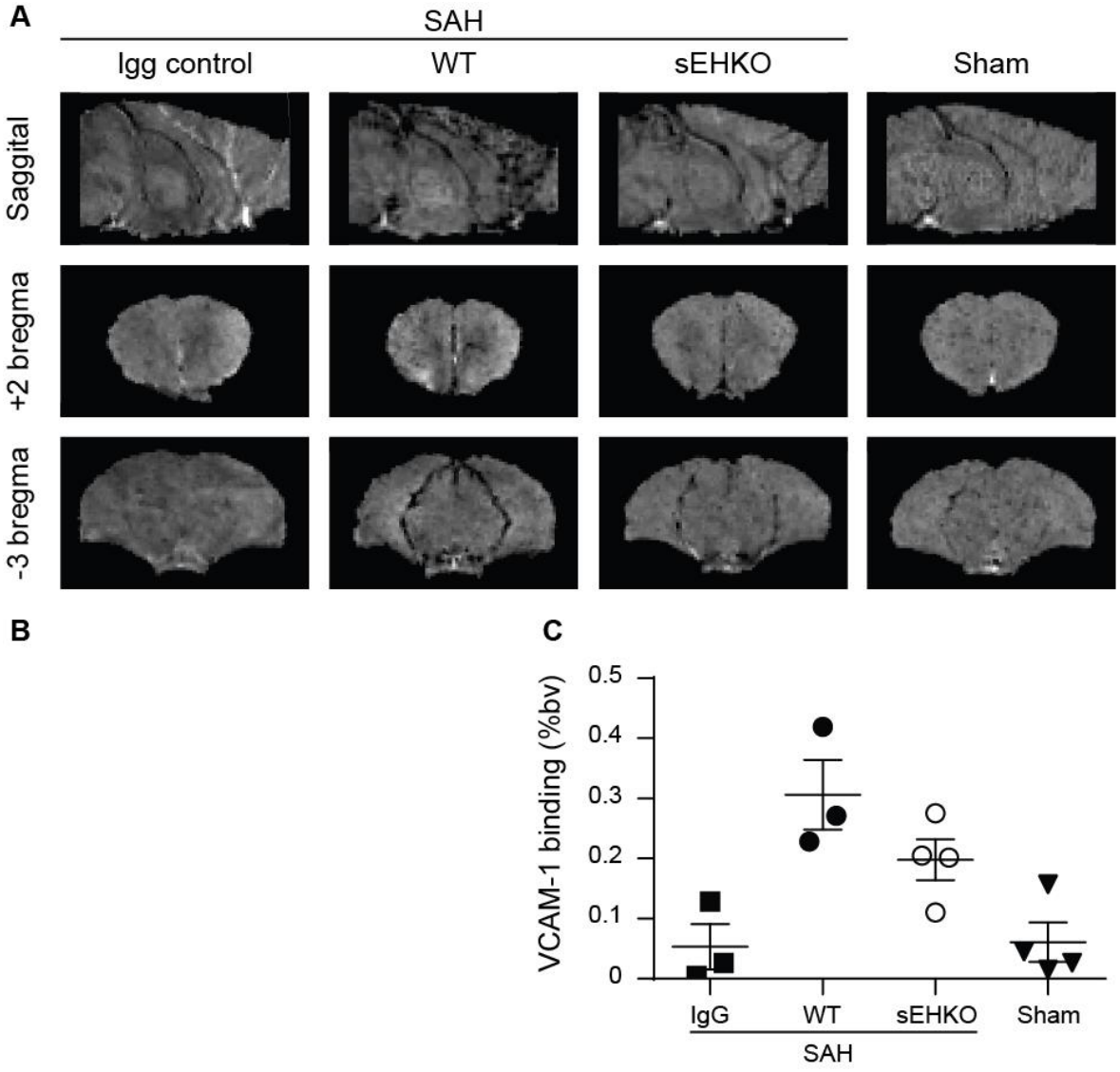

Figure 22. sEHKO mice may have less VCAM-1 expression than WT mice after SAH. A.) representative T2-star weighted images in SAH mice (IgG control, WT, and sEHKO) and sham operated mice. Deposition of the VCAM-1 MPIO causes hypointensity on MRI and was greatest along the vasculature in the midline of the animals as well as vasculature surrounding the midbrain. B.) Histology shows MPIO deposition within the vasculature. C.) Quantification of MPIO deposition as percent of brain volume (bv) in IgG control (n = 3) WT SAH (n =3) sEHKO SAH (n =4) and Sham (n =4). sEHKO mice have reduced MPIO deposition compared to WT mice (not significant).

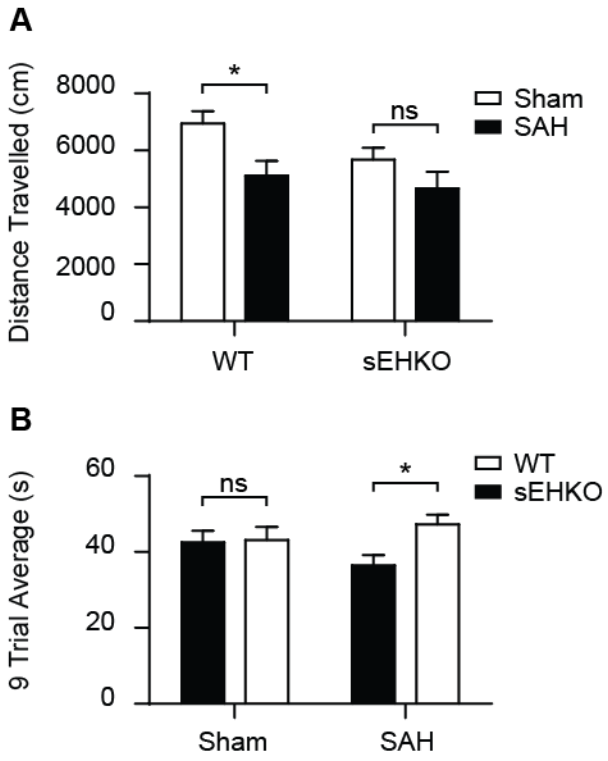

Figure 23. sEHKO mice have improved outcome after SAH. A.) 96h after SAH (WT n = 12, sEHKO n = 10) or sham (WT n = 10, sEHKO n =10), mice were placed in the open field for 10 min. sEHKO mice perform differently on the open field, so comparison within genotype was necessary. SAH reduces movement on open field for WT mice (* = $p<0.05$) but not sEHKO mice (ns = no significance) B.) 96h after SAH (WT = 12, sEHKO = 8) or sham (WT n = 10, sEHKO n = 10), animals were timed on the accelerated rotarod for three trials per day for three days. The average time to fall over the nine trials was increased in the sEHKO SAH mice compared to the WT SAH mice(* = $p< 0.05$)

Chapter 5

Discussion

5.1 Key Findings

- CSF flow into the brain parenchyma is completely blocked immediately after SAH due to fibrin deposition within CSF flow pathways. This blockade leads to intracranial hypertension and cortical hypoperfusion.

- Early tPA treatment can restore CSF flow in brain parenchyma after SAH which has effects on cortical perfusion that are independent of ICP.

- Both vasoconstrictive and vasodilatory P450 eicosanoids are elevated in the CSF after SAH. Concentrations of these eicosanoids in the CSF at early time points after SAH are capable of predicting the incidence of DCI in high risk patients.

- EETs are protective against both early and delayed microvascular dysfunction. In the early time point, sEHKO mice had reduced vascular inflammation and edema formation. Delayed decreases in cortical perfusion were also protected in sEHKO mice. This led to improved behavioral outcome in sEHKO mice after SAH.

- SAH induces a rapid acute communicating hydrocephalus and cerebral edema in mice.

5.2 Discussion

5.2.1 Blockade of CSF flow by fibrin after SAH

There are four known potential pathways of CSF flow out of the cranium. There are the arachnoid villi, the cervical lymphatics, the paravascular pathway and the spinal pathway. This study is unable to ascertain the status of all but the paravascular pathway, which can be clearly visualized as Evan's Blue dye movement into the brain (Figure 8). Nevertheless, this pathway is completely blocked within minutes of SAH and remains so for at least 24 hours (Figure 9). Theoretically, loss of this pathway represents complete loss of CSF function in conditioning the extracellular space of the brain parenchyma, the consequences of which are wholly unknown. There is substantial evidence that the

extracellular environment is altered after SAH in humans and animal models. This includes disruption of glucose homeostasis [115], elevated glutamate levels, elevated lactate/pyruvate ratios [204] and altered ionic homeostasis [205]. It is presumed that these are markers of cerebral ischemia, but an alternative hypothesis is that these are a consequence of impaired parenchymal CSF flow. This is testable using cerebral microdialysis [93] to assess how these levels change during SAH and after restoration of CSF flow.

While paravascular CSF flow may be critical for extracellular homeostasis, there is uncertainty as to the pathway's relative contribution to ICP determination. The cervical lymphatic pathway is thought to account for a significant portion of CSF outflow [87]. This pathway is also capable of accommodating whole red blood cells (personal observation) and may serve an important purpose in clearance of blood from the CSF. Does fibrin have a similar effect on flow through this pathway? Visualizing CSF flow through these cervical lymphatics is possible using either MRI or fluorescent tracers.

Chronic hydrocephalus has been associated with scarring within the subarachnoid space [206]. Does long term deposition of fibrin within CSF flow pathways promote subarachnoid scarring and chronically impaired CSF flow pathways? Does CSF diversion, which would hypothetically reduce positive pressure on these blocked pathways, exacerbate this process? This is testable by allowing the SAH mouse to survive for longer periods of time to determine if scarring occurs. CSF diversion could be accomplished using an external ventricular drain to test for exacerbation of pathway scarring.

5.2.2 Restoration of CSF Flow with tPA

tPA has been used as an off-label clot lysis therapy in SAH since 1991 [207], especially in patients who have large obstructive clots within the ventricular system. It's also thought that tPA can speed up removal of clots from the subarachnoid space to mitigate cerebral vasospasm [208]. However, employment of tPA on an SAH patient in

the early or ultra-early time points to prevent acute brain injury has not yet been considered. There is an important reason for this. In the early stages of SAH, most patients are *preoperative* meaning their aneurysm, a delicate piece of tissue that is prone to rupture, is still unsecured and may re-rupture at any time. The risk of aneurysm re-rupture within the first 6 hours of admission is 8% to 20% [209], and confers an 80% [8] risk of mortality or permanent neurological deficit. Because of this, any increase in the risk of re-rupture is unacceptable. It is assumed that introducing tPA into the same space as the aneurysm will increase the risk of re-rupture appreciably. However, pressure gradients in the brain (figure 24) are such that tPA would be unlikely to induce aneurysm rupture. Pre-operative tPA warrants further testing as a viable early therapy for SAH.

First and foremost, more work must be done to confirm the efficacy of tPA to reduce early brain injury in SAH. This includes assessment of other microvascular dysfunctions such as BBB disruption, inflammation and microthrombosis. Simultaneously, safety can be tested on a rudimentary level in rodent models. To test safety, the threshold for induced rupture by tPA in the mouse must be identified and compared to the threshold for effective prevention of early brain injury. Additionally, investigation of the re-rupture potential of combination therapy with intravenous anti-fibrinolytic drugs should be assessed. Plasma levels of tPA after cisterna injection should be measured, though the likelihood that cisternal tPA can appreciably raise plasma tPA levels is low due to the doses used. Finally, pressure-driven permeation is the key factor in the efficacy of tPA [146]. Can inducing a pressure gradient *inside* the subarachnoid space to drive tPA into the paravascular space improve the efficacy of therapy? The greatest limitation to study the safety of tPA therapy is the nature of the aneurysm, which may be more prone to bleed than an induced rupture in a rodent model. Ultimately, large animal testing will be necessary for establishment of a realistic therapeutic window.

5.2.3 P450 Eicosanoids can predict DCI

The value of an early test within the first 3 days of admission to reliably predict which patients are at high or low risk for DCI cannot be understated. The reason that SAH is so costly to treat is because the average SAH patient spends 12.6 days under observation in the intensive care unit [210]. The extended timeframe for the ICU stay is primarily due to the risk of DCI and the lack of predictive tests. The findings in Chapter 3 show that CSF P450 eicosanoid levels are able to stratify risk in individuals who were already at high risk for DCI. However, there are important limitations to the efficacy of this test that must be addressed. All analyses performed on the current testing thresholds were retrospectively established. Future studies examining the value of a P450 eicosanoid test should be a blinded prospective study of all comers with *a priori* testing criteria. Further, the current study relied on external ventricular drains for access to CSF, which limits qualified subjects to those being treated for intracranial hypertension. To test all SAH patients, a one-time lumbar puncture sample needs to be obtained. Is such a sample collection a viable and safe test with adequate temporal resolution? Considering that diagnostic criteria for SAH includes a lumbar puncture test, it is feasible that such a P450 eicosanoid test could be performed.

5.2.4 EETs are protective in early and delayed microvascular dysfunction after SAH

The findings in Chapters 3 and 4 show protection in sEHKO mice for both early and delayed microvascular dysfunction after SAH and identify EETs as an endogenous protective pathway in SAH. The greatest limitation to this finding is that all experiments were conducted in a genetically modified mouse which has elevated levels of basal EETs *before* induction of SAH. Because of the spontaneous nature of SAH, post ictal treatments are the only useful approach. Consequently, all of these findings must be repeated with use of a sEH inhibitor administered *after* SAH induction. Several potent sEH inhibitors [211] have been created that are effective in reducing infarct volume in models of cerebral ischemia [153]. Further, sEH inhibitors are currently in clinical trials for use in diabetes and hypertension.

It is not possible to attribute the beneficial effects of elevated EETs to protection via a single mechanism as multiple dysfunctional pathways are being affected. Additionally, EETs could have effects on microvascular dysfunctions after SAH not tested here including microthrombosis. Testing the effect of sEH inhibition on this microvascular pathology is warranted. Finally, there is building evidence that early brain injuries such as edema, early ischemia and hydrocephalus may contribute to the incidence of DCI. If sEH inhibitors are effective at mitigating early brain injury, then they may serve as a useful tool in exploring the relationship between early injury and DCI. To test this, sEH inhibitors would only be applied in the first 24 hours after SAH to determine if early treatment has an effect on delayed microvascular dysfunction.

5.2.5 A Mouse Model of Acute Communicating Hydrocephalus and Edema

Other models of hydrocephalus [182] lack the rapid development of communicating hydrocephalus found in this model, making this model ideal to gain an understanding of the mechanism behind SAH-induced hydrocephalus. The findings in Chapter 2 showing fibrin blockade of CSF flow pathways pose the question of whether early tPA treatment can prevent the formation of acute communicating hydrocephalus. The same questions regarding the development of chronic hydrocephalus can also be tested in this model.

The cerebral edema found in the mouse mimics the white matter-limited edema found in human patients [212]. Distinguishing between the sources of the edema is difficult however, given that both vasogenic and interstitial edema tend to congregate in the white matter [195]. However, the T2-weighted MRI modality represents a step above wet/dry brain water content measurements, which have no spacial resolution. Further, additional scanning modalities can be added on the same animal including dynamic contrast-enhanced MRI to study BBB permeability, diffusion-weighted MRI to characterize white matter water behavior [195] and T2-mapping to characterize absolute water level changes.

5.2.6 Multi-modal approach to treating subarachnoid hemorrhage.

As stated in the introduction, there are two known primary pathologies after SAH; transient global ischemia and blood in the subarachnoid space. It is likely that one therapy to reduce the effects of blood in the subarachnoid space will have little or no effect on the sequelae of transient global ischemia. Given that elevated levels of EETs in sEHKO mice do not alter hydrocephalus after SAH, but do reduce edema and inflammation, a logical question is whether intracisternal tPA's restoration of CSF flow could have a combinatorial effect on early brain injury. Further characterization of both potentially protective mechanisms individually and in combination with each other is warranted.

5.3 Technical Considerations

5.3.1 Anesthesia

There are known variations in outcome from the endovascular puncture model of SAH when induced under different anesthetic conditions. Specifically, isoflurane anesthesia has been demonstrated to be protective against mechanisms of microvascular dysfunction in SAH [213-215]. As isoflurane was used to induce SAH in all experiments of this thesis, this is an important consideration for two reasons. The first is that pathology reported in this thesis could be muted compared to what other labs using different anesthesia have reported. The second is that benefits seen in sEHKO mice or tPA-treated animals could be much larger than reported if isoflurane is masking some of the microvascular dysfunction. Future studies will address this consideration in anesthetic choice for studying SAH.

5.3.2 Behavioral Testing

Though we were able to identify differences in behavioral outcome between WT and sEHKO mice, there are several considerations for improving future studies on outcome in mice after SAH. The first is that sEHKO mice had different baseline behavior

on the open field test, which tests general locomotor activity but can be affected by anxiety. Second, the use of isoflurane might also be muting the differences between groups on behavioral testing. Finally, because we see white matter pathology after SAH, it may be beneficial to focus on tests of memory instead of the sensorimotor tests employed in Chapter 4. Future studies will explore memory-based tests for assessing efficacy of sEH inhibitors to protect in SAH.

5.4 Summary

SAH is a complex disease with many simultaneous pathological processes evolving together in the brain. The work in this thesis has identified one of the earliest pathologies that develops following SAH; blockade of CSF flow by fibrin. Reversal of this early pathology has the potential to prevent development of secondary sequelae. Additionally, this work has identified EETs as an endogenous protective pathway that modulates both early and delayed microvascular dysfunction and is amenable to augmentation through small molecule inhibition of its metabolizing enzyme sEH. Work in both of these therapeutic pathways is preliminary and requires further experimentation to confirm these findings.

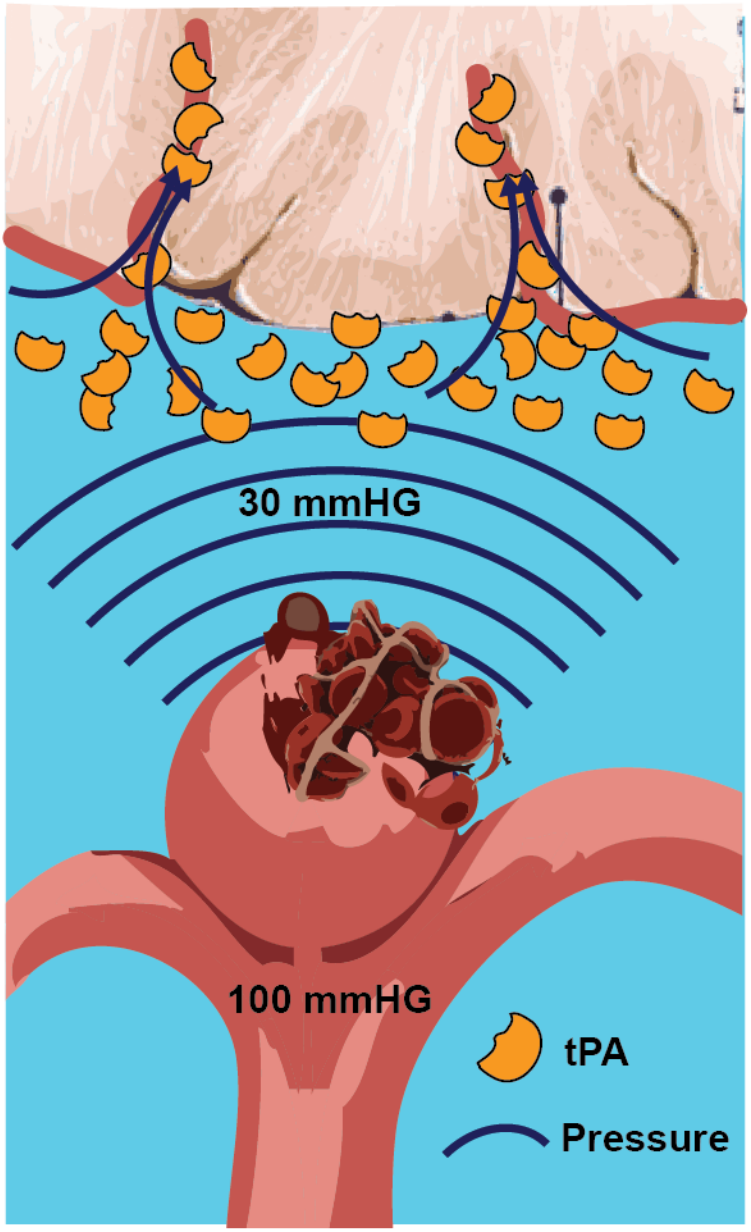

Figure 24 Pressure Driven Permeation Spares the Aneurysm. Tissue plasminogen activator (tPA) injected into the subarachnoid space will be driven into the parenchyma by prevailing pressure gradients. The large pressure gradient from the aneurysm into the subarachnoid space will not support lysis of the aneurysm clot.

References

1. Vernooij MW, Ikram MA, Tanghe HL, et al. Incidental Findings on Brain MRI in the General Population. New England Journal of Medicine 2007;357:1821-8.
2. Stegmayr B, Eriksson M, Asplund K. Declining Mortality From Subarachnoid Hemorrhage: Changes in Incidence and Case Fatality From 1985 Through 2000. Stroke 2004;35:2059-63.
3. Hop JW, Rinkel GJE, Algra A, van Gijn J. Case-Fatality Rates and Functional Outcome After Subarachnoid Hemorrhage: A Systematic Review. Stroke 1997;28:660-4.
4. le Roux AA, Wallace MC. Outcome and cost of aneurysmal subarachnoid hemorrhage. Neurosurgery clinics of North America 2010;21:235-46.
5. Dorhout Mees SM, Kerr RS, Rinkel GJ, Algra A, Molyneux AJ. Occurrence and impact of delayed cerebral ischemia after coiling and after clipping in the International Subarachnoid Aneurysm Trial (ISAT). Journal of neurology 2012;259:679-83.
6. Brinjikji W, Kallmes DF, Lanzino G, Cloft HJ. Hospitalization costs for endovascular and surgical treatment of ruptured aneurysms in the United States are substantially higher than Medicare payments. AJNR American journal of neuroradiology 2012;33:1037-40.
7. Taylor TN, Davis PH, Torner JC, Holmes J, Meyer JW, Jacobson MF. Lifetime cost of stroke in the United States. Stroke 1996;27:1459-66.
8. van Gijn J, Kerr RS, Rinkel GJE. Subarachnoid haemorrhage. The Lancet;369:306-18.
9. Hasan D, Vermeulen M, Wijdicks EF, Hijdra A, van Gijn J. Management problems in acute hydrocephalus after subarachnoid hemorrhage. Stroke 1989;20:747-53.
10. Claassen J, Carhuapoma JR, Kreiter KT, Du EY, Connolly ES, Mayer SA. Global Cerebral Edema After Subarachnoid Hemorrhage: Frequency, Predictors, and Impact on Outcome. Stroke 2002;33:1225-32.
11. Dorsch N. A clinical review of cerebral vasospasm and delayed ischaemia following aneurysm rupture. Acta neurochirurgica Supplement 2011;110:5-6.
12. Brathwaite S, Macdonald RL. Current Management of Delayed Cerebral Ischemia: Update from Results of Recent Clinical Trials. Translational stroke research 2013.
13. Wartenberg KE, Mayer SA. Medical Complications After Subarachnoid Hemorrhage. Neurosurgery clinics of North America 2010;21:325-38.
14. Al-Khindi T, Macdonald RL, Schweizer TA. Cognitive and Functional Outcome After Aneurysmal Subarachnoid Hemorrhage. Stroke 2010;41:e519-e36.
15. Bederson JB, Connolly ES, Batjer HH, et al. Guidelines for the Management of Aneurysmal Subarachnoid Hemorrhage: A Statement for Healthcare Professionals From a Special Writing Group of the Stroke Council, American Heart Association. Stroke 2009;40:994-1025.
16. Diringer MN, Bleck TP, Claude Hemphill J, 3rd, et al. Critical care management of patients following aneurysmal subarachnoid hemorrhage: recommendations from the Neurocritical Care Society's Multidisciplinary Consensus Conference. Neurocrit Care 2011;15:211-40.
17. Ecker A, Riemenschneider PA. Arteriographic Demonstration of Spasm of the Intracranial Arteries with Special Reference to Saccular Arterial Aneurisms*. Journal of Neurosurgery 1951;8:660-7.
18. Tso M, Macdonald RL. Subarachnoid Hemorrhage: a Review of Experimental Studies on the Microcirculation and the Neurovascular Unit. Translational stroke research 2014;5:174-89.
19. Shen J, Pan J-W, Fan Z-X, Xiong X-X, Zhan R-Y. Dissociation of vasospasm-related morbidity and outcomes in patients with aneurysmal subarachnoid hemorrhage treated with clazosentan: a meta-analysis of randomized controlled trials. Journal of Neurosurgery 2013;119:180-9.

20. Mima T, Yanagisawa M, Shigeno T, et al. Endothelin acts in feline and canine cerebral arteries from the adventitial side. Stroke 1989;20:1553-6.
21. Vatter H, Zimmermann M, Tesanovic V, Raabe A, Schilling L, Seifert V. Cerebrovascular characterization of clazosentan, the first nonpeptide endothelin receptor antagonist clinically effective for the treatment of cerebral vasospasm. Part I: Inhibitory effect on endothelinA receptor—mediated contraction. Journal of Neurosurgery 2005;102:1101-7.
22. Sabri M, Ai J, Macdonald RL. Dissociation of Vasospasm and Secondary Effects of Experimental Subarachnoid Hemorrhage by Clazosentan. Stroke 2011;42:1454-60.
23. Dupont S, Rabinstein AA. Extent of acute hydrocephalus after subarachnoid hemorrhage as a risk factor for poor functional outcome. Neurological research 2013;35:107-10.
24. Mokri B. The Monro–Kellie hypothesis: Applications in CSF volume depletion. Neurology 2001;56:1746-8.
25. Tso MK, Macdonald RL. Acute Microvascular Changes after Subarachnoid Hemorrhage and Transient Global Cerebral Ischemia. Stroke research and treatment 2013;2013:9.
26. Heuer GG, Smith MJ, Elliott JP, Winn HR, Leroux PD. Relationship between intracranial pressure and other clinical variables in patients with aneurysmal subarachnoid hemorrhage. Journal of Neurosurgery 2004;101:408-16.
27. Julow J, Ishii M, Iwabuchi T. Scanning electron microscopy of the subarachnoid macrophages after subarachnoid haemorrhage, and their possible role in the formation of subarachnoid fibrosis. Acta Neurochir (Wien) 1979;50:273-80.
28. Sonobe M, Suzuki J. Vasospasmogenic substance produced following subarachnoid haemorrhage, and its fate. Acta Neurochir (Wien) 1978;44:97-106.
29. Boullin DJ, Tagari P, du Boulay G, Aitken V, Hughes JT. The role of hemoglobin in the etiology of cerebral vasospasm. Journal of Neurosurgery 1983;59:231-6.
30. Kajita Y, Dietrich HH, Dacey RG, Jr. Effects of oxyhemoglobin on local and propagated vasodilatory responses induced by adenosine, adenosine diphosphate, and adenosine triphosphate in rat cerebral arterioles. Journal of neurosurgery 1996;85:908-16.
31. Allen GS, Henderson LM, Chou SN, French LA. Cerebral arterial spasm. Journal of Neurosurgery 1974;40:433-41.
32. Marbacher S, Fandino J, Kitchen ND. Standard intracranial in vivo animal models of delayed cerebral vasospasm. British journal of neurosurgery 2010;24:415-34.
33. Megyesi J, Vollrath B, Cook D, Findlay J. In Vivo Animal Models of Cerebral Vasospasm: A Review. 2000;46:448.
34. Schubert R, Mulvany MJ. The myogenic response: established facts and attractive hypotheses. Clin Sci 1999;96:313-26.
35. Michel F. Part 1: Multiple Functions of the Endothelial Cells—Focus on Endothelium-Derived Vasoactive Mediators. In: The Endothelium: Morgan & Claypool Life Sciences; 2011.
36. Ignarro LJ, Byrns RE, Buga GM, Wood KS. Endothelium-derived relaxing factor from pulmonary artery and vein possesses pharmacologic and chemical properties identical to those of nitric oxide radical. Circulation research 1987;61:866-79.
37. Busse R, Edwards G, Félétou M, Fleming I, Vanhoutte PM, Weston AH. EDHF: bringing the concepts together. Trends in Pharmacological Sciences 2002;23:374-80.
38. Koller A, Sun D, Kaley G. Role of shear stress and endothelial prostaglandins in flow- and viscosity-induced dilation of arterioles in vitro. Circulation research 1993;72:1276-84.
39. You J, Johnson TD, Marrelli SP, Bryan RM, Jr. Functional heterogeneity of endothelial P2 purinoceptors in the cerebrovascular tree of the rat. The American journal of physiology 1999;277:H893-900.
40. Cipolla MJ, Smith J, Kohlmeyer MM, Godfrey JA. SKCa and IKCa Channels, myogenic tone, and vasodilator responses in middle cerebral arteries and parenchymal arterioles: effect of ischemia and reperfusion. Stroke 2009;40:1451-7.

41. Golding EM, You J, Robertson CS, Bryan RM, Jr. Potentiated endothelium-derived hyperpolarizing factor-mediated dilations in cerebral arteries following mild head injury. Journal of neurotrauma 2001;18:691-7.
42. Dunn KM, Nelson MT. Neurovascular signaling in the brain and the pathological consequences of hypertension; 2014.
43. Bekar LK, Wei HS, Nedergaard M. The locus coeruleus-norepinephrine network optimizes coupling of cerebral blood volume with oxygen demand. Journal of cerebral blood flow and metabolism : official journal of the International Society of Cerebral Blood Flow and Metabolism 2012;32:2135-45.
44. Uhl E, Lehmberg J, Steiger H-J, Messmer K. Intraoperative Detection of Early Microvasospasm in Patients with Subarachnoid Hemorrhage by Using Orthogonal Polarization Spectral Imaging. 2003;52:1307-17.
45. Wiernsperger N, Schulz U, Gygax P. Physiological and morphometric analysis of the microcirculation of the cerebral cortex under acute vasospasm. Stroke; a journal of cerebral circulation 1981;12:624-7.
46. Ohkuma H, Suzuki S. Histological dissociation between intra- and extraparenchymal portion of perforating small arteries after experimental subarachnoid hemorrhage in dogs. Acta Neuropathol 1999;98:374-82.
47. Ohkuma H, Itoh K, Shibata S, Suzuki S. Morphological changes of intraparenchymal arterioles after experimental subarachnoid hemorrhage in dogs. Neurosurgery 1997;41:230-5; discussion 5-6.
48. Johshita H, Kassell NF, Sasaki T, Ogawa H. Impaired capillary perfusion and brain edema following experimental subarachnoid hemorrhage: a morphometric study. Journal of neurosurgery 1990;73:410-7.
49. Sehba FA, Friedrich V, Jr., Makonnen G, Bederson JB. Acute cerebral vascular injury after subarachnoid hemorrhage and its prevention by administration of a nitric oxide donor. Journal of neurosurgery 2007;106:321-9.
50. Friedrich V, Flores R, Muller A, Sehba FA. Luminal platelet aggregates in functional deficits in parenchymal vessels after subarachnoid hemorrhage. Brain research 2010;1354:179-87.
51. Sun BL, Zheng CB, Yang MF, Yuan H, Zhang SM, Wang LX. Dynamic alterations of cerebral pial microcirculation during experimental subarachnoid hemorrhage. Cellular and molecular neurobiology 2009;29:235-41.
52. Friedrich B, Muller F, Feiler S, Scholler K, Plesnila N. Experimental subarachnoid hemorrhage causes early and long-lasting microarterial constriction and microthrombosis: an in-vivo microscopy study. Journal of cerebral blood flow and metabolism : official journal of the International Society of Cerebral Blood Flow and Metabolism 2012;32:447-55.
53. Koide M, Wellman GC. SAH-induced suppression of voltage-gated K(+) (K (V)) channel currents in parenchymal arteriolar myocytes involves activation of the HB-EGF/EGFR pathway. Acta neurochirurgica Supplement 2013;115:179-84.
54. Nystoriak MA, O'Connor KP, Sonkusare SK, Brayden JE, Nelson MT, Wellman GC. Fundamental increase in pressure-dependent constriction of brain parenchymal arterioles from subarachnoid hemorrhage model rats due to membrane depolarization. American journal of physiology Heart and circulatory physiology 2011;300:H803-12.
55. Park KW, Metais C, Dai HB, Comunale ME, Sellke FW. Microvascular endothelial dysfunction and its mechanism in a rat model of subarachnoid hemorrhage. Anesthesia and analgesia 2001;92:990-6.
56. Vollmer DG, Takayasu M, Dacey RG, Jr. An in vitro comparative study of conducting vessels and penetrating arterioles after experimental subarachnoid hemorrhage in the rabbit. Journal of neurosurgery 1992;77:113-9.

57. Katusic ZS, Milde JH, Cosentino F, Mitrovic BS. Subarachnoid hemorrhage and endothelial L-arginine pathway in small brain stem arteries in dogs. Stroke; a journal of cerebral circulation 1993;24:392-9.
58. Park IS, Meno JR, Witt CE, et al. Impairment of intracerebral arteriole dilation responses after subarachnoid hemorrhage. Laboratory investigation. Journal of neurosurgery 2009;111:1008-13.
59. Britz GW, Meno JR, Park IS, et al. Time-dependent alterations in functional and pharmacological arteriolar reactivity after subarachnoid hemorrhage. Stroke; a journal of cerebral circulation 2007;38:1329-35.
60. Koide M, Bonev AD, Nelson MT, Wellman GC. Subarachnoid blood converts neurally evoked vasodilation to vasoconstriction in rat brain cortex. Acta neurochirurgica Supplement 2013;115:167-71.
61. Koide M, Bonev AD, Nelson MT, Wellman GC. Inversion of neurovascular coupling by subarachnoid blood depends on large-conductance Ca2+-activated K+ (BK) channels. Proceedings of the National Academy of Sciences of the United States of America 2012;109:E1387-95.
62. Reese TS, Karnovsky MJ. FINE STRUCTURAL LOCALIZATION OF A BLOOD-BRAIN BARRIER TO EXOGENOUS PEROXIDASE. The Journal of Cell Biology 1967;34:207-17.
63. Brightman MW, Reese TS. JUNCTIONS BETWEEN INTIMATELY APPOSED CELL MEMBRANES IN THE VERTEBRATE BRAIN. The Journal of Cell Biology 1969;40:648-77.
64. DeBault LE, Cancilla PA. $\gamma $-Glutamyl Transpeptidase in Isolated Brain Endothelial Cells: Induction by Glial Cells in vitro. Science 1980;207:653-5.
65. Muldoon LL, Alvarez JI, Begley DJ, et al. Immunologic privilege in the central nervous system and the blood-brain barrier. Journal of cerebral blood flow and metabolism : official journal of the International Society of Cerebral Blood Flow and Metabolism 2013;33:13-21.
66. Tailor A, Cooper D, Granger DN. Platelet–Vessel Wall Interactions in the Microcirculation. Microcirculation 2005;12:275-85.
67. Kaynar MY, Tanriverdi T, Kafadar AM, et al. Detection of soluble intercellular adhesion molecule—1 and vascular cell adhesion molecule—1 in both cerebrospinal fluid and serum of patients after aneurysmal subarachnoid hemorrhage. J Neurosurg 2004;101:1030-6.
68. Frijns CJM, Fijnheer R, Algra A, van Mourik JA, van Gijn J, Rinkel GJE. Early circulating levels of endothelial cell activation markers in aneurysmal subarachnoid haemorrhage: associations with cerebral ischaemic events and outcome. Journal of Neurology, Neurosurgery & Psychiatry 2006;77:77-83.
69. Ansar S, Edvinsson L. Subtype activation and interaction of protein kinase C and mitogen-activated protein kinase controlling receptor expression in cerebral arteries and microvessels after subarachnoid hemorrhage. Stroke 2008;39:185-90.
70. Friedrich V, Flores R, Muller A, Bi W, Peerschke E, Sehba F. Reduction of neutrophil activity decreases early microvascular injury after subarachnoid haemorrhage. Journal of Neuroinflammation 2011;8:103.
71. Sabri M, Ai J, Lakovic K, D'Abbondanza J, Ilodigwe D, Macdonald RL. Mechanisms of microthrombi formation after experimental subarachnoid hemorrhage. Neuroscience 2012;224:26-37.
72. Ishikawa M, Kusaka G, Yamaguchi N, et al. PLATELET AND LEUKOCYTE ADHESION IN THE MICROVASCULATURE AT THE CEREBRAL SURFACE IMMEDIATELY AFTER SUBARACHNOID HEMORRHAGE. Neurosurgery 2009;64:546-54 10.1227/01.NEU.0000337579.05110.F4.
73. Zhou N, Xu T, Bai Y, et al. Protective Effects of Urinary Trypsin Inhibitor on Vascular Permeability Following Subarachnoid Hemorrhage in a Rat Model. CNS Neuroscience & Therapeutics 2013;19:659-66.

74. Yatsushige H, Ostrowski RP, Tsubokawa T, Colohan A, Zhang JH. Role of c-Jun N-terminal kinase in early brain injury after subarachnoid hemorrhage. Journal of neuroscience research 2007;85:1436-48.
75. Germanò A, d'Avella D, Imperatore C, Caruso G, Tomasello F. Time-Course of Blood-Brain Barrier Permeability Changes After Experimental Subarachnoid Haemorrhage. Acta Neurochir (Wien) 2000;142:575-81.
76. Suzuki H, Ayer R, Sugawara T, et al. Protective effects of recombinant osteopontin on early brain injury after subarachnoid hemorrhage in rats. Critical care medicine 2010;38:612-8.
77. Gules I, Satoh M, Nanda A, Zhang JH. Apoptosis, blood-brain barrier, and subarachnoid hemorrhage. Acta neurochirurgica Supplement 2003;86:483-7.
78. Prunell GF, Svendgaard NA, Alkass K, Mathiesen T. Delayed cell death related to acute cerebral blood flow changes following subarachnoid hemorrhage in the rat brain. J Neurosurg 2005;102:1046-54.
79. Sehba FA, Friedrich V. Cerebral microvasculature is an early target of subarachnoid hemorrhage. Acta neurochirurgica Supplement 2013;115:199-205.
80. Granger DN SE. Inflammation and the Microcirculation. In: Morgan & Claypool Life Sciences; 2010.
81. Sehba FA, Mostafa G, Friedrich V, Bederson JB. Acute microvascular platelet aggregation after subarachnoid hemorrhage. Journal of neurosurgery 2005;102:1094-100.
82. Pisapia JM, Xu X, Kelly J, et al. Microthrombosis after experimental subarachnoid hemorrhage: Time course and effect of red blood cell-bound thrombin-activated pro-urokinase and clazosentan. Experimental Neurology 2012;233:357-63.
83. Bell JD, Thomas TC, Lass E, et al. Platelet-mediated changes to neuronal glutamate receptor expression at sites of microthrombosis following experimental subarachnoid hemorrhage. Journal of neurosurgery;0:1-8.
84. Sabri M, Ai J, Lass E, D'Abbondanza J, Macdonald RL. Genetic elimination of eNOS reduces secondary complications of experimental subarachnoid hemorrhage. Journal of cerebral blood flow and metabolism : official journal of the International Society of Cerebral Blood Flow and Metabolism 2013;33:1008-14.
85. Brinker T, Stopa E, Morrison J, Klinge P. A new look at cerebrospinal fluid circulation. Fluids and Barriers of the CNS 2014;11:10.
86. Rubin RC, Henderson ES, Ommaya AK, Walker MD, Rall DP. The Production of Cerebrospinal Fluid in Man and Its Modification by Acetazolamide. Journal of Neurosurgery 1966;25:430-6.
87. Pollay M. The function and structure of the cerebrospinal fluid outflow system. Cerebrospinal Fluid Research 2010;7:9.
88. Gijn J, Dongen KJ. The time course of aneurysmal haemorrhage on computed tomograms. Neuroradiology 1982;23:153-6.
89. Pluta RM, Afshar JKB, Boock RJ, Oldfield EH. Temporal changes in perivascular concentrations of oxyhemoglobin, deoxyhemoglobin, and methemoglobin after subarachnoid hemorrhage. Journal of Neurosurgery 1998;88:557-61.
90. Brinker T, Seifert V, Stolke D. Acute changes in the dynamics of the cerebrospinal fluid system during experimental subarachnoid hemorrhage. Neurosurgery 1990;27:369-72.
91. Brinker T, Seifert V, Dietz H. Subacute hydrocephalus after experimental subarachnoid hemorrhage: its prevention by intrathecal fibrinolysis with recombinant tissue plasminogen activator. Neurosurgery 1992;31:306-11; discussion 11-2.
92. Bragin DE, Bush RC, Nemoto EM. Effect of Cerebral Perfusion Pressure on Cerebral Cortical Microvascular Shunting at High Intracranial Pressure in Rats. Stroke 2013;44:177-81.
93. Persson L, Valtysson J, Enblad P, et al. Neurochemical monitoring using intracerebral microdialysis in patients with subarachnoid hemorrhage. Journal of Neurosurgery 1996;84:606-16.

94. Doczi T, Joo F, Szerdahelyi P, Bodosi M. Regulation of brain water and electrolyte contents: the opposite actions of central vasopressin and atrial natriuretic factor (ANF). Acta neurochirurgica Supplementum 1988;43:186-8.
95. Iliff JJ, Jia J, Nelson J, Goyagi T, Klaus J, Alkayed NJ. Epoxyeicosanoid signaling in CNS function and disease. Prostaglandins & other lipid mediators 2010;91:68-84.
96. Dietrich HH, Horiuchi T, Xiang C, Hongo K, Falck JR, Dacey RG, Jr. Mechanism of ATP-induced local and conducted vasomotor responses in isolated rat cerebral penetrating arterioles. Journal of vascular research 2009;46:253-64.
97. Gebremedhin D, Ma YH, Falck JR, Roman RJ, VanRollins M, Harder DR. Mechanism of action of cerebral epoxyeicosatrienoic acids on cerebral arterial smooth muscle. 1992;263:H519-H25.
98. Zhang G, Kodani S, Hammock BD. Stabilized epoxygenated fatty acids regulate inflammation, pain, angiogenesis and cancer. Progress in Lipid Research 2014;53:108-23.
99. Koerner IP, Jacks R, DeBarber AE, et al. Polymorphisms in the human soluble epoxide hydrolase gene EPHX2 linked to neuronal survival after ischemic injury. The Journal of neuroscience : the official journal of the Society for Neuroscience 2007;27:4642-9.
100. Liu M, Alkayed NJ. Hypoxic preconditioning and tolerance via hypoxia inducible factor (HIF) 1alpha-linked induction of P450 2C11 epoxygenase in astrocytes. Journal of cerebral blood flow and metabolism : official journal of the International Society of Cerebral Blood Flow and Metabolism 2005;25:939-48.
101. Dhanasekaran A, Al-Saghir R, Lopez B, et al. Protective effects of epoxyeicosatrienoic acids on human endothelial cells from the pulmonary and coronary vasculature. American journal of physiology Heart and circulatory physiology 2006;291:H517-31.
102. Yang B, Graham L, Dikalov S, et al. Overexpression of cytochrome P450 CYP2J2 protects against hypoxia-reoxygenation injury in cultured bovine aortic endothelial cells. Molecular pharmacology 2001;60:310-20.
103. Heizer ML, McKinney JS, Ellis EF. 14,15-Epoxyeicosatrienoic acid inhibits platelet aggregation in mouse cerebral arterioles. Stroke 1991;22:1389-93.
104. Chacos N, Capdevila J, Falck JR, et al. The reaction of arachidonic acid epoxides (epoxyeicosatrienoic acids) with a cytosolic epoxide hydrolase. Archives of Biochemistry and Biophysics 1983;223:639-48.
105. Sinal CJ, Miyata M, Tohkin M, Nagata K, Bend JR, Gonzalez FJ. Targeted Disruption of Soluble Epoxide Hydrolase Reveals a Role in Blood Pressure Regulation. Journal of Biological Chemistry 2000;275:40504-10.
106. Zhang W, Iliff JJ, Campbell CJ, Wang RK, Hurn PD, Alkayed NJ. Role of soluble epoxide hydrolase in the sex-specific vascular response to cerebral ischemia. Journal of cerebral blood flow and metabolism : official journal of the International Society of Cerebral Blood Flow and Metabolism 2009;29:1475-81.
107. Zhang W, Otsuka T, Sugo N, et al. Soluble epoxide hydrolase gene deletion is protective against experimental cerebral ischemia. Stroke 2008;39:2073-8.
108. Manhiani M, Quigley JE, Knight SF, et al. Soluble epoxide hydrolase gene deletion attenuates renal injury and inflammation with DOCA-salt hypertension. 2009;297:F740-F8.
109. Johanson C, Duncan J, Klinge P, Brinker T, Stopa E, Silverberg G. Multiplicity of cerebrospinal fluid functions: New challenges in health and disease. Cerebrospinal Fluid Research 2008;5:10.
110. Caner B, Hou J, Altay O, Fuj M, 2nd, Zhang JH. Transition of research focus from vasospasm to early brain injury after subarachnoid hemorrhage. Journal of neurochemistry 2012;123 Suppl 2:12-21.
111. de Rooij NK, Greving JP, Rinkel GJE, Frijns CJM. Early Prediction of Delayed Cerebral Ischemia After Subarachnoid Hemorrhage: Development and Validation of a Practical Risk Chart. Stroke 2013.

112. Kreiter KT, Copeland D, Bernardini GL, et al. Predictors of Cognitive Dysfunction After Subarachnoid Hemorrhage. Stroke 2002;33:200-9.
113. Yan J, Li L, Khatibi NH, et al. Blood–brain barrier disruption following subarchnoid hemorrhage may be faciliated through PUMA induction of endothelial cell apoptosis from the endoplasmic reticulum. Experimental Neurology 2011;230:240-7.
114. Sarrafzadeh A, Haux D, Sakowitz O, et al. Acute Focal Neurological Deficits in Aneurysmal Subarachnoid Hemorrhage: Relation of Clinical Course, CT Findings, and Metabolite Abnormalities Monitored With Bedside Microdialysis. Stroke 2003;34:1382-8.
115. Sakowitz OW, Santos E, Nagel A, et al. Clusters of Spreading Depolarizations Are Associated With Disturbed Cerebral Metabolism in Patients With Aneurysmal Subarachnoid Hemorrhage. Stroke 2013;44:220-3.
116. Lee J-Y, He Y, Sagher O, Keep R, Hua Y, Xi G. Activated autophagy pathway in experimental subarachnoid hemorrhage. Brain research 2009;1287:126-35.
117. Endo H, Nito C, Kamada H, Yu F, Chan PH. Reduction in oxidative stress by superoxide dismutase overexpression attenuates acute brain injury after subarachnoid hemorrhage via activation of Akt/glycogen synthase kinase-3beta survival signaling. Journal of cerebral blood flow and metabolism : official journal of the International Society of Cerebral Blood Flow and Metabolism 2007;27:975-82.
118. Westermaier T, Jauss A, Eriskat J, Kunze E, Roosen K. Acute vasoconstriction: decrease and recovery of cerebral blood flow after various intensities of experimental subarachnoid hemorrhage in rats. Journal of Neurosurgery 2009;110:996-1002.
119. Woernle CM, Winkler KML, Burkhardt J-K, et al. Hydrocephalus in 389 patients with aneurysm-associated subarachnoid hemorrhage. Journal of Clinical Neuroscience 2013;20:824-6.
120. Schubert G, Seiz M, Hegewald A, Manville J, Thomé C. Hypoperfusion in the Acute Phase of Subarachnoid Hemorrhage. In: Feng H, Mao Y, Zhang J, eds. Early Brain Injury or Cerebral Vasospasm: Springer Vienna; 2011:35-8.
121. Iliff JJ, Wang M, Liao Y, et al. A Paravascular Pathway Facilitates CSF Flow Through the Brain Parenchyma and the Clearance of Interstitial Solutes, Including Amyloid β. Science Translational Medicine 2012;4:147ra11.
122. Jackowski A, Crockard A, Burnstock G, Russell RR, Kristek F. The time course of intracranial pathophysiological changes following experimental subarachnoid haemorrhage in the rat. Journal of cerebral blood flow and metabolism : official journal of the International Society of Cerebral Blood Flow and Metabolism 1990;10:835-49.
123. Wang RK, Jacques SL, Ma Z, Hurst S, Hanson SR, Gruber A. Three dimensional optical angiography. Opt Express 2007;15:4083-97.
124. Jia Y, Alkayed N, Wang RK. Potential of optical microangiography to monitor cerebral blood perfusion and vascular plasticity following traumatic brain injury in mice in vivo. Journal of biomedical optics 2009;14:040505.
125. Sozen T, Tsuchiyama R, Hasegawa Y, et al. Role of interleukin-1beta in early brain injury after subarachnoid hemorrhage in mice. Stroke 2009;40:2519-25.
126. Schubert GA, Seiz M, Hegewald AA, Manville J, Thome C. Acute hypoperfusion immediately after subarachnoid hemorrhage: a xenon contrast-enhanced CT study. Journal of neurotrauma 2009;26:2225-31.
127. Abbott NJ. Evidence for bulk flow of brain interstitial fluid: significance for physiology and pathology. Neurochemistry International 2004;45:545-52.
128. Preston SD, Steart PV, Wilkinson A, Nicoll JAR, Weller RO. Capillary and arterial cerebral amyloid angiopathy in Alzheimer's disease: defining the perivascular route for the elimination of amyloid β from the human brain. Neuropathology and Applied Neurobiology 2003;29:106-17.

129. Schubert GA, Poli S, Mendelowitsch A, Schilling L, Thome C. Hypothermia reduces early hypoperfusion and metabolic alterations during the acute phase of massive subarachnoid hemorrhage: a laser-Doppler-flowmetry and microdialysis study in rats. Journal of neurotrauma 2008;25:539-48.
130. Chung WY, Lee LS. The effect of tissue plasminogen activator (t-PA) on cerebral vasospasm in canine subarachnoid hemorrhage. Zhonghua yi xue za zhi = Chinese medical journal; Free China ed 1993;52:298-306.
131. Findlay JM, Weir BKA, Kanamaru K, Grace M, Baughman R. The Effect of Timing of Intrathecal Fibrinolytic Therapy on Cerebral Vasospasm in a Primate Model of Subarachnoid Hemorrhage. Neurosurgery 1990;26:201-6.
132. Findlay JM, Weir BKA, Steinke D, Tanabe T, Gordon P, Grace M. Effect of intrathecal thrombolytic therapy on subarachnoid clot and chronic vasospasm in a primate model of SAH. Journal of Neurosurgery 1988;69:723-35.
133. Suzuki H, Kanamaru K, Kuroki M, Sun H, Waga S, Miyazawa T. Effects of unilateral intrathecal administrations of low dose tissue-type plasminogen activator on clot lysis, vasospasm and brain phospholipid hydroperoxidation in a primate model of bilateral subarachnoid hemorrhage. Neurological research 1998;20:625-31.
134. Asada M, Kong J, Nakamura M, Tamaki N. Thrombolytic therapy with tissue plasminogen activator for prevention of vasospasm in experimental subarachnoid hemorrhage: its efficacy and problems. Neurological research 1996;18:342-4.
135. Kawada S, Kinugasa K, Meguro T, et al. Experimental Study of Intracisternal Administration of Tissue-Type Plasminogen Activator Followed by Cerebrospinal Fluid Drainage in the Ultra-Early Stage of Subarachnoid Haemorrhage. Acta Neurochir (Wien) 1999;141:1331-8.
136. Brinker T, Seifert V, Stolke D. Effect of intrathecal fibrinolysis on cerebrospinal fluid absorption after experimental subarachnoid hemorrhage. J Neurosurg 1991;74:789-93.
137. Litrico S, Almairac F, Gaberel T, et al. Intraventricular fibrinolysis for severe aneurysmal intraventricular hemorrhage: a randomized controlled trial and meta-analysis. Neurosurg Rev 2013:1-9.
138. Kinouchi H, Ogasawara K, Shimizu H, Mizoi K, Yoshimoto T. Prevention of Symptomatic Vasospasm After Aneurysmal Subarachnoid Hemorrhage by Intraoperative Cisternal Fibrinolysis Using Tissue-Type Plasminogen Activator Combined With Continuous Cisternal Drainage. Neurologia medico-chirurgica 2004;44:569-77.
139. Ramakrishna R, Sekhar LN, Ramanathan D, et al. Intraventricular tissue plasminogen activator for the prevention of vasospasm and hydrocephalus after aneurysmal subarachnoid hemorrhage. Neurosurgery 2010;67:110-7; discussion 7.
140. Varelas PN, Rickert KL, Cusick J, et al. Intraventricular hemorrhage after aneurysmal subarachnoid hemorrhage: pilot study of treatment with intraventricular tissue plasminogen activator. Neurosurgery 2005;56:205-13; discussion -13.
141. Findlay JM, Jacka MJ. Cohort study of intraventricular thrombolysis with recombinant tissue plasminogen activator for aneurysmal intraventricular hemorrhage. Neurosurgery 2004;55:532-7; discussion 7-8.
142. Amin-Hanjani S, Ogilvy CS, Barker FG, 2nd. Does intracisternal thrombolysis prevent vasospasm after aneurysmal subarachnoid hemorrhage? A meta-analysis. Neurosurgery 2004;54:326-34; discussion 34-5.
143. Roos YB, Rinkel GJ, Vermeulen M, Algra A, van Gijn J. Antifibrinolytic therapy for aneurysmal subarachnoid haemorrhage. Cochrane Database Syst Rev 2003:CD001245.
144. Hillman J, Fridriksson S, Nilsson O, Yu Z, Säveland H, Jakobsson K-E. Immediate administration of tranexamic acid and reduced incidence of early rebleeding after aneurysmal subarachnoid hemorrhage: a prospective randomized study. Journal of Neurosurgery 2002;97:771-8.

145. Iplikcioglu AC, Berkman MZ. The effect of short-term antifibrinolytic therapy on experimental vasospasm. Surgical Neurology 2003;59:10-6.
146. Diamond SL, Anand S. Inner clot diffusion and permeation during fibrinolysis. Biophysical Journal 1993;65:2622-43.
147. Diamond SL. Engineering Design of Optimal Strategies for Blood Clot Dissolution. Annual Review of Biomedical Engineering 1999;1:427-61.
148. Dankbaar JW, de Rooij NK, Velthuis BK, Frijns CJ, Rinkel GJ, van der Schaaf IC. Diagnosing delayed cerebral ischemia with different CT modalities in patients with subarachnoid hemorrhage with clinical deterioration. Stroke 2009;40:3493-8.
149. Pluta RM, Hansen-Schwartz J, Dreier J, et al. Cerebral vasospasm following subarachnoid hemorrhage: time for a new world of thought. Neurological research 2009;31:151-8.
150. Macdonald RL. Delayed neurological deterioration after subarachnoid haemorrhage. Nature reviews Neurology 2014;10:44-58.
151. Poloyac SM, Reynolds RB, Yonas H, Kerr ME. Identification and quantification of the hydroxyeicosatetraenoic acids, 20-HETE and 12-HETE, in the cerebrospinal fluid after subarachnoid hemorrhage. Journal of neuroscience methods 2005;144:257-63.
152. Cambj-Sapunar L, Yu M, Harder DR, Roman RJ. Contribution of 5-hydroxytryptamine1B receptors and 20-hydroxyeiscosatetraenoic acid to fall in cerebral blood flow after subarachnoid hemorrhage. Stroke 2003;34:1269-75.
153. Zhang W, Koerner IP, Noppens R, et al. Soluble epoxide hydrolase: a novel therapeutic target in stroke. Journal of cerebral blood flow and metabolism : official journal of the International Society of Cerebral Blood Flow and Metabolism 2007;27:1931-40.
154. Node K, Huo Y, Ruan X, et al. Anti-inflammatory properties of cytochrome P450 epoxygenase-derived eicosanoids. Science 1999;285:1276-9.
155. Nation DA, Edland SD, Bondi MW, et al. Pulse pressure is associated with Alzheimer biomarkers in cognitively normal older adults. Neurology 2013;81:2024-7.
156. Iliff JJ, Fairbanks SL, Balkowiec A, Alkayed NJ. Epoxyeicosatrienoic acids are endogenous regulators of vasoactive neuropeptide release from trigeminal ganglion neurons. Journal of neurochemistry 2010;115:1530-42.
157. McGirt MJ, Lynch JR, Parra A, et al. Simvastatin Increases Endothelial Nitric Oxide Synthase and Ameliorates Cerebral Vasospasm Resulting From Subarachnoid Hemorrhage. Stroke 2002;33:2950-6.
158. Sugawara T, Ayer R, Jadhav V, Zhang JH. A new grading system evaluating bleeding scale in filament perforation subarachnoid hemorrhage rat model. Journal of neuroscience methods 2008;167:327-34.
159. An L, Qin J, Wang RK. Ultrahigh sensitive optical microangiography for in vivo imaging of microcirculations within human skin tissue beds. Opt Express 2010;18:8220-8.
160. Abramoff MD, Magalhaes, P.J., Ram, S.J. Image Processing with ImageJ. Biophotonics International 2004;11:36-42.
161. Jouihan SA, Zuloaga KL, Zhang W, et al. Role of soluble epoxide hydrolase in exacerbation of stroke by streptozotocin-induced type 1 diabetes mellitus. J Cereb Blood Flow Metab 2013.
162. Reilly C, Amidei C, Tolentino J, Jahromi BS, Macdonald RL. Clot volume and clearance rate as independent predictors of vasospasm after aneurysmal subarachnoid hemorrhage. J Neurosurg 2004;101:255-61.
163. Crago EA, Thampatty BP, Sherwood PR, et al. Cerebrospinal fluid 20-HETE is associated with delayed cerebral ischemia and poor outcomes after aneurysmal subarachnoid hemorrhage. Stroke 2011;42:1872-7.

164. Barden AE, Croft KD, Beilin LJ, Phillips M, Ledowski T, Puddey IB. Acute effects of red wine on cytochrome P450 eicosanoids and blood pressure in men. Journal of hypertension 2013;31:2195-202; discussion 202.
165. Pradilla G, Chaichana KL, Hoang S, Huang J, Tamargo RJ. Inflammation and cerebral vasospasm after subarachnoid hemorrhage. Neurosurgery clinics of North America 2010;21:365-79.
166. Alkayed NJ, Goyagi T, Joh HD, et al. Neuroprotection and P450 2C11 upregulation after experimental transient ischemic attack. Stroke 2002;33:1677-84.
167. Kawasaki T, Marumo T, Shirakami K, et al. Increase of 20-HETE synthase after brain ischemia in rats revealed by PET study with 11C-labeled 20-HETE synthase-specific inhibitor. Journal of cerebral blood flow and metabolism : official journal of the International Society of Cerebral Blood Flow and Metabolism 2012;32:1737-46.
168. Martini R, Ward J, Siler D, et al. Genetic variation in soluble epoxide hydrolase is associated with outcome after aneurysmal subarachnoid hemorrhage. Journal of Neurosurgery 2014;In Press.
169. Sehba FA, Hou J, Pluta RM, Zhang JH. The importance of early brain injury after subarachnoid hemorrhage. Progress in neurobiology 2012;97:14-37.
170. Fu C, Yu W, Sun L, Li D, Zhao C. Early cerebral infarction following aneurysmal subarachnoid hemorrhage: frequency, risk factors, patterns, and prognosis. Current neurovascular research 2013;10:316-24.
171. Rabinstein AA, Weigand S, Atkinson JL, Wijdicks EF. Patterns of cerebral infarction in aneurysmal subarachnoid hemorrhage. Stroke 2005;36:992-7.
172. Shimoda M, Takeuchi M, Tominaga J, Oda S, Kumasaka A, Tsugane R. Asymptomatic versus symptomatic infarcts from vasospasm in patients with subarachnoid hemorrhage: serial magnetic resonance imaging. Neurosurgery 2001;49:1341-8; discussion 8-50.
173. Etminan N, Vergouwen MD, Ilodigwe D, Macdonald RL. Effect of pharmaceutical treatment on vasospasm, delayed cerebral ischemia, and clinical outcome in patients with aneurysmal subarachnoid hemorrhage: a systematic review and meta-analysis. Journal of cerebral blood flow and metabolism : official journal of the International Society of Cerebral Blood Flow and Metabolism 2011;31:1443-51.
174. Deng Y, Edin ML, Theken KN, et al. Endothelial CYP epoxygenase overexpression and soluble epoxide hydrolase disruption attenuate acute vascular inflammatory responses in mice. The FASEB Journal 2011;25:703-13.
175. Iliff JJ, Alkayed NJ. Soluble epoxide hydrolase inhibition: targeting multiple mechanisms of ischemic brain injury with a single agent. Future Neurol 2009;4:179-99.
176. Ostergaard L, Aamand R, Karabegovic S, et al. The role of the microcirculation in delayed cerebral ischemia and chronic degenerative changes after subarachnoid hemorrhage. Journal of cerebral blood flow and metabolism : official journal of the International Society of Cerebral Blood Flow and Metabolism 2013;33:1825-37.
177. Milhorat TH. Acute hydrocephalus after aneurysmal subarachnoid hemorrhage. Neurosurgery 1987;20:15-20.
178. Hoh BL, Kleinhenz DT, Chi YY, Mocco J, Barker FG, 2nd. Incidence of ventricular shunt placement for hydrocephalus with clipping versus coiling for ruptured and unruptured cerebral aneurysms in the Nationwide Inpatient Sample database: 2002 to 2007. World Neurosurg 2011;76:548-54.
179. Vale FL, Bradley EL, Fisher WS. The relationship of subarachnoid hemorrhage and the need for postoperative shunting. J Neurosurg 1997;86:462-6.
180. Li T, Wang H, Ding Y, et al. Genetic elimination of Nrf2 aggravates secondary complications except for vasospasm after experimental subarachnoid hemorrhage in mice. Brain research 2014;1558:90-9.

181. Sozen T, Tsuchiyama R, Hasegawa Y, et al. Role of Interleukin-1β in Early Brain Injury After Subarachnoid Hemorrhage in Mice. Stroke; a journal of cerebral circulation 2009;40:2519-25.
182. Bloch O, Auguste KI, Manley GT, Verkman AS. Accelerated progression of kaolin-induced hydrocephalus in aquaporin-4-deficient mice. J Cereb Blood Flow Metab 2006;26:1527-37.
183. New paradigms in inflammatory signaling in vascular endothelial cells; 2014.
184. Node K, Huo Y, Ruan X, et al. Anti-inflammatory Properties of Cytochrome P450 Epoxygenase-Derived Eicosanoids. Science 1999;285:1276-9.
185. Serres S, Mardiguian S, Campbell SJ, et al. VCAM-1-targeted magnetic resonance imaging reveals subclinical disease in a mouse model of multiple sclerosis. The FASEB Journal 2011;25:4415-22.
186. McAteer MA, Sibson NR, von zur Muhlen C, et al. In vivo magnetic resonance imaging of acute brain inflammation using microparticles of iron oxide. Nat Med 2007;13:1253-8.
187. Smith SM, Jenkinson M, Woolrich MW, et al. Advances in functional and structural MR image analysis and implementation as FSL. NeuroImage 2004;23, Supplement 1:S208-S19.
188. Jenkinson M, Bannister P, Brady M, Smith S. Improved Optimization for the Robust and Accurate Linear Registration and Motion Correction of Brain Images. NeuroImage 2002;17:825-41.
189. Jenkinson M, Smith S. A global optimisation method for robust affine registration of brain images. Medical Image Analysis 2001;5:143-56.
190. van Gijn J, Hijdra A, Wijdicks EF, Vermeulen M, van Crevel H. Acute hydrocephalus after aneurysmal subarachnoid hemorrhage. J Neurosurg 1985;63:355-62.
191. Braun KP, Dijkhuizen RM, de Graaf RA, et al. Cerebral ischemia and white matter edema in experimental hydrocephalus: a combined in vivo MRI and MRS study. Brain research 1997;757:295-8.
192. Tada T, Kanaji M, Shigeaki K. Induction of communicating hydrocephalus in mice by intrathecal injection of human recombinant transforming growth factor-β1. Journal of neuroimmunology 1994;50:153-8.
193. Zhang K, Sejnowski TJ. A universal scaling law between gray matter and white matter of cerebral cortex. Proceedings of the National Academy of Sciences 2000;97:5621-6.
194. Nag S, Manias JL, Stewart DJ. Pathology and new players in the pathogenesis of brain edema. Acta neuropathologica 2009;118:197-217.
195. Ebisu T, Naruse S, Horikawa Y, et al. Discrimination between different types of white matter edema with diffusion-weighted MR imaging. Journal of magnetic resonance imaging : JMRI 1993;3:863-8.
196. Ulu A, Harris TR, Morisseau C, et al. Anti-inflammatory Effects of [omega]-3 Polyunsaturated Fatty Acids and Soluble Epoxide Hydrolase Inhibitors in Angiotensin-II-Dependent Hypertension. Journal of Cardiovascular Pharmacology 2013;62:285-97 10.1097/FJC.0b013e318298e460.
197. Schmelzer KR, Kubala L, Newman JW, Kim I-H, Eiserich JP, Hammock BD. Soluble epoxide hydrolase is a therapeutic target for acute inflammation. Proceedings of the National Academy of Sciences of the United States of America 2005;102:9772-7.
198. Siler DA, Gonzalez JA, Wang RK, Cetas JS, Alkayed NJ. Intracisternal administration of tissue plasminogen activator improves cerebrospinal fluid flow and cortical perfusion after subarachnoid hemorrhage in mice. Translational stroke research 2014;5:227-37.
199. Greenwood J, Etienne-Manneville S, Adamson P, Couraud P-O. Lymphocyte migration into the central nervous system: Implication of ICAM-1 signalling at the blood–brain barrier. Vascular Pharmacology 2002;38:315-22.
200. Hoyte LC, Brooks KJ, Nagel S, et al. Molecular magnetic resonance imaging of acute vascular cell adhesion molecule-1 expression in a mouse model of cerebral ischemia. Journal of

cerebral blood flow and metabolism : official journal of the International Society of Cerebral Blood Flow and Metabolism 2010;30:1178-87.
201. Qiong Yu MC, Hailian Wang, Shiduo Lu, Hui Gao, Peiying Li, Yu Gan, Hong Shi, Weimin Liang, Jun Chen, Yanqin Gao. Sevoflurane preconditioning protects blood-brain-barrier against brain ischemia. Frontiers in Bioscience 2011;E3:10.
202. Koerner IP, Jacks R, DeBarber AE, et al. Polymorphisms in the Human Soluble Epoxide Hydrolase Gene EPHX2 Linked to Neuronal Survival after Ischemic Injury. The Journal of Neuroscience 2007;27:4642-9.
203. Dilation of cerebral arterioles by cytochrome P-450 metabolites of arachidonic acid; 1990.
204. Samuelsson C, Howells T, Kumlien E, Enblad P, Hillered L, Ronne-Engström E. Relationship between intracranial hemodynamics and microdialysis markers of energy metabolism and glutamate-glutamine turnover in patients with subarachnoid hemorrhage. Journal of Neurosurgery 2009;111:910-5.
205. Hubschmann OR, Kornhauser D. Effect of subarachnoid hemorrhage on the extracellular microenvironment. Journal of Neurosurgery 1982;56:216-21.
206. Suzuki S, Ishii M, Ottomo M, Iwabuchi T. Changes in the subarachnoid space after experimental subarachnoid haemorrhage in the dog: Scanning electron microscopic observation. Acta Neurochir (Wien) 1977;39:1-14.
207. Mizoi K, Yoshimoto T, Fujiwara S, Sugawara T, Takahashi A, Koshu K. Prevention of Vasospasm by Clot Removal and Intrathecal Bolus Injection of Tissue-Type Plasminogen Activator: Preliminary Report. 1991;28:807-13.
208. Zabramski JM, Spetzler RF, Lee KS, et al. Phase I trial of tissue plasminogen activator for the prevention of vasospasm in patients with aneurysmal subarachnoid hemorrhage. Journal of Neurosurgery 1991;75:189-96.
209. Larsen CC, Astrup J. Rebleeding After Aneurysmal Subarachnoid Hemorrhage: A Literature Review. World Neurosurgery 2013;79:307-12.
210. Witiw C, Ibrahim G, Fallah A, Macdonald RL. Early Predictors of Prolonged Stay in a Critical Care Unit Following Aneurysmal Subarachnoid Hemorrhage. Neurocrit Care 2013;18:291-7.
211. Liu J-Y, Tsai H-J, Hwang SH, Jones PD, Morisseau C, Hammock BD. Pharmacokinetic optimization of four soluble epoxide hydrolase inhibitors for use in a murine model of inflammation. British journal of pharmacology 2009;156:284-96.
212. Nag S, Manias JL, Stewart DJ. Pathology and new players in the pathogenesis of brain edema. Acta Neuropathol 2009;118:197-217.
213. Park KW, Dai HB, Metais C, Comunale ME, Sellke FW. Isoflurane does not further impair microvascular vasomotion in a rat model of subarachnoid hemorrhage. Canadian journal of anaesthesia = Journal canadien d'anesthesie 2002;49:427-33.
214. Altay O, Hasegawa Y, Sherchan P, et al. Isoflurane delays the development of early brain injury after subarachnoid hemorrhage through sphingosine-related pathway activation in mice. Critical care medicine 2012;40:1908-13.
215. Altay O, Suzuki H, Hasegawa Y, et al. Isoflurane attenuates blood-brain barrier disruption in ipsilateral hemisphere after subarachnoid hemorrhage in mice. Stroke 2012;43:2513-6.